Single and Multiple Emitter Localization in Cognitive Radio Networks

by

Suzan Ureten

Thesis submitted to the
Faculty of Graduate and Postdoctoral Studies
In partial fulfillment of the requirements
For the Ph.D. degree in
Electrical and Computer Engineering

School of Electrical Engineering and Computer Science
Faculty of Engineering
University of Ottawa

Abstract

Cognitive radio (CR) is often described as a context-intelligent radio, capable of changing the transmit parameters dynamically based on the interaction with the environment it operates. The work in this thesis explores the problem of using received signal strength (RSS) measurements taken by a network of CR nodes to generate an interference map of a given geographical area and estimate the locations of multiple primary transmitters that operate simultaneously in the area. A probabilistic model of the problem is developed, and algorithms to address location estimation challenges are proposed. Three approaches are proposed to solve the localization problem. The first approach is based on estimating the locations from the generated interference map when no information about the propagation model or any of its parameters is present. The second approach is based on approximating the maximum likelihood (ML) estimate of the transmitter locations with the grid search method when the model is known and its parameters are available. The third approach also requires the knowledge of model parameters but it is actually based on generating samples from the joint posterior of the unknown location parameter with Markov chain Monte Carlo (MCMC) methods, as an alternative for the highly computationally complex grid search approach.

For RF cartography generation problem, we study global and local interpolation techniques, specifically the Delaunay triangulation based techniques as the use of existing triangulation provides a computationally attractive solution. We present a comparative performance evaluation of these interpolation techniques in terms of RF field strength estimation and emitter localization. Even though the estimates obtained from the generated interference maps are less accurate compared to the ML estimator, the rough estimates are utilized to initialize a more accurate algorithm such as the MCMC technique to reduce the complexity of the algorithm. The complexity issues of ML estimators based on full grid search are also addressed by various types of iterative grid search methods. One challenge to apply the ML estimation algorithm to multiple emitter localization problem is that, it requires a pdf approximation to summands of log-normal random variables for likelihood calculations at each grid location. This inspires our investigations on sum of log-normal approximations studied in literature for selecting the appropriate approximation to our model assumptions. As a final extension of this work, we propose our own approximation based on distribution fitting to a set of simulated data and compare our approach with Fenton-Wilkinson's well-known approximation which is a simple and computational efficient approach that fits a log-normal distribution to sum of log-normals by matching the first and second central moments of random variables. We demonstrate that the location estimation accuracy of the grid search technique obtained with our proposed approximation is higher than the one obtained with Fenton-Wilkinson's in many different case scenarios.

Acknowledgements

I would like to express deepest gratitude to my supervisor Prof. Abbas Yongacoglu for his full support, expert guidance, understanding and encouragement throughout my study and research. Without his incredible patience and counsel, my thesis work would have been a frustrating and overwhelming pursuit. In addition, I express my appreciation to my co-supervisor Prof. Emil Petriu and also to Prof. Halim Yanikomeroglu for having served on my committee. Their thoughtful questions and comments were valued greatly.

Thanks also go to the University of Ottawa which granted me an admission scholarship for the entire four year term. Without this scholarship, I wouldn't have been able to continue my studies on a full-time basis.

Special thanks go to my colleagues, Dr. Zhenxia Zhang, Chao Li, Kerem Karatas and my other friends who helped me throughout this academic exploration.

Finally I would like to thank my family for their patience, guidance, support and love in every aspect of my life.

Table of Contents

List of Figures

Nomenclature

Abbreviations

AOA	Angle of arrival
CPSO	Constriction particle swarm optimization
CR	Cognitive radio
CRLB	Cramer Rao lower bound
CRN	Cognitive radio network
CWLS	Constrained weighted least squares
EM	Expectation maximization
FIM	Fisher information matrix
GDOP	Geometric dilution of precision
GIS	Geographic information systems
GPS	Global positioning system
GSM	Global system for mobile communications
IEEE	Institute of electrical and electronics engineers
IM	Interference management
LS	Least squares
MAC	Media access control
MCMC	Markov chain Monte Carlo
ME	Mean error
MH	Metropolis-Hastings
MH-Linear	Linear interpolation initialized MH
MH-Max	Maximum power reading sensor's location initialized Metropolis-Hastings
MH-NN	Nearest neighbor interpolation initialized Metropolis-Hastings
MH-RND	Randomly initialized Metropolis-Hastings
ML	Maximum likelihood
MLE	Maximum likelihood estimation
MMSE	Minimum mean squared error
MSE	Mean squared error
PHY	Physical layer
REA	Radio environmental awareness
REM	Radio environment map
RF	Radio frequency
RIFE	Radio interference field estimation

RJMCMC	Reversible jump Markov chain Monte Carlo
RMS	Root mean square
RMSE	Root mean squared error
ROI	Region of interest
RRM	Radio resource management
RSS	Received signal strength
RSSD	Received signal strength difference
TDOA	Time difference of arrival
TOA	Time of arrival
TSA	Tree search algorithm
WSN	Wireless sensor network
WTLS	Weighted total least squares

Mathematical Symbols

α	path-loss exponent
β	constant that reflects carrier frequency and antenna gain
$\hat{\boldsymbol{\theta}}$	$(\hat{T}_x, \hat{T}_y)$ emitter's estimated location
$\boldsymbol{\theta_c}$	current state of location parameter
$\boldsymbol{\theta_i}$	initial state of location parameter
$\boldsymbol{\theta_{new}}$	new state of location parameter
$\boldsymbol{\theta_p}$	proposed state of location parameter
$\boldsymbol{\theta}$	(T_x, T_y) emitter's actual location
ϵ	$\frac{\ln 10}{10}$
η	efficiency
$\gamma(.)$	semivariance function
κ	RMSE of emitter localization
Ł	likelihood function
$Ł_c$	likelihood value of current location
$Ł_p$	likelihood value of proposed location
$Ł_R$	likelihood ratio
$Ł_{Fenton}$	likelihood value of Fenton approximation
$Ł_{fitted}$	likelihood value of fitted approximation
$Ł_{mar}$	marginalized likelihood function
λ	wavelength
$\phi(.)$	basis function
σ	shadowing spread
$\mathbf{M}$	signal model
$\mathbf{r}$	vector of RSS measurements
d_j	distance between jth sensor and the emitter
d_{corr}	decorrelation distance
$E(.)$	statistical expectation operator
E_{rms}	root mean squared value of received power estimation error
G	geometric dilution of precision
H	number of simulations
I	number of iterations (levels)
J_{ij}	Fisher information matrix
L	length of square search area
$LN(.)$	log-normal operator
$ln(Ł)$	log-likelihood function
N_s	number of sensors
N_t	number of emitters
$N_{selected}$	number of selected sensors
P_t	emitter power
Q	number of grid elements
r_j	received power at jth sensor

s_j	total mean received power at jth sensor
$SLN(.)$	sum of log-normal
Δ	step size of MH algorithm
μ_j	mean value of sum-of-log-normal distribution
$\sigma^2_{sum_j}$	variance of sum-of-log-normal distribution
a	acceptance ratio
d_{ij}	distance between jth sensor and ith emitter
r_{ij}	power at jth sensor due to ith emitter
s_{ij}	mean power at jth sensor due to ith emitter

Chapter 1

Introduction

An increasing number of wireless systems and applications are being integrated into our daily lives in a variety of forms, such as entertainment devices, defense, security applications and health care systems. Any such wireless system needs radio frequency (RF) spectrum allocation for its proper operation, therefore spectrum scarcity has become a critical issue due to the increased demand for wireless systems and applications.

The RF spectrum is considered as a natural source and traditionally its use has been strictly regulated and managed by government on a licensing basis. These strict regulations do not allow the use of spectrum by other radio technologies or different users other than the specific ones initially defined, i.e. license holders are not allowed to reallocate the spectrum to different technologies or to other users. However, several spectrum measurement campaigns carried out in several places have demonstrated that major licensed bands such as those allocated for television broadcasting, amateur radio or paging systems are under-utilized, i.e. the allocated spectrum is idle at different times and geographical locations. Therefore it is believed that the existing problem is the inefficient utilization of the spectrum due to the current regulation scheme rather than the scarcity of the spectrum.

The concept of cognitive radio has been recently proposed to address the under-utilization problem due to current spectrum regulation regime. A cognitive radio is a device that can change the transmit parameters dynamically based on the interaction with the environment it operates. The objective of the cognitive radio is to achieve better spectrum utilization by allowing unlicensed users to access the spectrum if their usages do not cause unacceptable interference to the original license holders. In practice, the unlicensed users, also called **secondary users** or cognitive users, need to sense the spectrum continuously to find a suitable spectrum band for possible utilization without causing interference to the licensed users, also called **primary users**.

Spectrum sensing task is a critical part of a **dynamic spectrum access** system and complicated by several factors such as requirement of detecting the primary user at very low signal-to-noise ratio levels, measurement uncertainties, shadow fading and hidden terminal problems. Errors in sensing can cause performance degradation both in the primary or the secondary user systems. When the secondary users misses detecting the primary user (called **missed detection**) and transmits, it causes interference to the primary user. On

the other hand, if the sensing result indicates presence of the primary user when the spectrum is actually idle (called **false alarm**), then a transmission opportunity is lost and secondary user efficiency suffers. A promising idea to address these difficulties is to perform sensing collaboratively among several radios in the network. In order to assist cognitive radio to perform these tasks, a concept called **radio environment map (REM)** is proposed. The REM is a tool to provide network support to cognitive radio. It identifies the location of transmitters and geo-spatial properties of parameters such as terrain, service availability, policy requirements and hardware type. It contains several kinds of information such as geographical structure of the area and the spectrum regulations in the area or the location of transmitters. If the locations and the transmit powers of primary users can be extracted from such tools, then a protection region can be set around the primary emitters. This protected region is known as **primary exclusion region** or **zone** and primary users are protected from harmful interference due to secondary users inside this region. This type of approach will help efficient spectrum exploitation which is an essential step in dynamic spectrum access networks. Therefore there exists a need to identify the location of primary emitters to predict the primary exclusion region as the emitters cannot or will not identify their own location and/or communicate it to a REM due to non-cooperative nature of primary networks.

Spatial estimation of the location of signal sources, or source (node) localization problem has been considered extensively in the literature where the goal is to locate the position of a source based on the measurements taken at the sensors. Source localization has several applications in various fields such as logistics and tracking [54]. For example, accurate localization of cell phones in an emergency has been mandated in the United States [89]. Similarly, microphone arrays can be used to determine the location of an acoustic source [11] or to aid automatic camera tracking [77]. In source localization, received power measurements can be utilized to estimate the distances between the source and the sensors by using a protocol in which the source with unknown location transmits a signal with known power and the sensors deduce their distance from it based on the received signal power measurements and a given path-loss model. The distances from several monitors are then combined to obtain an estimate of the relative location of the transmitter [18]. The problem can also be extended to a network of multiple sensors whose locations must be determined based on the known locations of a group of nodes and pairwise node distances [6]. The literature on source localization has been developing on efficient and/or distributed algorithms for minimizing the localization error. An important constraint of source localization problem is that the source (to be localized) is not cooperating and its transmit power is unknown; this makes it infeasible to compute the distance between the source and the monitor. The problem is even more complicated when there are multiple sources to localize and their number is unknown.

Measurements for source localization include received signal strength (RSS) [11], angle of arrival (AOA) [66] and time difference of arrival (TDOA) [14] at multiple receivers. The drawbacks of AOA measurements is that determining the AOA requires a phased array antenna at each sensor rather than a single antenna and the quality of the final position estimate degrades rapidly as the monitors move away from the source node. Due to its simplicity in terms of both hardware and computational requirements, RSS is frequently

used and is an attractive source of measurements with wide applicability for low-cost sensor systems. However, RSS measurements are not very accurate and a large, dense network is often required for precise location estimates. RSS techniques typically assume that the transmitted power and the path-loss exponent are known and the transmitting antenna is isotropic. TDOA methods do not make such assumptions, but they require significantly higher communications overhead than AOA or RSS-based methods.

In addition to the existing localization methods, fingerprinting based localization is also an attractive source of RSS based measurement. It simply relies on the recording of the signal strength from several access points in range and storing this information in a database along with the known coordinates of the client device in an offline phase. This information can be deterministic [8] or probabilistic [81]. During the online tracking phase, the current RSS measurement at an unknown location is compared to those stored in the fingerprint and the closest match is returned as the estimated user location. Its main disadvantage is that any changes of the environment may change the fingerprint that corresponds to each location, requiring an update to the fingerprint database. However, the integration with other sensors can be used in order to deal with the environmental interference [10].

Emitter localization problem in general has been considered extensively in the literature; see for example [43] for an overview of localization techniques. Localization may be accomplished via the above mentioned techniques. Among these techniques, less accurate RSS-based techniques are often of interest as they require simpler hardware. The challenge of RSS-based localization is due to numerous factors affecting the energy decay between the transmitter and emitter such as shadowing, multipath, path-loss exponent estimation errors, geometric configuration of the nodes and antenna orientation. Despite having several sources of error, RSS-based techniques are expected to perform satisfactorily when a large number of spatially separated sensors are employed.

1.1 Problem Definition

In this thesis, we consider the problem of generating an interference map of a given geographical area, and estimating the locations of multiple radio transmitters that operate simultaneously in adjacent coverage areas by using the received signal strength measurements taken at different locations. We develop a probabilistic model of the problem and propose algorithms to address location estimation challenges. The efficiencies of the algorithms are also of interest, hence we explore complexity-performance trade-offs as well as the distribution of computations over the network.

A mathematical definition of the problem including model assumptions and constraints will be presented in Section 3.3.1 and Section 4.2.2 for single and multiple emitter case scenarios respectively. The assumption of model parameters will be stated for different localization techniques in each related section. However, a table that summarizes the assumptions of model parameters can also be found in Appendix A.

In this chapter, we will justify the motivation of our efforts and briefly review the existing literature.

1.2 Motivation

The problem of locating and tracking signal-emitting sources has attracted attention for the last 60 years [21]. Early applications in radar and sonar typically involved a few sensors. In the last six decades, there has been a considerable increase in the sophistication of wireless networks. Dramatic advances in radio frequency have been made possible through the use of large networks of wireless sensors for a variety of new monitoring and control applications. These advancements have led to the broadening of techniques employed for localization as well as the applications where localization is important. Examples of today's applications for source localization that serve as the major reason for current research include the following:

- Monitoring and tracking for safety and security reasons [62]
- Location based billing [62]
- Fraud protection [62]
- Asset tracking [62]
- Fleet management [62]
- Alternative to global positioning system (GPS) navigation [62, 21]

For outdoor localization, GPS systems have been used in a wide range of applications including tracking, transport navigation, and guidance [32]. Although GPS works extremely well in outdoor localization, it does not perform well indoors. Therefore alternatives to GPS navigation is being sought to overcome its limitations. When inside large buildings or in an underground or a tunnel, there is often no direct line from the satellite signals to the GPS receiver and the signal weakens or distorts as it travels through the building. The GPS works better when the device has a clear line of sight to the sky. The more GPS satellites that a device can access, the more accurate location estimates it provides. The construction materials in a building also affect how well a GPS device will work indoors. GPS signals pass through glass much more easily than they do through thick, solid materials such as brick, metal, stone or wood. For example, if one is in a house and stand near enough to the windows, or in an office tower with large windows, the device could still work.

Spatial estimation of the location of signal sources, or source (node) localization is already discussed in the Introduction Section with some other applications. Besides source localization, spectrum cartography, i.e. multiple transmitter localization and communication footprint identification has also applications in cognitive radio white space networking

and spectrum enforcement. An accurate and fast method of obtaining up-to-date transmitter footprint information is necessary for frequency based networking and optimal routing of cognitive radios, while ensuring minimal interference to higher priority primary users. Moreover, recent studies have revealed that knowledge of the primary users' location and interference tolerance can dramatically improve spectrum sensing performance, and therefore reduce interference to the primary system [35]. For example, once the location of the primary emitter is known, the secondary user that is the closest to the emitter can detect either the primary is on or off. We consider the problem of using RSS measurements taken by the secondary users to estimate the locations of multiple primary transmitters that operate simultaneously in adjacent coverage areas. We develop a probabilistic model of the problem and propose algorithms to address location estimation challenges. The proposed algorithms provide a mechanism for secondary users to obtain their information about nearby primary systems by processing distributed measurements. The efficiency of the algorithms is also of interest, and hence we explore complexity-performance trade-off as well as the distribution of computations over the network.

Localization of multiple emitters can also be applied to dynamic spectrum access in cellular networks [50] where the possibility of deploying a cognitive network that can opportunistically access the spectrum allocated to a primary cellular network is studied. The main problem is that detecting spectrum opportunities in the frequency bands allocated to cellular networks is more challenging than in TV white space due to several problems in the former, namely the requirement for coverage, the presence of different services with different quality constraints, dynamic traffic patterns, the presence of several neighboring primary transmitters and adaptive primary transmit powers. The approach in [50] assumes that the cognitive network knows the positions of the primary base stations and its own base stations through a local or regional database without knowing their transmit powers. It utilizes a **maximum likelihood estimator (MLE)** to detect the activity of neighboring primary base stations and exploits this information to determine the power with which a cognitive radio can transmit. The results show the possibility of using such a method to deploy an IEEE 802.11-like network as a cognitive network under specific constraints related to the position, to the number and to the distribution of the spectrum monitoring sensors inside the primary network.

Another challenge for opportunistically accessing the spectrum in cellular networks is that the secondary users need to detect a wide-band of 20 MHz spectrum, a typical bandwidth of a GSM network so that they can decide whether the primary user is on or off. This requires wide-band power spectrum estimation which is highly costly. Besides, distinguishing channels allocated to neighboring cells and to the own cell of a secondary user requires FFT analysis and fast signal processing algorithms that would cause latency in the cognitive network. Instead, low-cost sensors that monitor the activities of primary base stations can be distributed in the network and the measurements collected at these sensors can then be sent to a fusion center where the information is utilized to localize multiple primary base stations. When there are multiple base stations transmitting in the same band, energy detection techniques are insufficient to localize the base stations that are transmitting simultaneously. This is because each base station contributes different unknown portions of power at the sensor nodes. Simple methods based on received power

measurements are inconclusive. Isolating each base station based on the its signature is essential to estimate its location in this scenario. There is a trade-off between the cost and complexity of the sensors. When we require complex signal processing algorithms in the sensors, the cost of the devices increases. Thus, there is a need for signal processing and detection algorithms which can be implemented at low cost. The time taken for localization directly impacts the time to find the white spaces in the spectrum. In highly dynamic networks like cellular networks where white spaces do not last long, time to localize needs to be short so that secondary users can make better use of white spaces. Hence algorithms that take less time to localize are preferable in cognitive radio networks.

The possibility that REMs can also be used as databases that provide a variety of network and user-related context information for improving interference management (IM) and radio resource management (RRM) in two-tier cellular networks comprising macro and femto-cells [83] is another motivation for us to study emitter localization problem in cognitive radio networks. A cognitive femto-cell is a femto-cell that intelligently and dynamically allocates air interface resources based on the usage of nearby macro-cells [33]. The framework is essentially a dynamic spectrum access framework in which the macro-cell is the primary user and the femto-cell is the secondary user. The femto-cell senses what time-frequency resources are in use by the macro-cell and dynamically allocates resources such that it does not interfere with the macro-cell's transmissions. Dynamic allocation offers greater flexibility and potentially improved spectral efficiency over fixed allocations. Given the strong interest in femto-cells in the mobile networking industry, it is likely that cognitive femto-cells will represent a key use of dynamic spectrum access technologies in coming years.

Another potential application of dynamic spectrum access in a mobile cellular network is device-to-device communication. Device-to-device communication is a direct mode of communication between nearby mobile devices that would otherwise be routed through the base station and associated infrastructure. It is proposed to offload traffic from potentially congested infrastructure as well as to provide communication opportunities in the absence of a link to the base station (e.g. indoor scenario). Commercial networks, such as media sharing and gaming that offers proximity based services, have interest in device-to-device communication. There is also interest in non-commercial networks. For example, the public safety network, such as FirstNet (First Responder Network Authority) that is designed to serve the needs of the first responder community, uses direct mode communication between emergency responders on the network [61]. As the first responder community migrates to broadband cellular networks, a device-to-device capability is an active research topic in order to preserve this critical mode of communication. The 3rd Generation Partnership Project (3GPP) has studied the feasibility of proximity-based services in preparation for inclusion in Release 12 of Long Term Evolution (LTE) specifications [38]. Since device-to-device connections can be controlled by the cellular network infrastructure [22], a framework in which the connections are established in a decentralized fashion by the devices themselves is also possible. Such a framework would allow for a device-to-device communication in the absence of a link to the base station, which is highly desirable in the public safety community. In the decentralized scenario, the peer-to-peer network would function as a secondary network, sensing for and giving priority to

the primary transmissions.

Dynamic spectrum access can also play an important role in unlicensed spectrum. As more devices appear on unlicensed bands, it may become necessary to prioritize traffic. For example, it is common to have multiple WiFi devices in a home connected to the internet through a single access point. Currently, they access the medium as peers. But it may be more appropriate to set priorities among the devices. For example, the device running a video streaming application may have a higher priority than the smart fridge reporting its temperature. Using dynamic spectrum access technology, the smart fridge can transmit its packets when it detects white space in the spectrum, rather than competing with the video streaming application.

Furthermore, by sharing information about the radio environment through REM dissemination, the hidden node problem can be mitigated and the secondary users can co-exist with primary users with minimal harmful interference [85].

1.3 Contributions

This thesis makes 4 major contributions:

- A number of interpolation techniques have been used for generating **interference cartographs** in the literature but there is no such relative performance comparison of these techniques where the data to be interpolated are the RF field strength values. As one of our contribution to the area of interference map generation problem in CR networks, we present a comparative performance evaluation of the interpolation techniques used in interference cartography generation. Specifically, we investigate the performance of **Delaunay triangulation** based interpolation techniques in generating interference maps as the use of existing triangulation provides a computationally attractive solution for the map generation problem. Furthermore, we propose to estimate the locations of the primary emitters from the generated interference map and explore complexity-performance trade-offs of these interpolation techniques.

- As the accuracy of the estimation obtained from interference maps is low, we investigate more accurate algorithms, develop a probabilistic model of the problem and propose algorithms to address location estimation challenges. The existing maximum-likelihood estimation (MLE) based on **grid search** method gives accurate location estimations with a constriction of unknown emitter power for the single emitter case scenario. However, since the grid elements must be chosen small to obtain more accurate location estimations, this estimator requires a high number of computations. Therefore we propose an efficient RSS- based localization algorithm, referred to as **iterative grid-search** method that closely approaches the MLE method, particularly at small shadowing spread values with significantly reduced computational complexity.

- As an alternative to MLE-based grid search algorithms, we propose to apply a **Markov chain Monte Carlo (MCMC)** based technique to the emitter localization

problem. The main reason for this is, MCMC based techniques provide lower computational complexity solutions to parameter estimation problems especially when the number of parameters to be estimated is large. To the best of our knowledge, MCMC techniques have not been applied to multiple emitter localization in the literature. The major drawback of these techniques is that they require a large number of iterations to converge if the design parameters of the algorithm, such as burn-in samples and step size are not tuned in advance. To overcome this problem, we propose to initialize the algorithm with the knowledge fed-back from the interference map generated by using low-complexity interpolation techniques. Hence the smart initialization of MCMC technique we propose, eliminates tedious parameter tuning process and achieves significantly better localization performance than randomly initialized ones at a fraction of iterations.

- The grid search technique used for multiple emitter localization requires the knowledge of the pdf of the sum of log-normal distributions which does not have an exact closed form. In this work, we use the Fenton-Wilkinson approximation due to its simplicity and applicability to non-iid log-normal random variables that represent different mean received power values for each emitter sensor pair in the network. However, the estimation accuracy of this approach is low at high dB spread values. Hence we propose a new approximation where the pdf of sum of log-normals is estimated from a set of simulated data. Our proposed approach addresses the problem with the Fenton-Wilkinson approach and gives higher estimation accuracies, even at high dB spread values. This approach is our final contribution to the area of RSS based multiple emitter localization.

1.4 Thesis Organization

The outline of the thesis is as follows:

Chapter 2 provides a literature overview for interference map generation, RSS-based localization, such as maximum likelihood estimation and iterative grid search techniques, **Cramer Rao lower bound (CRLB)** for RSS-based localization and also in multiple emitter localization.

Chapter 3 explains the importance of **environmental awareness** and the use of REM in cognitive radio networks followed by a brief overview of the interpolation techniques considered in generating the interference map. The RF cartography generation techniques studied in this thesis include global interpolation techniques such as **thin-plate spline** and **Kriging interpolation** and local interpolation techniques that are based on Delaunay triangulation. Followed by the definition of the probabilistic signal model and network assumptions, a comparative performance evaluation of RF cartography generation techniques in terms RF field strength estimation and emitter localization accuracy for both single and multiple emitter case scenarios is given in this chapter.

Chapter 4 investigates the emitter localization problem in detail with the aim of improving the location estimation accuracy obtained from the generated inference map and

presents a framework that leads to a proposed approach to address the multiple emitter localization problem. Performance analysis of the existing MLE based on full grid search method is given and its performance is compared with Cramer Rao lower bound for a single emitter case. Remarking the problems with the grid search method, the chapter continues with a study of proposed MCMC based localization technique with its performance analysis. After summarizing the challenges of multiple emitter localization and the investigation into sum of log-normal random variables, the chapter concludes the study of multiple emitter localization problem by proposing a novel approach called **pdf estimation approach** from simulated sum of log-normals. The simulation results that demonstrate the performance evaluations of grid search method with the proposed approach and Fenton's approximation are also presented.

Chapter 5 explores the complexity reduction of the localization algorithms studied in the thesis. It presents different iterative grid search techniques and smart initialization of MCMC techniques with their performance analysis.

Chapter 6 concludes the thesis and points out open problems for future work in the related area.

1.5 Publications

The related publications are as follows:

S. Ureten, A. Yongacoglu and E. Petriu, A comparison of interference cartography generation techniques in cognitive radio networks in Communications (ICC), 2012 IEEE International Conference on, pages 1879-1883.

S. Ureten, A. Yongacoglu and E. Petriu, Interference map generation based on Delaunay triangulation in cognitive radio networks in Signal Processing Advances in Wireless Communications (SPAWC), 2012 IEEE 13th International Workshop on, pages 134-138.

S. Ureten, A. Yongacoglu and E. Petriu, Primary emitter localization using smartly initialized Metropolis-Hastings algorithm in Signal Processing Conference (EUSIPCO), 2013 Proceedings of the 21st European, pages 1-5.

S. Ureten, A. Yongacoglu and E. Petriu, A reduced complexity iterative grid search for RSS- based emitter localization in Communications (QBSC), 2014 27th Queens Biennial Symposium on, pages 149-152.

S. Ureten, A. Yongacoglu and E. Petriu, Iterative grid search for RSS- based emitter localization in Signal Processing Conference (EUSIPCO), 2014 22nd European Signal Processing Conference, pages 1507-1511.

Chapter 2

Literature Survey

In this chapter we review the literature on interference map generation, RSS-based geolocation algorithms and multiple emitter localization in cognitive radio networks.

2.1 Interference Map Generation

Cognitive radios (CRs) are goal-oriented and aware of their operational environment, learn from experience and adopt themselves to changing operating conditions. The radio environment map (REM) concept has been proposed to support their operations. The map itself is an integrated database that characterizes the radio environment for CRs. It represents the radio environment in multiple domains such as geographical features, available services, spectral regulations, locations and activities of radios, relevant policies and experiences. In [87], a cost-efficient approach is proposed to improve spectrum utilization in both space and time domains by using the REM-enabled CRs as secondary users. The paper also evaluates the performance of spectrum sharing wireless networks when CR uses the global REM and the local REM. In [85], it is shown that the REM can be exploited by the CRs for various cognitive functionalities such as situation awareness, reasoning, learning, planning and decision support. The authors present the system flow and framework of REM-enabled situation aware learning algorithms in the paper. In [7], a prototype of a REM for storing and reasoning about spectrum data obtained from heterogeneous sources is described and shown that information such as transmitter locations and estimates of spectrum occupancy over space and time can be obtained through the REM.

In [2], interference cartography concept is presented in secondary spectrum usage. An interference cartograph is a map that displays the level of interference over the area of interest and it can constitute one of the layers of REM. Interference cartography involves combining measurements coming from different radio network entities together with the geo-location information and applying effective spatial interpolation techniques to obtain a map which indicates interference levels at each grid point over the area of interest. Utilization of interference cartography in a secondary spectrum usage permits the secondary network to be aware of local interference tolerance levels so that it becomes possible to

detect, identify and use spectrum opportunities without disturbing the primary users or other secondary users in the network. A number of spatial interpolation techniques have been used for generating interference cartographs in the literature. In [2], Kriging is applied on spatial interference data obtained from a radio network simulator as a simple and efficient spatial interpolation method. The original interference map is obtained from partial knowledge of interference data points. Different percentage values of partial knowledge are investigated and the results demonstrate that interference cartography constitute a viable solution for efficient secondary spectrum usage. In [59], the Kriging interpolation technique is adopted to estimate the spatial power spectral density. An iterative REM building process based on Kriging interpolation is presented in [30]. The thin-plate spline interpolation technique is employed to accommodate shadow fading in spectrum cartography generation [46].

There have been many different interpolation techniques studied in the interference cartography literature. For example, the techniques used in the above reviewed papers are the global interpolation methods. The local interpolation techniques which require data only from the neighboring nodes have also been studied recently. Specifically, triangulation is a generic tool that serves as a basis for many geometry-based algorithms in wireless networks to enable local information processing. Delaunay triangulation is the one that has been frequently used for many networking tasks such as routing [12] and topology control [40]. The interpolation technique based on Delaunay triangulation is used to generate an interpolated map grid as a simple and a fast solution in the context of 802. 11 networks in [23].

One of the most challenging tasks in interference cartography through interpolation is choosing the most appropriate technique as the validity of each method depends on the type of data being interpolated. The importance of the evaluation of the relative performances of interpolation techniques has been recognized in various fields, including remote sensing [25], image reconstruction [41] and wireless sensor networks [69]. However, there is no such relative performance comparison of the interference cartography generation techniques, where the data to be interpolated are the RF field strength values. The RF field strength estimation has also been studied in radio propagation prediction literature, where the objective is to predict the field strength values in the region of interest (ROI) for a given emitter location and power information. In the context of CR networks, however, the desire is to estimate the location and power of the primary emitter in addition to estimating the field strength values at any location in the ROI using a limited number of field strength measurements. In this thesis, we provide a comparison of the performances of some common interpolation techniques studied in literature. Our goal is to provide a comparative analysis of the techniques in terms of RF field strength estimation and emitter localization for single and multiple emitter case scenarios.

2.2 RSS-based Single Emitter Localization

The literature on RSS-based primary emitter localization has been on developing efficient algorithms for accurate location estimation. An important constraint of primary emitter

localization problem is that the primary user is not cooperating and its transmission power is unknown. This limitation is critical in localizing primary users because most schemes using RSS measurements require transmission power of the RF signal. In [36], the primary emitter power and location estimation are modeled as a constrained optimization problem with a weighting factor. The proposed scheme uses the linearization technique to approximate the relationship between RSS measurements and unknown power and coordinates of the primary user to set the weighting factor that considers the differences of the quality of measurements. This approach is shown to outperform the least squares technique. In [44], a scheme is proposed to characterize the spatial size of the perceived spectrum hole in terms of the maximum permissible transmit power using signal measurements taken by a group of frequency agile radios. In [76], single source localization problem with unknown transmit power is studied by using an approach that approximates the ML problem to a convex optimization problem. The proposed approach is shown to have remarkable performance close to ML estimator. Linearizing RSS model, least squares (LS) and weighted total least squares algorithms (WTLS) are also derived for the problem in [76] and it is shown that WTLS has a better performance than LS. Another study for RSS linear estimators is reviewed in [16]. In [16], a constrained weighted least squares (CWLS) positioning approach that encompasses different measurement cases such as TDOA, AOA and RSS is presented. It is shown that CWLS location estimators can achieve the Cramer-Rao lower bound when measurement error variances are small.

In addition to the mentioned localization techniques, maximum likelihood technique is one of the most frequently used method in the literature. Among the others, ML estimation offers an attractive approach for localization problems since it is asymptotically efficient, unbiased and does not require any prior information of the transmit power [65]. In fact, it has been shown that MLE method achieves the Cramer-Rao lower bound (CRLB) at small shadow variances [80]. However, because of non-convex behavior of ML estimator, intensive computations are required to achieve its global minimum. In [55], the ML estimator and the CRLB are derived for self-localization of a network of sensors, in which a small subset of the sensors are anchor nodes at known locations. In [82], a maximum likelihood based approach is given and two numerical solutions are proposed based on simplex optimization and grid search. In my thesis, I study the grid search technique as a numerical solution to the MLE method for locating a single emitter with unknown emitter power and for locating two emitters with known and equal emitter power values. In a grid search approach, the algorithm scans all the possible grid points in the localization space. The grid point that maximizes the likelihood is selected as the location of the emitter. The size of the grid elements must be chosen small to obtain more accurate location estimates. However, smaller grid size increases the computational complexity. In order to reduce the complexity, different iterative grid search techniques are studied in the literature. For example, a variable-mesh, derivative-free optimization algorithm, namely contracting grid search method, is used to derive interaction locations in compact gamma cameras in [31]. In [34], the location of a sound source in a distributed sensor network is estimated using a grid based multi-resolution search to reduce the complexity of an exhaustive maximum likelihood estimator and a smarter multi-resolution search is proposed based on searching around the highest energy reading sensor. [56] proposes a low-complexity positioning

procedure that simply searches for the global minimum around the sensor exhibiting the smallest local maximum of the cost function and it is shown that it outperforms the naive approach that searches for the global minimum around the sensor reporting the largest signal strength. In [3], a tree search algorithm (TSA) is used to reduce the computational complexity of grid search algorithm in sensor networks assuming that the power of the transmitter to be located is known and it is shown that the performance of the TSA algorithm closely achieves the performance of least squares estimator with significantly reduced computational complexity. In my thesis, I use three different iterative grid search techniques and present their performance analysis in localizing a single emitter with the assumption of unknown emitter power. Our regular iterative algorithm sets a search space centred at the origin of the ROI and it does not rely on any sensor measurements or sensor measurement related metric in setting the initial search space. However the other two approaches rely on sensor measurements with the rational given in [34] and [56] for setting the initial search space.

2.3 Multiple Emitter Localization

Multiple emitter localization and communication footprint identification are recent topics of research. In [48], the location and average power estimation problem of two transmitting sources which is based on the measurements of the power received by sensors that are placed in known locations in a given area is studied. A technique for obtaining radio interference field estimation (RIFE) by estimating average transmit power via maximizing the likelihood function (ML criterion) in a shadow fading environment is presented. Simulated annealing technique is used for maximization. The effect of number of sensors, grid size, shadowing variance and additive noise variance on the averaged estimated power are investigated. It is shown that increasing the number of sensors beyond certain level does not result in higher estimation accuracy. The estimated power on the actual source locations is also shown to be decreasing when the shadow fading variance increases.

In [82], **blind estimation** (i.e. estimation without any prior knowledge about the transmitters location or any statistical characterization of its transmit power) of a wireless node′s transmit power based on received power measurements at multiple sensor nodes is studied. First, through geometrical analysis, it is shown that there is a fundamental limitation on uniquely estimating the unknown transmit power and location of a node for certain topologies of sensor placements even though infinite measurements are considered. In other words, regular placement of monitors in the ROI with uniform spacing does not provide sufficient measurement diversity to yield a unique estimate. Second, analytical expressions for the maximum likelihood estimator under log-normal fading model are obtained. Third, it is shown that the ML estimator is asymptotically optimal for a random topology of monitor placement, i.e. the transmit power estimate converges to the actual value as the number of sensors goes to infinity.

In [52], the number of transmitters and their transmit powers are assumed to be known, and a global optimization approach for locating multiple transmitters within a geographical area is proposed. A set of sensor nodes are assumed to be present in the region to

measure the total received power at their respective locations. These measurements are sent to a processing node, which uses particle swarm optimization to find the transmitter locations that minimize the difference between the true received power and the estimated power values at the sensor locations. Clustering is used to generate initial estimates of the transmitter locations, thereby increasing the likelihood that the particle-based optimizer reaches the global minimum. Simulation results show that global optimization is an effective method for multiple transmitter localization and that generating "smart" initial conditions via clustering improves the performance.

In [51], estimating multiple transmitter locations based on received signal measurements of randomly located receivers under log-normal shadowing with quasi expectation maximization (EM) technique is studied. Simulated performance of quasi EM algorithm is compared to random guessing and global optimization using constriction particle swarm (CPSO). Results showed that the proposed quasi EM algorithm outperforms the alternative methods, especially as the number of transmitter increases. In this work, the number of transmitters is assumed to be known and all the transmitters are assumed to have the same constant transmit power.

In [49], the number of transmitters is estimated by minimizing the sum of mean squared error (MSE) in the location and power estimates. The two main criteria are presented to determine the total number of transmitters in the primary system. The first criterion is called the net minimum mean squared error (MMSE) criterion, which uses the Cramer-Rao lower bound on localization accuracy. The second criterion is an information theoretic criterion namely minimum description length. Both of these criteria lead to measurement clustering algorithms in a natural way. Although only signal strength measurements are considered, the approach in [49] is predicted to be generalized to include other types of observations (e.g., time and angle information) with independent measurements in additive noise. The numerical results demonstrate the effectiveness of the proposed approach to measurement clustering.

In [88], an iterative multiple primary user localization algorithm which estimates the positions non-cooperatively based on k-mean clustering is proposed and its performance is compared with the traditional EM algorithm. Here, similar to [51], the number of transmitters is assumed to be known and their power values are assumed to be equal. The received signals by sensing nodes from each primary user are assumed to be uncorrelated. Authors claim that the proposed iterative method achieves better performance than the EM algorithm where the proposed iterative method has lower computational complexity than EM algorithm as the EM requires some complex matrix operations.

All of these methods are based on transmitting the RSS measurements from multiple sensors to a central node prior to location estimates. Compared to other physical layer measurements, such as the time of arrival and angle of arrival of radio signals, measuring the received power is simple in terms of both hardware and computational requirements, and thus, it is an attractive source of measurements with wide applicability for low-cost sensor systems. In the thesis, we extend our studies of grid search technique to the localization of multiple emitters by using the RSS measurements collected at multiple sensors. The MLE algorithm requires the knowledge of the pdf of the sum of log-normal random variables

that represent the portion of received power values for each emitter sensor pair in the network. However, the sum does not have an exact closed form. Therefore approximations for sum of log-normal random variables are of interest for emitter localization methods, such as MLE, EM and MCMC methods that are utilizing the RSS measurements at sensors for estimation. We have also investigated the existing sum of log-normal approximations in Section 4.2.2 and proposed a novel approach that improves the performance of our multiple emitter localization algorithm compared to the existing Fenton-Wilkinson′s [64] sum of log-normal approximation approach.

As an alternative to MLE-based grid search algorithms, we also study the **Metropolis Hastings (MH)** algorithm which is an MCMC based technique to the emitter localization problem since MCMC based techniques provide a lower computational complexity solutions to parameter estimation problems especially when the number of parameters to be estimated is large. To our best knowledge, MCMC techniques have not been applied to multiple emitter localization in the literature. Smartly initialized MH algorithms are our additional contributions to the area of RSS based emitter localization.

Chapter 3

Interference Map Generation

3.1 Radio Environmental Awareness (REA) and Radio Environment Map (REM)

Cognitive radios have been introduced as a new paradigm for increasing the efficiency of spectrum utilization, providing more reliable radio services, reducing harmful interference, and helping the cooperativeness of different wireless networks. CRs can autonomously be aware of situations and the radio environment, learn from experience, and adapt by responding to dynamic operational conditions. An essential step before applying any cognitive algorithm is to build a system's radio environmental awareness (REA). To provide CR networks with up to-date global radio environment information, the radio environment map is proposed as an abstraction from real world radio scenarios and as a vehicle of network support [86]. Ideally, REM can offer multi-domain environmental information, such as geographical features, available services, spectral regulations, locations and activities of radios, relevant policies, and experiences. To keep REM information current, updates to the REM database should be made with observations from distributed CR nodes and then distributed throughout the CR network. The REM can also be viewed as an extension to the available resource map (ARM) which has been proposed as a real-time map of all radio activities in the network for cognitive radio applications in unlicensed wide area networks. The idea behind REM is digitizing and indexing radio environment information. The more clearly the radio environment is characterized and modeled, the better the CR can learn from experience and environment. The REM can also incorporate the policy layer, application layer, optimization layer, topology, and network layer information, all of which are important to CR networks. To obtain situation awareness, CRs don't need to conduct sophisticated spectrum sensing algorithms as it maintains or has access to an up-to-date REM through the network support [86]. The REM enables CR to obtain situation awareness in a very efficient way. For example, the REM can inform the CR with what kind of radio networks could be in service at a certain location. Based upon the radio interface specifications stored in the REM database, the CR will know the possible frequency bands and modulation types used by the primary users. The CR can even obtain some prior knowledge of primary users by analyzing the historical REM data and learning from ex-

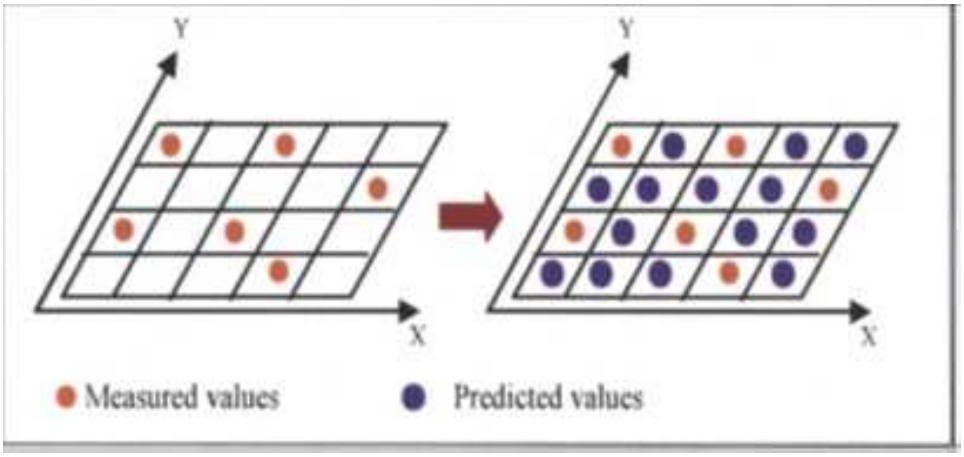

Figure 3.1: Spatial interpolation

perience. Therefore, CR can conduct primary detection with focused attention instead of spending excessive processing time performing complex spectrum sensing algorithms. This type of approach for primary user detection is very effective in CR networks. Furthermore, REM has the potential to support global cross-layer optimization by enabling CRs to look through various layers: from policy layer, application layer, optimization layer, topology layer, down to the network, MAC, and PHY layers [85].

A typical setting for building REA is to characterize the power profile over a geographical area of interest at a particular time instant. We will refer to it as **interference cartography generation**. Interference cartography combines measurements performed by different network entities (mobile terminals, base stations, access points) with the geolocation information and applies simple and effective **spatial interpolation** techniques to achieve a map which indicates the level of interference experienced at each mesh over the area of interest. Using this information, a secondary network can detect the presence of a primary network (or of other secondary networks) and can use spectrum opportunities without causing harmful interference to them.

3.2 RF Cartography Generation Techniques

Spatial interpolation [19] is a well-known procedure, commonly used in geographic information systems (GIS). GIS refers to any system manipulating geographical referenced data for capture, storage, analysis and management purposes in many application areas such as agriculture, meteorology, mining, geology, climate and urbanization. Formally, spatial interpolation is a statistical procedure that estimates missing values at unobserved locations within a given area, based on a set of available observations of a random field (see Fig.3.1).

One of the most challenging tasks in field reconstruction through interpolation is choosing the most appropriate technique as the validity of each method depends on the type of data being interpolated. The importance of the evaluation of the relative performances of interpolation techniques has been recognized in various fields, including remote sensing

[25], image reconstruction [41] and wireless sensor networks [69]. However, there is no such relative performance comparison of the interference cartography generation techniques, where the data to be interpolated are the RF field strength values. The RF field strength estimation has been studied in radio propagation prediction literature, where the objective is to predict the field strength values in an area of interest for given emitter location and power. In the context of cognitive radio networks, however, the desire is to estimate the location and power of the primary emitter in addition to estimating the field strength values in any location in the ROI using a limited number of field strength measurements.

The spatial interpolation techniques can be classified into two main categories as global and local. In local techniques only the data which fall within the given point's local neighborhood are used for calculating the interpolation values. Global techniques use a weighted sum of all data to do the interpolation.

The RF cartography generation techniques studied in this thesis include global interpolation techniques such as thin-plate spline and Kriging interpolation and local interpolation techniques that are based on Delaunay triangulation as they have been proposed as candidates of estimating RF field strength in the literature (refer to Section 2.1). In this chapter, we will give a brief overview of these techniques and study their comparative performance in terms RF field strength estimation and emitter localization for both single and multiple emitter case scenarios.

3.2.1 Global Interpolation Techniques

Thin-plate Spline Interpolation

The thin-plate spline interpolation is a global interpolation technique and a special form of radial basis function interpolation. In radial basis function interpolation, a radial basis function is centered on each input sample and the interpolated value $f(\mathbf{x})$, at any given output point $\mathbf{x}$, is calculated as a weighted sum of the contributions from each input point $\mathbf{x}_i$:

$$f(\mathbf{x}) = \sum_{i=1}^{N} w_i \phi(||\mathbf{x} - \mathbf{x}_i||), \tag{3.1}$$

where N is the number of input points, $||.||$ is the Euclidean norm, w_i is the set of weights and $\phi(.)$ is the basis function which is given by

$$\phi(r) = r^2 \ln(r) \tag{3.2}$$

for thin-plate spline. The values of weights w_i can be found by solving the linear system

$$\mathbf{A}\mathbf{w} = \mathbf{f} \tag{3.3}$$

where $\mathbf{A}$ is a matrix of evaluated basis functions for every possible input value and $\mathbf{w}$ and $\mathbf{f}$ are the column vectors of weights and input values, respectively. This interpolation

technique has higher computational complexity because of calculation of matrix **A** and and solving the linear system.

Kriging Interpolation

Kriging interpolation is also a global interpolation technique and based on empirical semivariograms obtained from the input points, i.e. measurements at sample locations. It consists of the following steps:

1. An empirical semivariogram is formed.

   Semivariogram is a graph showing the semivariance as a function of separations (distances). It indicates the degree of spatial correlation in measurements at sample locations. The semivariance is defined as:

   $$\gamma(\mathbf{h}) = 0.5\frac{1}{n(h)}\sum_{i=1}^{n(h)}(f(\mathbf{x}) - f(\mathbf{x}+\mathbf{h}))^2 \tag{3.4}$$

   where $f(\mathbf{x})$ is the point values at a given location $\mathbf{x}$ and $f(\mathbf{x}+\mathbf{h})$ is the point value separated from $\mathbf{x}$ by the distance vector $\mathbf{h}$ and $n(h)$ is the number of paired data at a distance of h.

2. A model is fitted to the empirical semivariogram to form the theoretical semivariogram such as exponential, Gaussian and spherical.

3. The interpolated output value at any given point is determined by using a weighted average of the N input points:

   $$f(\mathbf{x}) = \sum_{i=1}^{N} w_i f(\mathbf{x}_i) \tag{3.5}$$

   The weights, w_i are calculated by minimizing the kriging variance, which is the difference between the estimated and the actual variance values. Since it minimizes the variance of the output, kriging is often called the best linear unbiased estimator. However, the performance of the interpolation depends on the semivariogram model selection and the parameter N. There is a trade-off between performance and complexity. Larger N values result in better performance at the cost of increased computational complexity.

In Fig. 3.2, an empirical semivariogram obtained from RF power measurements is shown. The theoretical semivariogram used to fit the empirical data for this figure is an exponential model.

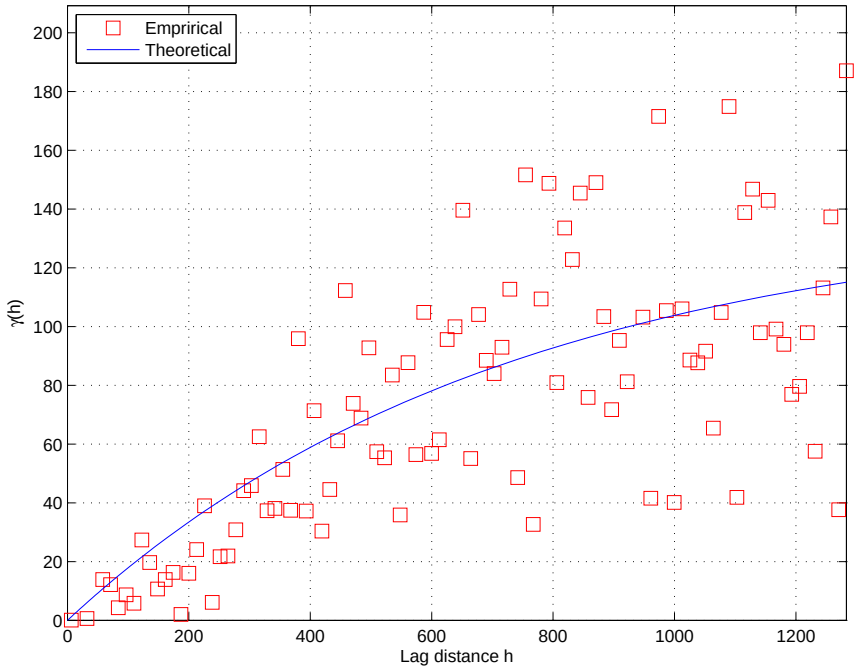

Figure 3.2: An example of empirical and theoretical semivariograms

3.2.2 Local Interpolation Techniques Based on Delaunay Triangulation

The Delaunay triangulation and its dual, the Voronoi decomposition are important data structures in computational geometry and have been used in many fields such as cartography and geostatistics. In the following sections the nearest and natural neighbor interpolations are explained by using Voronoi decomposition and the polynomial (linear, quadratic and cubic) interpolations are explained by using Delaunay triangulation for convenience.

Delaunay Triangulation

For a given set of nodes, Delaunay triangulation of the set is formed by the following steps:

1. Let P be a set of nodes in the plane and C, the convex hull of the nodes.
2. Draw straight lines (not crossing each other) from nodes on the interior to nodes on the boundary of the convex hull (or to each other), until the entire convex hull is divided into a set of polygons, with all the vertices being elements of P.
3. If any of the polygons are not triangles, divide them into triangles by drawing more lines between vertices of the polygons. This will give a triangulation of the set of nodes (see Fig. 3.3).

The Delaunay triangulation has the following properties:

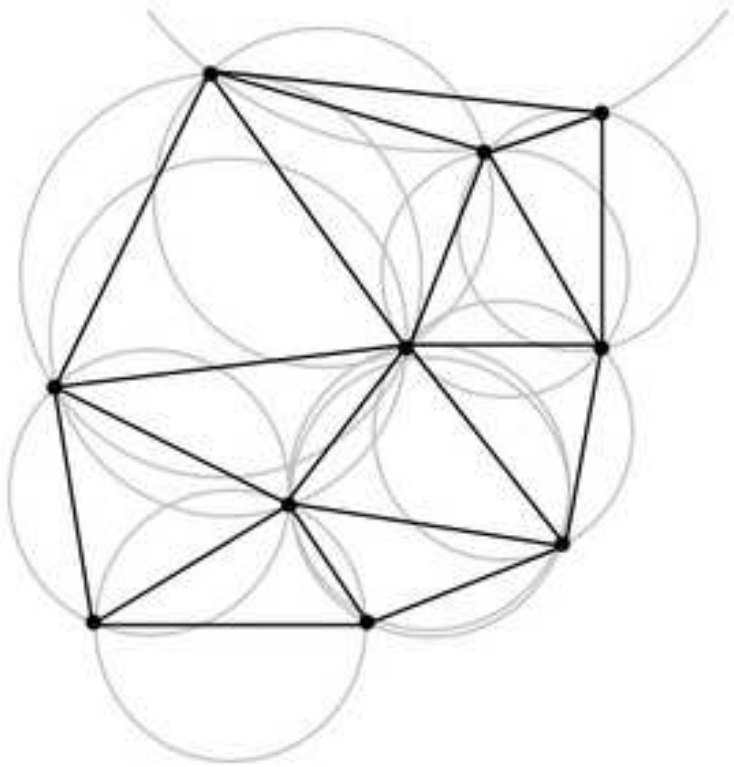

Figure 3.3: Delaunay triangulation of a set of 10 nodes with the circumcircles

1. There is no node in the set that falls in the interior of the circumcircle of any triangle in the triangulation, i.e. the circumcircle of every triangle contains no other nodes. This property is known as Delaunay condition. Triangulation that satisfy the condition is shown in Fig. 3.4 and the one that doesn't satisfy the condition is shown in Fig. 3.5.

2. Every line is also contained within some circle which contains no other nodes.

3. This triangulation maximizes the minimum angle of all the angles of the triangles in the triangulation.

4. This triangulation is unique except for when 4 or more nodes are on the same circle (e.g. the vertices of a rectangle); each of the two possible triangulations that split the quadrangle into two triangles satisfies the Delaunay condition. This can be avoided by choosing in such a way that the other nodes are outside of the circle, thus it is assumed that this case does not occur.

Sample Delaunay triangulations of random sets of 20 and 100 points on a 2D plane can be found in Fig. 3.6 and Fig. 3.7.

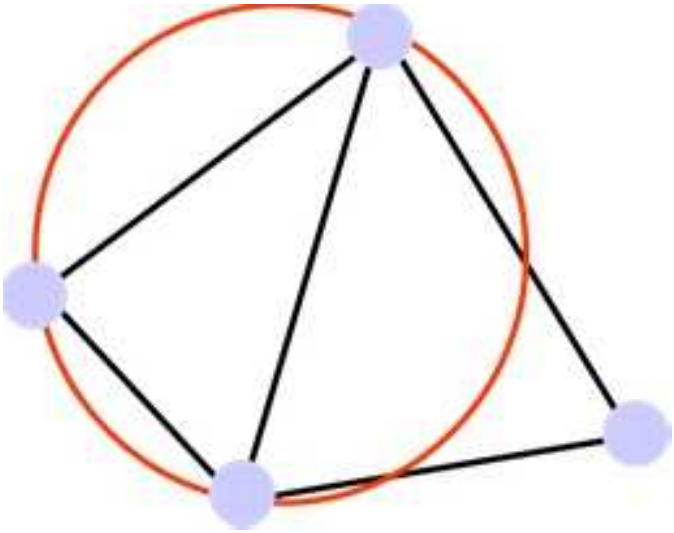

Figure 3.4: Delaunay condition of triangulations (conditions satisfied)

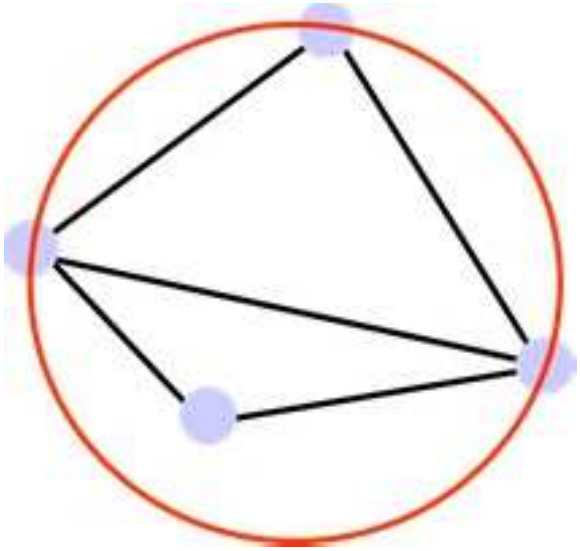

Figure 3.5: Delaunay condition of triangulations (conditions not satisfied)

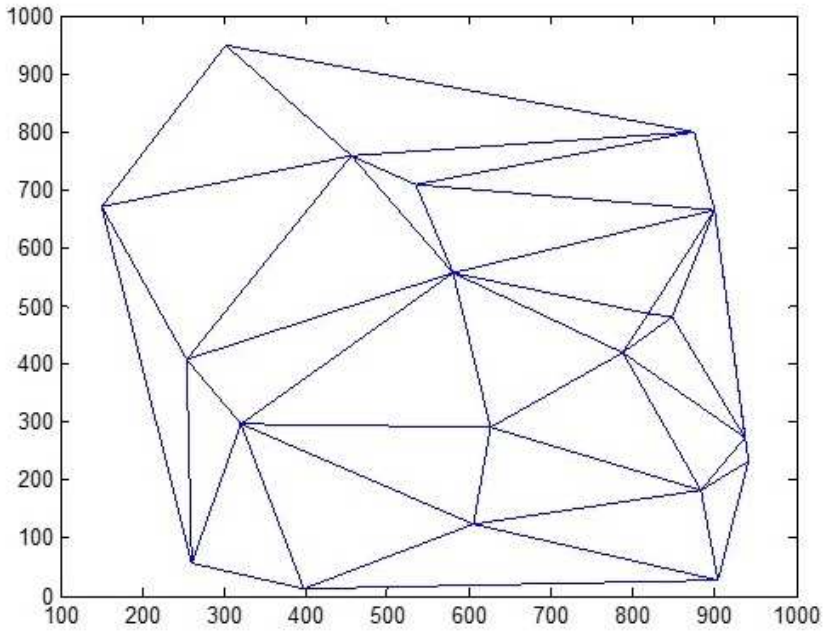

Figure 3.6: Delaunay triangulations of a random set consisting 20 points

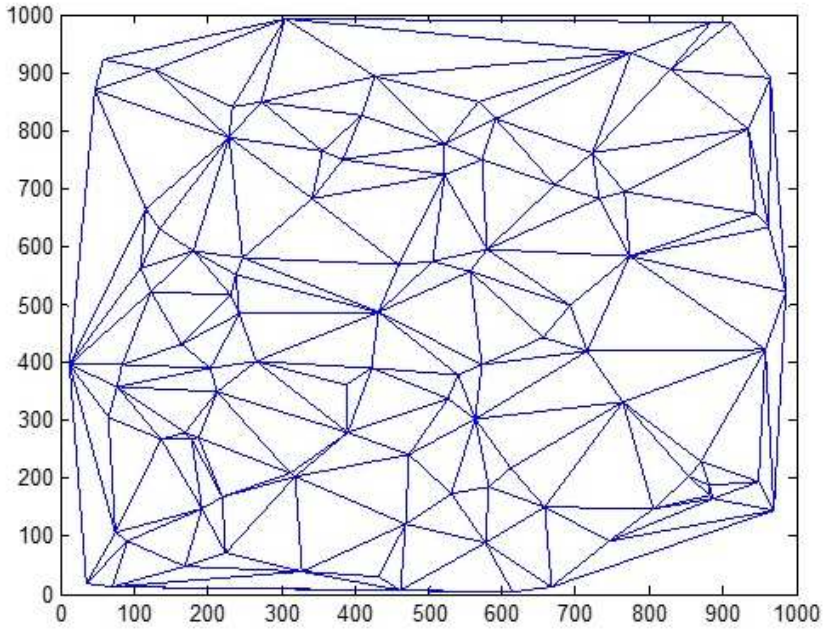

Figure 3.7: Delaunay triangulations of a random set consisting 100 points

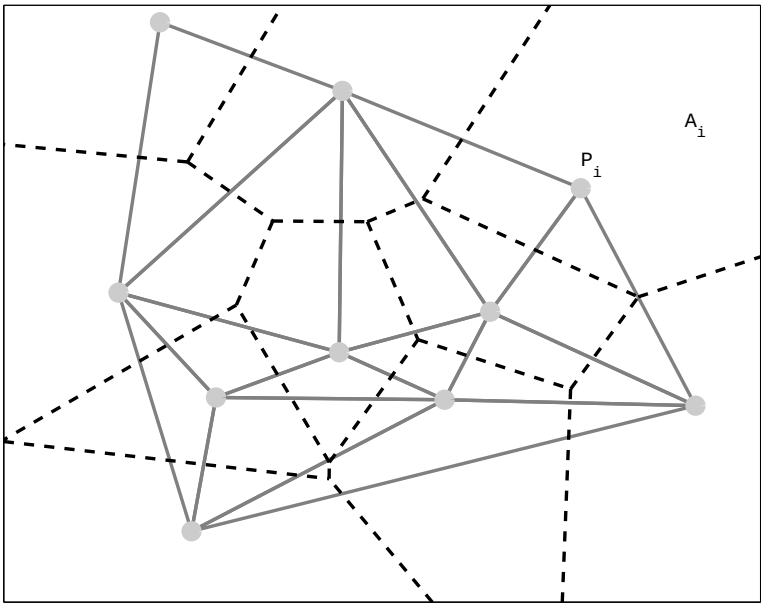

Figure 3.8: Delaunay triangulation and the corresponding Voronoi tessellation of a set of 10 points

Voronoi Decomposition

The Voronoi decomposition is the partitioning of a plane with points into convex polygons such that each polygon contains exactly one generating point and every point in a given polygon is closer to its generating point than to any other. Each node in a given set is called Voronoi sites and the decomposition generates a cell for each site. The decomposition can be obtained by connecting the centers of the circumcircles of the Delaunay triangulation. Voronoi decomposition is actually the dual representation of Delaunay triangulation.

In Fig. 3.8, an example of the Delaunay triangulation of a set of 10 points is shown with solid lines. The dashed lines show Voronoi decomposition of the same set.

Nearest Neighbor Interpolation

The nearest neighbor interpolation is straightforward once the Voronoi decomposition of the sensor set is obtained. The RSS value at the given node is assigned to all the points inside the Voronoi cell, i.e. all the points inside a cell take the value of that Voronoi site. For example, all the points inside the cell A_1 in Fig. 3.8 are assigned to the measured value of P_1.

Natural Neighbor Interpolation

The natural neighbor interpolation is another local interpolation technique based on Voronoi tessellation of a set of given points in the plane. The interpolation consists of the following steps:

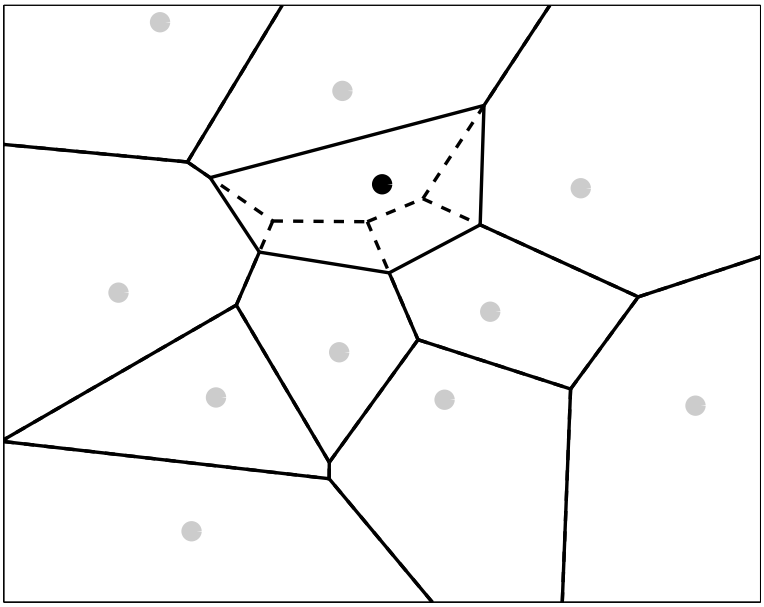

Figure 3.9: Natural neighbor interpolation using Voronoi tessellations

1. The tessellation obtained from the input points serves as a reference for the interpolation.

2. Include the output point (new point) in the input data set and retessellate the resulting set. The new point adds a new Voronoi cell which overlaps with the cells of the reference (see Fig. 3.9)

3. Calculate the interpolated output value at any point $\mathbf{x}$ by using a weighted sum of the values at its neighbors $\mathbf{x}_i$, $i = 1, .., M$ and M is the number of neighbors of $\mathbf{x}$. The weights w_i are given by the ratio of the area of overlap to the total area of the new cell.

$$f(\mathbf{x}) = \sum_{i=1}^{M} w_i f(\mathbf{x}_i) \tag{3.6}$$

In Fig. 3.9, gray circles represent measurement data locations and the dark circle is the location at which the field is to be estimated. Tessellations before and after adding new data are shown in dashed and solid lines, respectively. The areas between solid and dashed lines determine the weights of the interpolation. Note that the natural-neighbor interpolation technique requires that the points interpolated to be in the convex hull of the measurement locations as the Voronoi cells of outer data points are open-ended polygons with an infinite area.

The natural neighbor interpolation is suitable for distributed estimation as it considers information only from the neighbors in the estimation process.

Polynomial Interpolations

The polynomial interpolations we study here are based on Delaunay triangulation. After the triangulation is obtained, each node in the data set is connected to several others by triangle vertices. For a given set of triangle's nodes (f_i), e.g. f_i representing a received power level at the corresponding sensor location of (x_i, y_i), the interpolated value of any point (x, y) within the triangle is calculated by:

$$f(x,y) = \sum_{i=1}^{3} \phi_i(x,y) f_i \tag{3.7}$$

where $\phi_i(\mathbf{x})$ is the interpolating basis function that weighs the contributions of the inputs, i.e. readings of the three sensors that are located at the vertices of the Delaunay triangle. For the linear interpolation case the basis function can be replaced by a simple first order polynomial;

$$f(x,y) = c_1 x + c_2 y + c_3 \tag{3.8}$$

The coefficients $\mathbf{c} = (c_1, c_2, c_3)$ can be found by solving $\mathbf{Ac} = \mathbf{f}$ where $\mathbf{f} = (f_1, f_2, f_3)^T$ and $\mathbf{A}$ is a 3x3 matrix of rows with the form $(x_i, y_i, 1)$, where i is the row number as below.

$$A = \begin{bmatrix} x_1 & y_1 & 1 \\ x_2 & y_2 & 1 \\ x_3 & y_3 & 1 \end{bmatrix} \tag{3.9}$$

Therefore $c = fA^{-1}$

$$c = (c_1, c_2, c_3) = \begin{bmatrix} f_1 \\ f_2 \\ f_3 \end{bmatrix} \begin{bmatrix} x_1 & y_1 & 1 \\ x_2 & y_2 & 1 \\ x_3 & y_3 & 1 \end{bmatrix}^{-1} \tag{3.10}$$

For quadratic and cubic interpolation case, the basis function is a second and third order polynomials respectively. Note that higher order polynomials require larger number of inputs.

3.3 Performance Evaluations of RF Cartography Generation Techniques

3.3.1 Network and Signal Model with Assumptions

Network Model

We consider a cognitive radio network consisting of N_s secondary users deployed at known but arbitrary locations in a given geographical area. These nodes act as RF sensors that

measure the received signal strength due to the primary transmitter(s) at a given frequency and bandwidth. The secondary radios report their power measurements and location information to a fusion center through a common channel. The fusion center processes this information to estimate the interference level over the entire area so that a map of the RF field strength of the considered region can be constructed. We assume that individual sensor measurements are perfect and there is no information loss in the delivery of sensor measurements to the central node.

For simplicity, we first define the signal model for the single emitter case scenario. Additionally, the signal model for the multiple emitter case scenario is given in Section 4.2.2. The ROI is assumed to be 1 km square area with a certain constraint on the emitter and sensor geometries. For the single emitter case scenario, all sensors are assumed to be at least 50 m away from the emitter, a constraint required to guarantee that the log-distance propagation model yields realistic results [28].

Signal Model

We assume that all transmissions are omnidirectional and the signal propagation is governed by a distance dependent path loss model such that the noise-free received power at the jth receiver, j = 1, 2,. . . ,N_s from the primary transmitter is given by

$$s_j = \frac{\beta P_t}{(d_j)^\alpha} \tag{3.11}$$

where P_t is the emitter power, β is a constant that reflects the carrier frequency and antenna properties given by $\beta = (\frac{\lambda}{4\pi})^2$, λ is the wavelength, α is the path-loss exponent and d_j is the distance between sensor j and the primary emitter located at $\boldsymbol{\theta} = (T_x, T_y)$.

We assume that each sensor experiences log-normal shadowing. If the fast fading effects are sufficiently averaged then the resulting unknown measured power from the emitter to the jth sensor is given by

$$r_j = s_j 10^{\frac{W}{10}} \tag{3.12}$$

where $W \sim \mathcal{N}(0, \sigma^2)$ is the gain/loss in dB due to shadowing and σ is called the shadowing spread. The received power at a distance from the emitter is a log-normal random variable with mean s_j and variance σ^2 and its pdf is given by

$$p(r_j; s_j, \sigma) = \frac{1}{\sigma\sqrt{2\pi}\epsilon r_j} \exp\left(-\frac{(10log_{10}r_j - 10log_{10}s_j)^2}{2\sigma^2}\right) \tag{3.13}$$

where $\epsilon = \frac{ln10}{10}$.

3.3.2 Performance Evaluations for RF Field Strength Estimation

In this section we compare the RF field strength estimation performances of the interpolation techniques commonly used in the generation of interference cartographs. Obtaining

field strength estimates is important, specifically in setting the acceptable transmit power for secondary users.

We consider a simulated CR network and a propagation model as described in Section 3.3.1. Sensors are randomly deployed at locations on a planar square of length 1 km with the given emitter and sensor geometry restriction above. A path-loss exponent of 3 is assumed. The shadowing values depend on the terrain structure and they show a spatial correlation as terrain structures do not show fast spatial changes in real environments. Random shadow fading is generated from log-normal distribution with given spread at points separated by the decorrelation distance d_{corr}, which is the distance at which shadow fading becomes independent. The correlated shadow fading values in between independent locations are then computed by applying spline interpolation [24]. A sample figure that shows the shadow loss of a 1km by 1km area, generated at a shadowing spread of 6 dB with a decorrelation distance of 50 m is illustrated in Fig. 3.10. In this figure, the correlated shadow values between indepedent points at which random shadow fading is generated, are calculated for each 1m by 1m grid points and the calcaluted values are transformed into a colored image. Simulated received RF strength values at given sensor locations are used to obtain the interpolant function for any given interpolation method. After the area is divided into grids, the RF field strength at each tile center is interpolated by using the given interpolant function. Hence an interference map is generated over the area of interest. For our simulations, the grid size is taken as 100 m by 100 m. It should be noted that, the grid is used only to determine the points at which the the RF strength values will be estimated and not utilized in calculating the interpolants. Hence a quantization error due to grid size is not a concern for our estimations with any of the interpolation techniques unlike the grid search method described in Section 4.1.2.

Assuming that only one primary user is active with 1 W emitter power at any given time, performance evaluations of the interpolation techniques are studied in two categories; first performances of global methods are compared with a local method's performance, second the performances of local methods based on Delaunay triangulation are compared within each other. Note that, the knowledge of the propagation model and/or any parameter related with the environment such as path-loss exponent, shadowing spread or emitter power are not taken into account for any of the interpolation methods since these techniques do not use this knowledge that may be available and they require only the measured received power values at sensors and their locations to make estimations.

Global and Local Interpolation Techniques:

Sensor measurements are simulated based on the correlated shadowing model and given sensor and primary emitter locations. The simulations are performed for networks with 100 nodes. A number of sensors are selected randomly among all sensors and their measurements are used to calculate the interpolant functions. The RF strength values at the remaining nodes are then estimated based on the interpolants using a local that is natural neighbor and global interpolation techniques that are thin-plate spline and kriging interpolation techniques. Note that output sites that are outside the convex hull of the input sites are excluded in performance evaluations, as these techniques cannot extrapolate outside

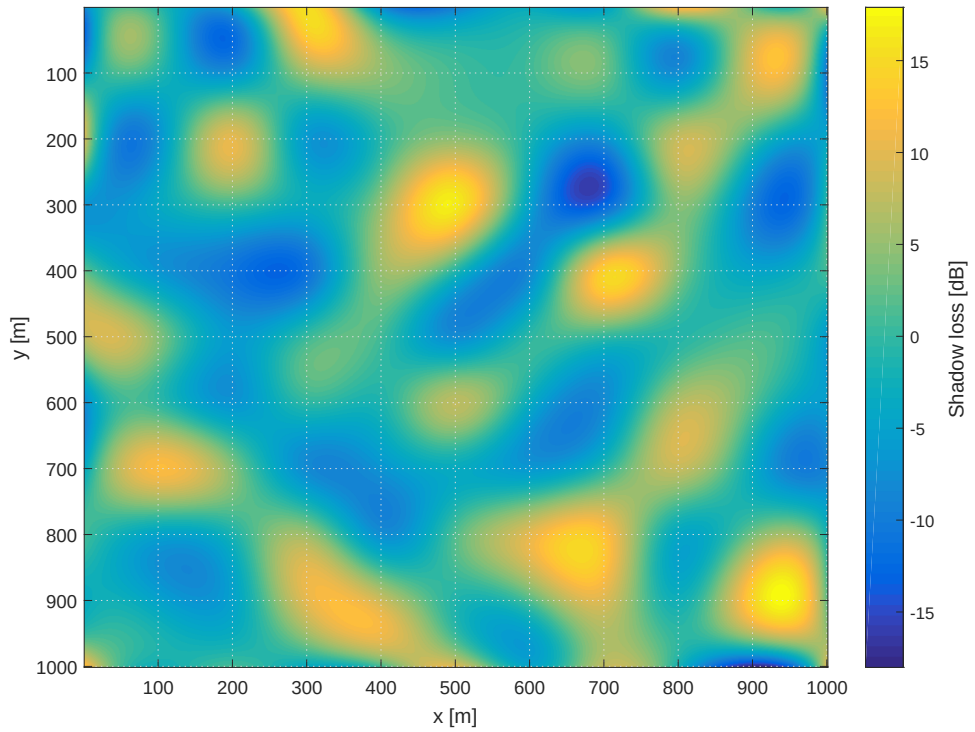

Figure 3.10: Example of two-dimensional shadow fading map with spline interpolated (correlated) shadow fading variables for $\sigma = 6$ dB, $\alpha = 3$, L = 1 km, $d_{corr} = 50$ m

the convex hull of the input sites. An example simulation of sensor placements can be seen in Fig. 3.11. In this figure 20 sensors (input sites) shown with red circles are used to estimate the location of remaining 80 sensors (output sites) shown with blue crosses. The large red polygon that surrounds the input sites, shows the convex hull in which the output sites can be interpolated as the Voronoi cells of outer data points are open-ended polygons with an infinite area. The Voroni tesselation of input sites and their convex hull is also illustrated in Fig. 3.12. The difference between the estimated and simulated RF strength values in dB determine the estimation error, E. We define the efficiency, η is defined as the probability that the RMS value of the RF power estimation error, E_{rms} is less than the dB spread of the shadowing, σ;

$$\eta = Pr(E_{rms} < \sigma) \tag{3.14}$$

Sensor measurements simulated at 20 nodes are used to estimate the RF strength values at the remaining 80 nodes using the three interpolation techniques. The efficiency is calculated for 10000 Monte Carlo simulations for dB spread values ranging from 1 to 10 dB at 1 dB intervals and decorrelation distances of 50 to 500 m at 50 m intervals. Fig. 3.13 shows the efficiency results averaged over the shadowing spread values as a function of decorrelation distance. As can be seen from the figure, average efficiency of all interpolation techniques improves with increased shadowing decorrelation. The performance difference between the interpolation methods is negligible when the decorrelation distance is higher than 250m.

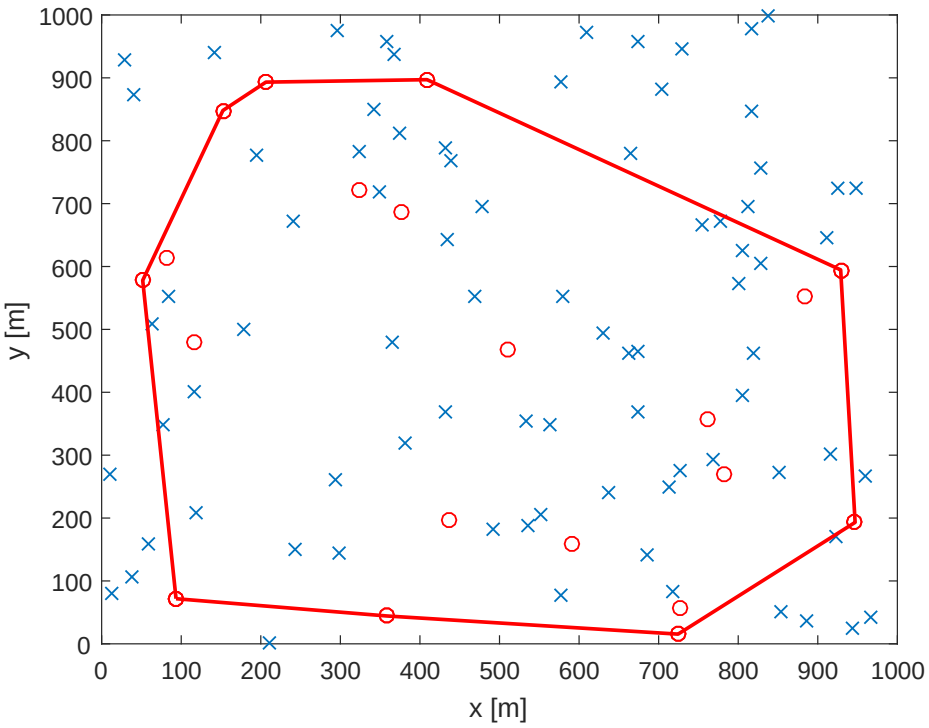

Figure 3.11: A simulation example: RF field strength estimation at output sites using input sites ($N_s = 100, N_{selected} = 20$)

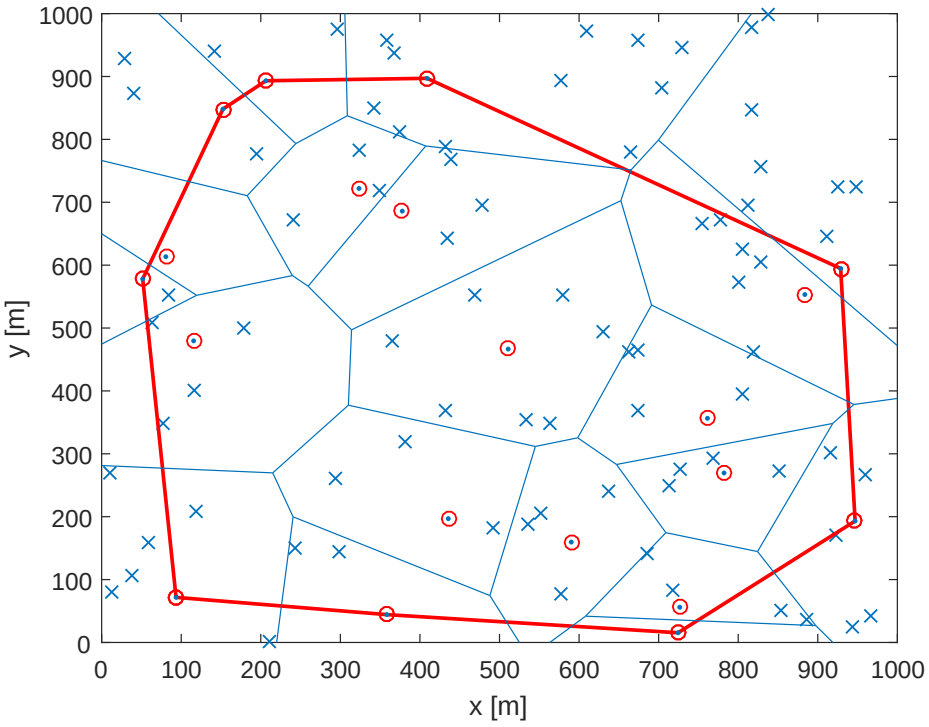

Figure 3.12: Voronoi tesselation and convex hull of input sites ($N_s = 100, N_{selected} = 20$)

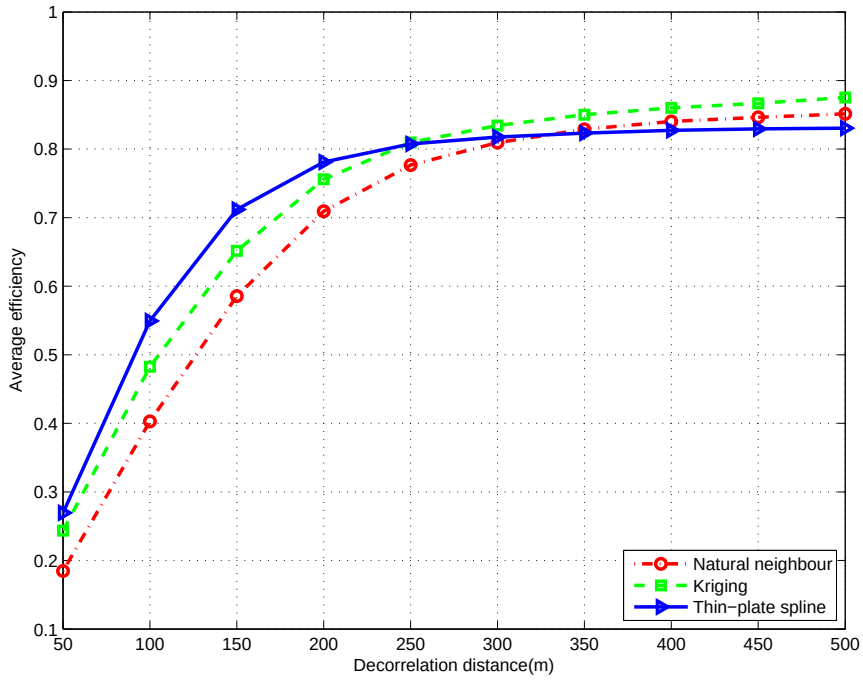

Figure 3.13: Average efficiency of the RF field strength estimates in correlated shadowing for estimating the RF power values at 80 nodes by using the RF power values at 20 nodes ($N_t = 1$, $N_s = 100$, $N_{selected} = 20$, $\alpha = 3$, $P_t = 1$ W, $L = 1$ km, grid size = 100m by 100m)

The effect of number of interpolation points to the efficiency of the RF power estimates is also evaluated by varying the number of nodes. In the simulations the number of nodes is ranging from 10 to 40. Shadowing spread and decorrelation distance are set to 6 dB and 250 m respectively. The calculated efficiencies are shown in Fig. 3.14. As seen from the figure, the efficiency of the thin-plate spline interpolation is better than the other techniques, however the performance gap becomes negligible as the number of sensors increase.

The thin-plate spline interpolation outperforms the other two interpolation techniques in terms of RF field strength estimation. Note that the kriging and thin-plate spline methods are both global interpolation techniques which require a central node to process the information from individual nodes, but natural neighbor interpolation is a local technique.

On the other hand, local interpolation techniques such as natural neighbor interpolation, require information only from the neighboring nodes; thus a central fusion node is not required. This characteristic may provide desirable features such as robustness and better adaptation to local changes, for example due to mobility in CRNs. For this reason local interpolation techniques are suitable for distributed estimation. Particularly, in the context of ad hoc networks where the nodes can form into a network without an infrastructure, it is more efficient to perform local computations rather than implementing network wide updates.

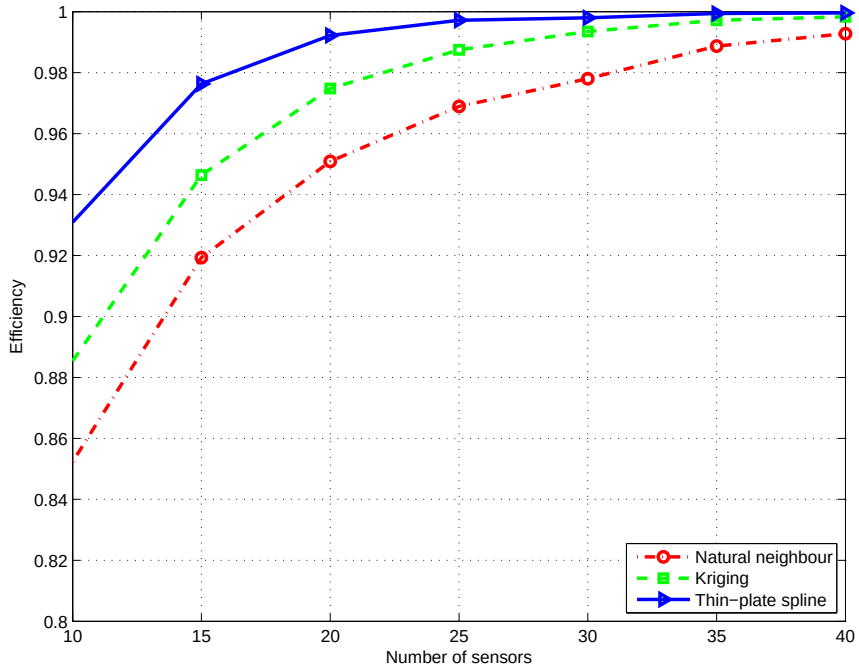

Figure 3.14: Efficiency of the RF field strength estimates in correlated shadowing as a function of number of sensors ($\sigma = 6$ dB, $d_{corr} = 250$ m, $N_t = 1$, $N_s = 100$, $N_{selected} = 10 - 40$, $\alpha = 3$, $P_t = 1$ W, $L = 1$ km, grid size = 100 m by 100 m)

Delaunay Based Interpolation Techniques:

In this section we compare the performances of the local interpolation techniques based on Delaunay triangulation in generating interference cartographs. These are nearest neighbor, natural neighbor, linear, quadratic and cubic interpolation techniques.

Here we consider an ad hoc network consisting of secondary users (nodes) deployed at known but arbitrary locations in a given geographical area as described in Section 3.3.1. We assume that the nodes discovering their one-hop neighbors are triangulated for networking tasks such as routing [12] or topology control [40], and our aim is to utilize the existing triangulation for interference map generation in order to avoid complex computations while generating the interference map. Each node measures the local RSS due to the primary emitter at a given frequency and sends the information to its one-hop neighbors. The nodes process RSS measurements using the Delaunay triangulation to estimate the field strength values by local interpolation techniques.

Sensor measurements simulated at 20 randomly selected nodes are used to find the interpolant functions and then estimation of the RF strength values at the remaining 80 nodes are done based on the calculated interpolants using the five interpolation techniques. The efficiency was calculated over 10000 Monte Carlo simulations for dB spread value of 6 dB and decorrelation distances of 50 to 250 m at 50 m intervals. Fig. 3.15 shows the field strength estimation efficiency results averaged over the shadowing spread values as a function of decorrelation distance. As seen from this figure, average efficiency of all in-

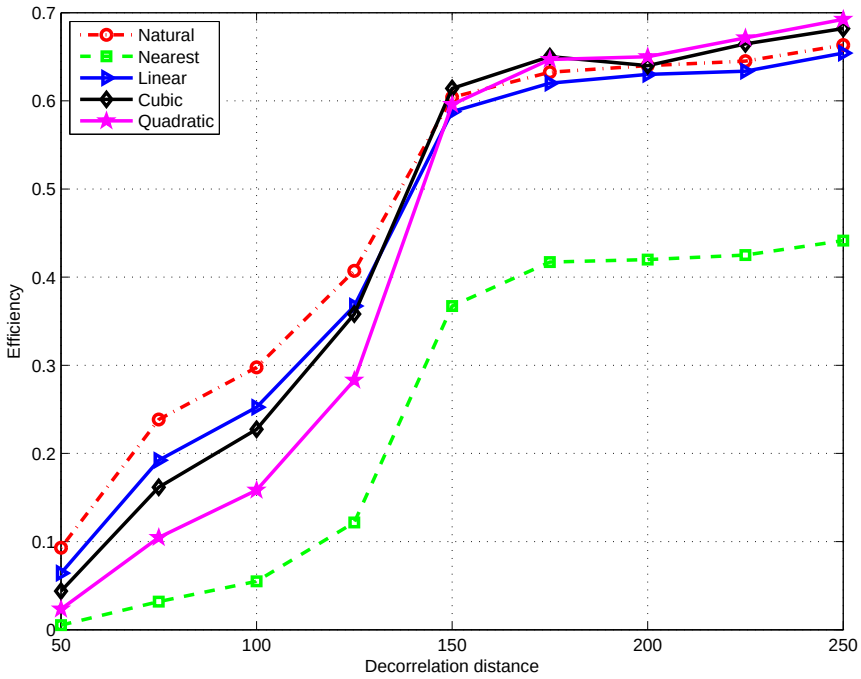

Figure 3.15: Efficiency of RSS estimates in correlated shadowing as a function of decorrelation distance ($N_t = 1$, $N_s = 100$, $N_{selected} = 20$, $\alpha = 3$, $\sigma = 6$ dB, $P_t = 1$ W, $L = 1$ km, grid size = 100m by 100m)

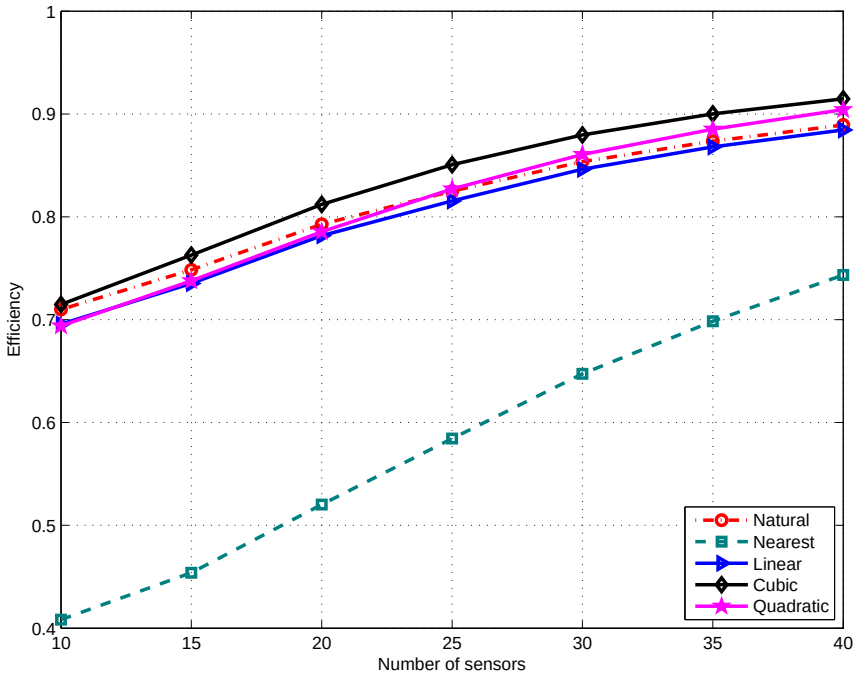

Figure 3.16: Efficiency of RSS estimates in correlated shadowing as a function of number of sensors($\sigma = 6$ dB, $d_{corr} = 250$ m, $N_t = 1$, $N_s = 100$, $N_{selected} = 10 - 40$, $\alpha = 3$, $P_t = 1$ W, $L = 1$ km, grid size = 100 m by 100 m)

terpolation techniques improves with increased shadowing decorrelation. The performance differences between the interpolation methods are negligible except for the nearest neighbor interpolation that performs poorly. The effect of number of interpolation points to the efficiency of the RF power estimates is also shown in Fig. 3.16 as simulations are repeated by varying the number of nodes ranging from 10 to 40. In all simulations, shadowing spread and decorrelation distance are set to 6 dB and 250 m respectively. As seen from the figure, the efficiency of nearest neighbor interpolation is worse than any of the other techniques that have comparable performances.

As a result, among the five considered techniques above, nearest neighbor interpolation is the least complex method, however its performance is the worst. Since all the other techniques based on Delaunay triangulation have comparable performances, linear interpolation would be better than the other RSS interpolation techniques to use because of its less complexity.

3.4 Emitter Localization Using the Generated Radio Environment Map

An interference cartograph provides field strength values at any desired location in the area and emitter location can be estimated simply by selecting the peak location of the field. Even though this estimator has lower accuracy compared to the ML estimator, the achieved accuracy level may be enough for applications where a high level of accuracy is not required. Besides, rough estimates obtained from the interference cartograph can be used to initialize more accurate localization algorithms to reduce their computational complexity or to improve estimation accuracy. (Refer to Section 5.2)

In our simulations in Section 3.3.2, the emitter's location is estimated at the center of the tile that contains the peak value of the interpolated RF field strength in the given area. Performance evaluations of the interpolation techniques are also presented in terms of primary emitter localization accuracy. We define localization error as the difference between estimated and the actual transmitter location and calculate the root mean squared error (RMSE) of localization for each interpolation technique by averaging the simulations.

3.4.1 Single Emitter Case

Performance Comparison of Global and Local Interpolation Techniques:

Assuming that one primary emitter is active with 1 W emitter power at any given time, simulations have been run for dB spread values ranging from 1 to 10 dB at 1 dB intervals for independent shadow fading case and the number of sensors ranging from 5 to 30. Fig. 3.17 shows the RMSE performance versus shadowing spread for networks of 10 sensors and Fig. 3.18 displays the RMSE performance versus number of sensors for shadowing spread of 6 dB. As seen from these figures, both kriging and natural-neighbor interpolations perform

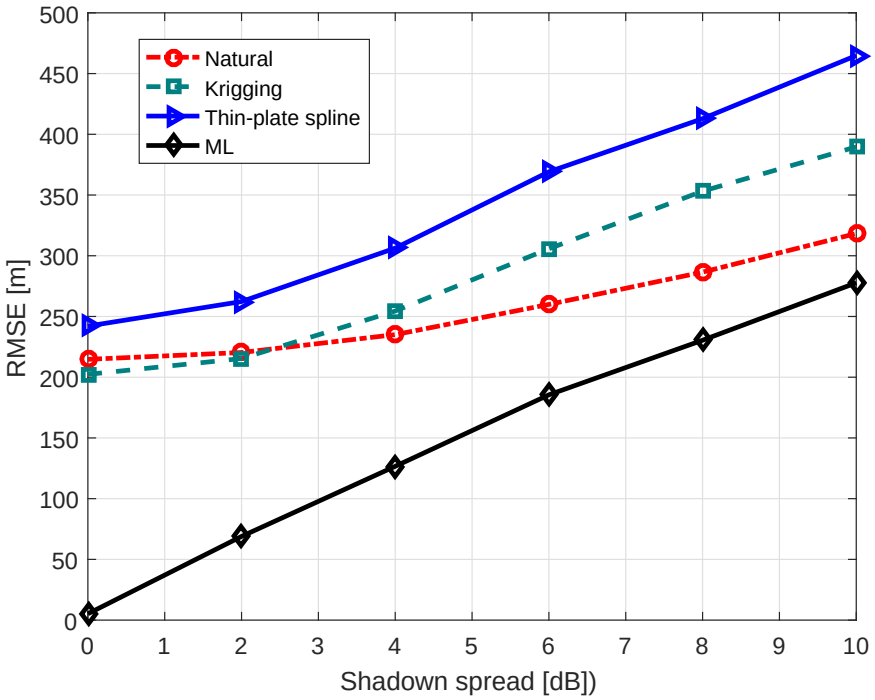

Figure 3.17: Localization errors of cartography generation techniques at different shadowing spread values with uncorrelated shadowing ($N_t = 1$, $N_s = 10$, $\alpha = 3$, $P_t = 1$ W, $L = 1$ km, grid size for ML = 10 m by 10 m)

similarly when the channel and/or measurement uncertainty is lower. When the channel and/or measurement uncertainty increase, natural-neighbor interpolation technique outperforms the kriging in terms of primary emitter localization performance.

For a baseline comparison for emitter localization, the performance of the ML estimator based on grid search is also included in Fig. 3.17 and 3.18. The ML estimator is derived based on the assumption that the received signal strength values are independently distributed, each having a log-normal density. The likelihood of receiving sensor measurements is calculated for each tile on a regular grid and the center of the tile that gives the maximum likelihood value is selected as an estimate of the emitter location. To implement the ML method, we divided the one square kilometer simulation region into 10 m by 10 m square tiles for which the likelihood values are calculated. As seen from the figures, the ML estimator based on grid search provides more accurate primary emitter location estimates than the three interpolation techniques. It should be noted that, the RMSE error of ML estimate at zero shadow spread is 5 m. However, it requires the knowledge of the propagation model and the path-loss exponent. Furthermore, it is computationally more complex as it requires the calculation of the likelihood function for each tile in the grid.

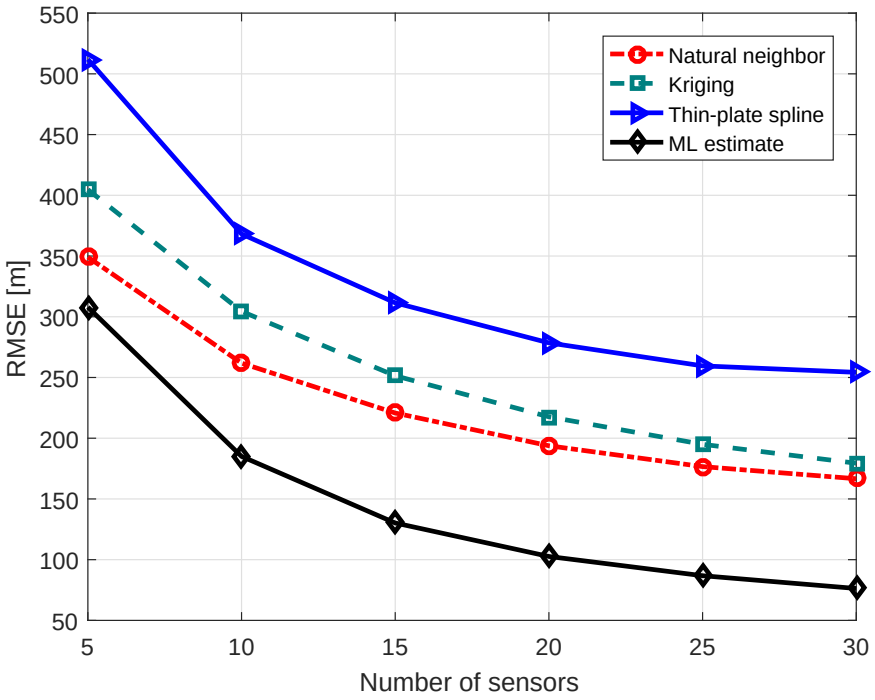

Figure 3.18: Localization errors of cartography generation techniques as a function of number of sensors with uncorrelated shadowing ($\sigma = 6$ dB, $N_t = 1$, $N_s = 100$, $\alpha = 3$, $P_t = 1$ W, $L = 1$ km, grid size for ML = 10 m by 10 m)

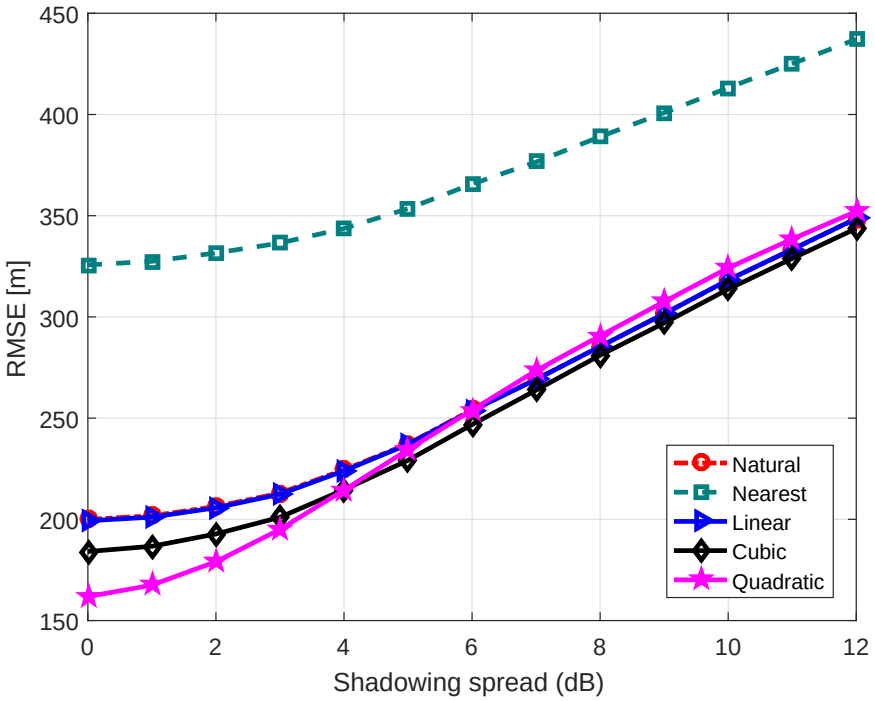

Figure 3.19: Comparison of localization errors at different shadowing spread values for 10 sensors ($N_t = 1$, $N_s = 10$, $\alpha = 3$, $P_t = 1$ W, $L = 1$ km, grid size = 100 m by 100 m)

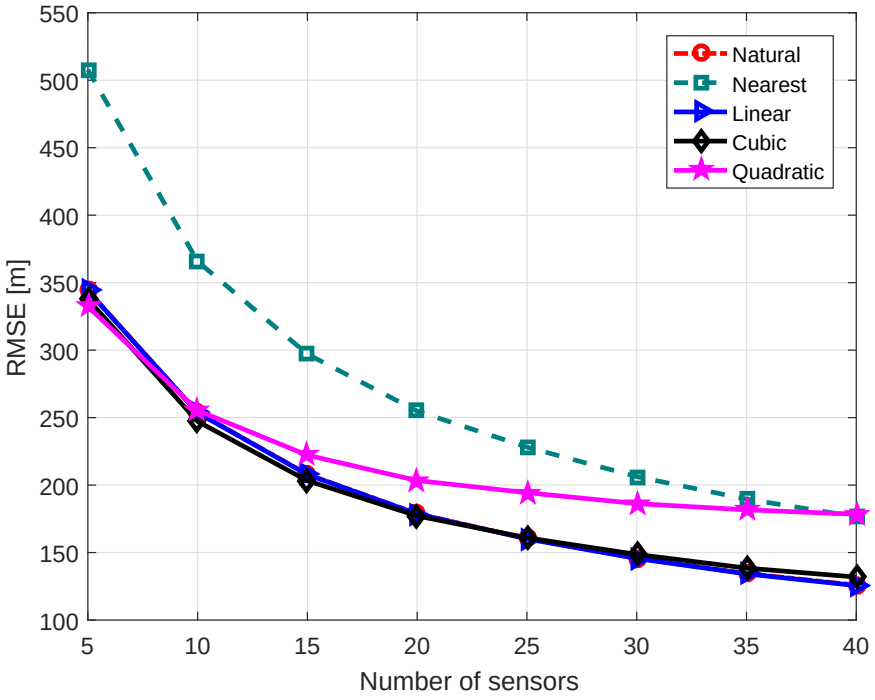

Figure 3.20: Comparison of localization errors as a function of number of sensors ($\sigma = 6$ dB, $N_t = 1$, $\alpha = 3$, $P_t = 1$ W, $L = 1$ km, grid size = 100 m by 100 m)

Performance Comparison of Delaunay Based Interpolation Techniques:

Simulations have been run for dB spread values ranging from 1 to 12 dB at 1 dB intervals and the number of sensors ranging from 5 to 40. Figure 3.19 displays the RMSE performance against shadowing spread for networks of 10 sensors and Fig. 3.20 shows the RMSE performance versus number of sensors in a channel with shadowing spread of 6 dB. As seen from the figures, the localization performances of all interpolation techniques degrade as the shadowing spread increases. Increasing the number of sensors improves the localization performance. In these figures, the RMSE values of natural neighbor and linear interpolation are the same, therefore their curves overlap. Nearest neighbor interpolation has the worst performance among the others. All the other techniques have comparable performances.

3.4.2 Multiple Emitter Case

In the above simulations, we have studied the RF cartography generation techniques with the assumption that one active primary emitter exists in the network. When there are more than one primary emitters, all transmitting at the same time, the localization becomes quite challenging since there will be more than one peak of the RF field strength values to find in the reconstructed interference map. In this section we study the RF cartography generation techniques that are based on Delaunay triangulation for multiple emitter case. We first reconstruct the interference map from the simulated RF field strength measurements at

sensor locations and estimate the locations of emitters from the reconstructed map. Note that we assume all active primary transmitters are randomly located and all have equal transmit power value of 1 W with a certain constraint on the emitter and sensor geometries. The constraints and the selection of the value of other network parameters are justified in Section 4.2.5 considering a microcellular network with a cluster size of 3 and cell size of 100 m in detail. The first constraint is that the emitters are assumed to be seperated by at least 300 m, reflecting the physical reality that of primary transmitters using the same frequency band would interfere if they were too close together. The second constraint is, all sensors are assumed to be at least twice the reference distance (assumed to be 1 m for our simulations) from all emitters. This is a constraint required to guarantee that the log-distance propagation model yields realistic results [28] and taken as 10 m. The minimum distance between sensors is also assumed to be 10 m. The number of active emitters at a time is also assumed to be known which sets the number of peaks to be found in the reconstructed map. When a peak is found, no other peak with a position within a 300 m by 300 m square area centered at the first peak is detected. Peaks are found sequentially; for example, after the highest peak has been found, the second is found at the largest value in the estimated RF strength values excepting the first found peak. A detailed explanation of finding the number of the peaks and the location of the peaks of a 2D array can be found in [68].

In our simulations, a network of 100 randomly located sensors with a path-loss exponent of 3 in a 1 km by 1 km area is considered. Simulated RF field strength values at the sensors are used to estimate the field strength values on a 10 m by 10 m grid using a particular interpolation technique. We have run the simulations for 3, 4 or 5 emitters being active in the network under different shadowing spread values ranging from 0 to 6 dB with nearest neighbor, natural neighbor and linear interpolation methods. Examples of simulation results are illustrated in Fig. 3.21 through Fig. 3.23. Samples of the constructed cartographs with nearest interpolation method for 5 emitters under 4 dB of shadowing spread is shown in Fig. 3.21. Similarly, maps constructed with natural neighbor and linear interpolation methods for 5 emitters with 4dB shadowing spread values are shown in Fig. 3.22 and Fig. 3.23 respectively. In these figures, the interpolated RF field strength measurements are transformed into a colored image where the lowest field strength is mapped into a blue and the highest strength is mapped into a yellow color. The color bar on the right side shows the power levels between -35 and -70 dBm. The red circles represent the actual locations of emitters that are randomly generated and the blue rectangles represent their estimated locations. Ideally, the estimated emitter locations would lie on the yellow colored regions as the estimates are done at the center of the tile that contains the peak value of the interpolated RF field strength in the given area.

Although the estimated emitter locations were quite close to the actual locations on the illustrated simulation results, there are some occasions where peaks might be missed and estimates might fall further away from the peaks yielding in high location estimation errors. An example is illustrated in Fig. 3.24 for estimating the locations of 5 emitters by using the measurements of 30 sensors placed randomly in the area with natural neighbor interpolation. Simulated field strength values at the sensors are used to estimate the field strength values on a 10 m by 10 m grid using natural interpolation technique for a dB

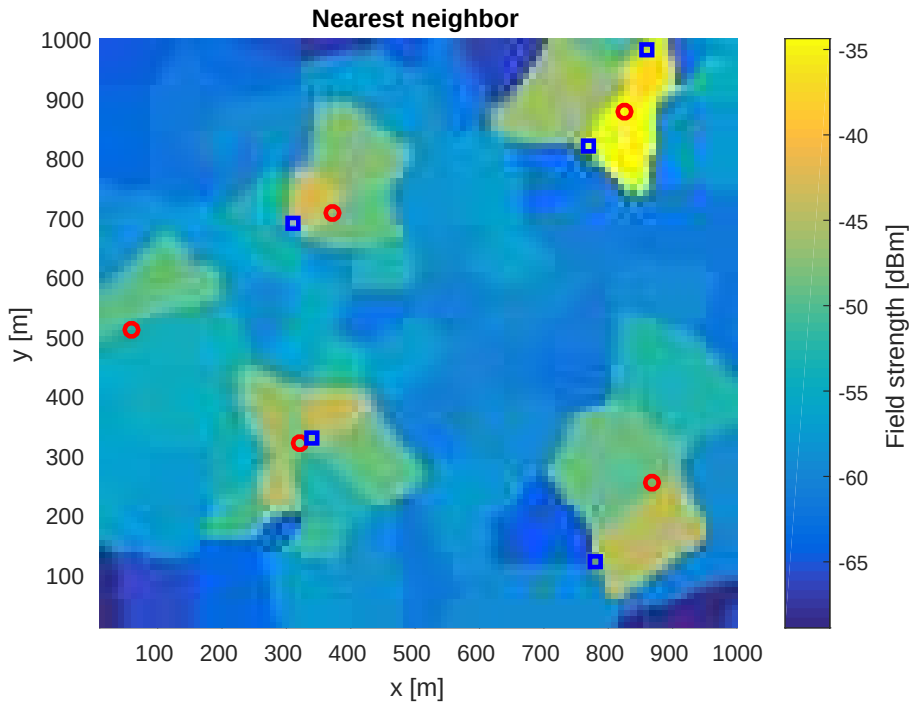

Figure 3.21: Nearest neighbor interpolation with multiple emitters ($N_t = 5$, $N_s = 100$, $\sigma = 4$ dB, $\alpha = 3$, $P_t = 1$ W, $L = 1$ km, grid size = 10 m by 10 m, red circles and blue rectangles are actual and estimated emitter locations, respectively)

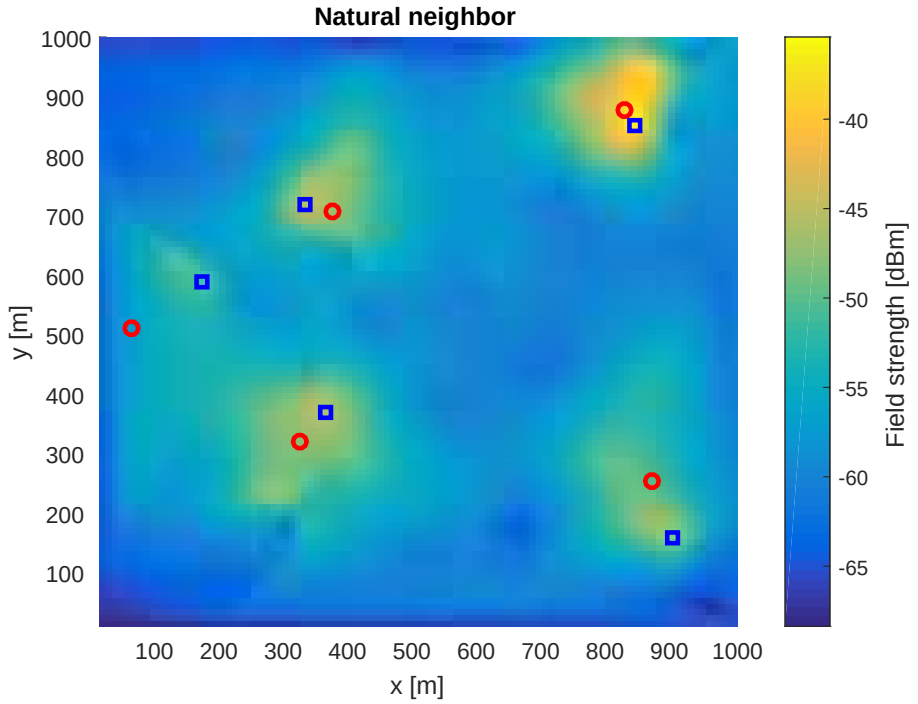

Figure 3.22: Natural neighbor interpolation with multiple emitters ($N_t = 5$, $N_s = 100$, $\sigma = 4$ dB, $\alpha = 3$, $P_t = 1$ W, $L = 1$ km, grid size = 10 m by 10 m, red circles and blue rectangles are actual and estimated emitter locations, respectively)

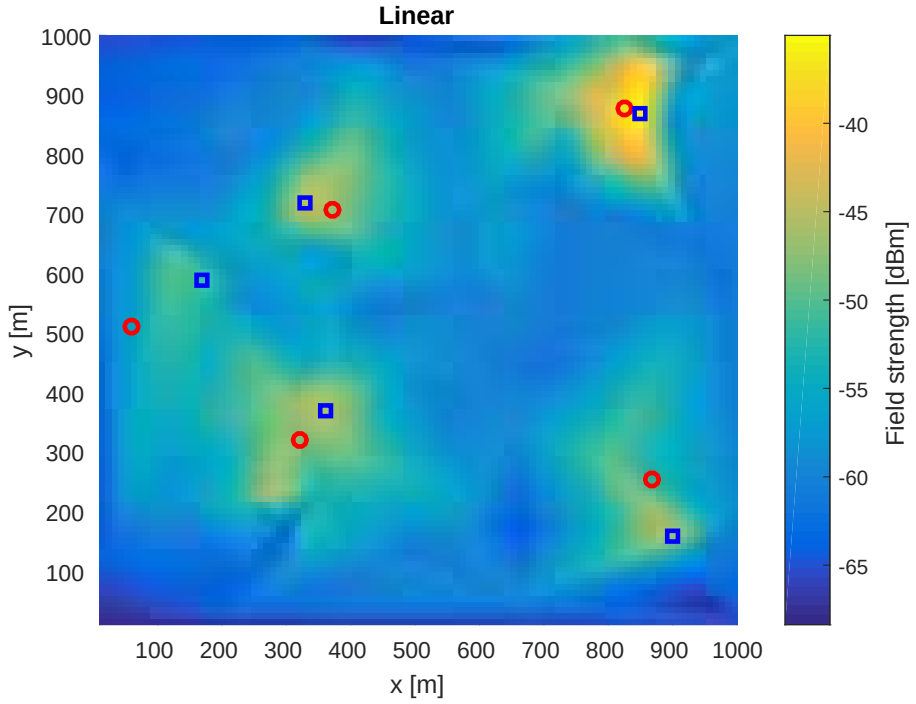

Figure 3.23: Linear interpolation with multiple emitters ($N_t = 5$, $N_s = 100$, $\sigma = 4$ dB, $\alpha = 3$, $P_t = 1$ W, $L = 1$ km, grid size = 10 m by 10 m, red circles and blue rectangles are actual and estimated emitter locations, respectively)

spread of 4 and a path-loss exponent of 3 within a 1 km by 1 km area. In the figure, the sensor locations are shown with red crosses. Idealy, we expect to see five peaks (estimates) near the actual emitter locations. However, findings for this particular example is quite different. As can be seen from the figure, the four estimates are near the actual locations, but the estimate of the emitter which is at the top right corner with the coordinates (950, 1000) is found to be further away from its actual location causing an high estimation error. This is due to the lack of sensors around that emitter whereas the other four emitters are surrounded by enough number of sensors. At this point, we can conclude that not only the number of sensors affects the estimation accuracy, but also the emitter-sensor geometry has an impact on the estimation performance. We discuss this issue in detail in the next chapter in Section 4.1.1.

A comparison of RF field strength estimation performances of the interpolation techniques for multiple emitter cartography generation is also studied. We consider a network of 200 randomly located sensors with a path-loss exponent of 2.5 in a 1 km by 1 km area. In order to analyze the error in estimating the RF field strength in an area of interest, 100 received power measurements at the sensors (input sites) that are randomly selected among the simulated measurements are used to obtain the Delaunay triangulation which forms the interpolant function. The field strength values at the remaining sensor locations (output sites) are then estimated based on the calculated interpolants using nearest neighbour, natural neighbor and linear interpolation techniques based on Delaunay triangulations. Note that the output sites that are outside the convex hull of the input sites are

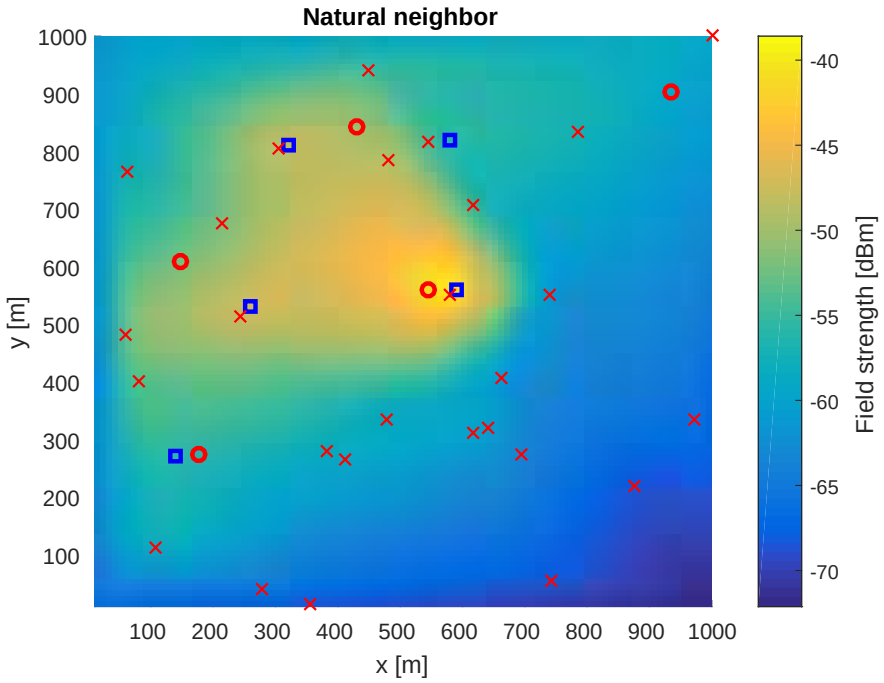

Figure 3.24: Natural neighbor interpolation with high estimation error ($N_t = 5$, $N_s = 30$, $\sigma = 4$ dB, $\alpha = 3$, $P_t = 1$ W, $L = 1$ km, grid size= 10 m by 10 m, red crosses are sensor locations, red circles and blue rectangles are actual and estimated emitter locations, respectively)

excluded in the performance evaluations, as these techniques cannot extrapolate outside the convex hull of the input sites. An example of a Delaunay triangulation formed with 100 randomly selected sensors among 200 randomly located ones in a square region of 1 km by 1 km can be seen in Fig. 3.25. In this figure, the power levels of sensors whose locations are shown with blue circles are used to estimate the power levels of the sensors with the locations shown in red. Four of the sensors are placed at the corners of the square region such that all sensors lie within the convex hull of the triangulation. Therefore each and every sensor measurement is included in performance evaluations.

Estimation errors are calculated as the differences between the estimated and simulated field strength values in dB. The simulations are performed with multiple primary emitters of 1 to 5. In order to evaluate the effect of shadow fading, the probability of RF field strength estimation error being less than 5dB is plotted as a function of dB spread values ranging from 0 to 12 dB with different number of transmitters in the network for the nearest neighbor, natural neighbour and linear interpolation methods in Fig. 3.26, Fig. 3.28 and Fig. 3.30 respectively. The probability of the estimation error being less than 10 dB for the three interpolation methods is also given in Fig. 3.27, Fig. 3.29 and Fig. 3.31 respectively. As can be seen from these figures, the estimation error increases as the shadowing spread in dB increases, as expected. But in terms of number of transmitters there isn't a certain proportion for the probability of error against dB spread, i.e. the effect of the number of transmitters to the power estimates depends on the shadowing spread. For shadowing spread of 3 dB or less, the estimation error increases with the increased

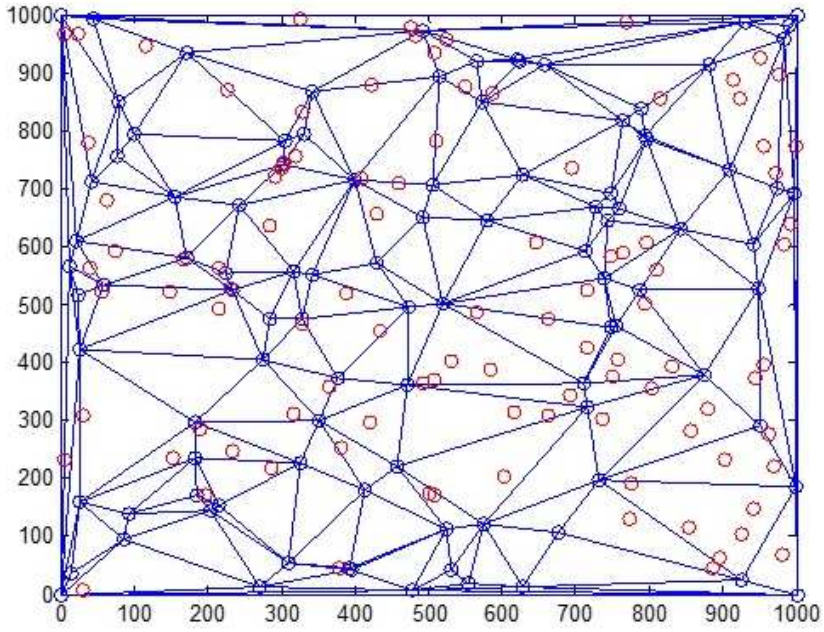

Figure 3.25: A Delaunay triangulation formed with 100 sensors to interpolate the power levels at the remaining sensors ($N_s = 200$, $N_{seleceted} = 100$)

number of transmitters in all methods. However for shadowing values bigger than 3 dB, the estimation error decreases with the increased number of transmitters which can be interpreted as the increase in the number of transmitters helps reducing the shadowing effects.

A comparison of field strength estimation error at different shadowing spread values for three transmitters is plotted for the three interpolation methods for 5 dBm and 10 dBm in Fig. 3.32 and Fig. 3.33 respectively. As seen from the figures, the estimation error increases for bigger values of shadowing spread. The worst performance among the three interpolation methods belongs to the nearest neighbour where natural neighbor and linear interpolation methods provide comparable performance levels. In terms of computational complexity, linear interpolation can be preferred for further analysis.

1000 simulations have been run for a number of selected sensors ranging from 50 to 150 using linear interpolation to estimate the RF field strength value at the rest of 200 sensors, as linear interpolation is advantageous due to its higher performance and lower computational complexity. The probability that the RF field strength estimation error is less than 5 dB and 10 dB is plotted as a function of the number of sensors for shadowing spread value of 6 dB for 1 to 5 transmitters in Fig. 3.34 and Fig. 3.35 respectively. As seen from the figures, the RF field estimation error decreases with the increased number of sensors. For a shadowing spread of 6 dB, the estimation error decreases with the increased number of transmitters as the increase in the number of emitters helps reducing the shadowing effect for higher shadowing values. The cdf of the RF field strength estimation error

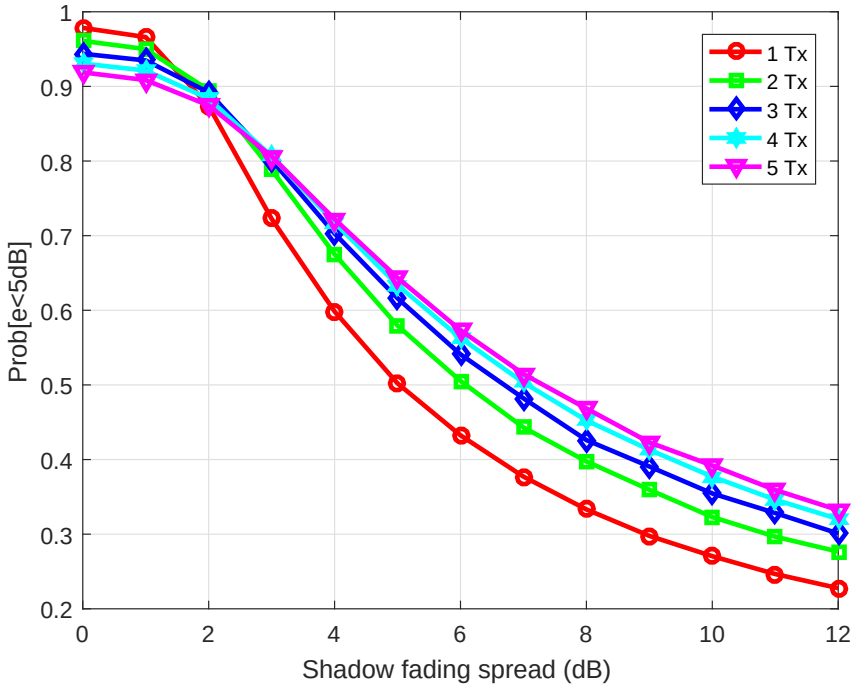

Figure 3.26: Prob. of RSS estimation error being less than 5 dB as a function of shadowing spread for nearest neighbor interpolation for multiple emitters (N_t = 1 - 5, N_s = 200, $N_{selected}$ = 100, α = 2.5, P_t = 1 W, L = 1 km, grid size = 10 m by 10 m)

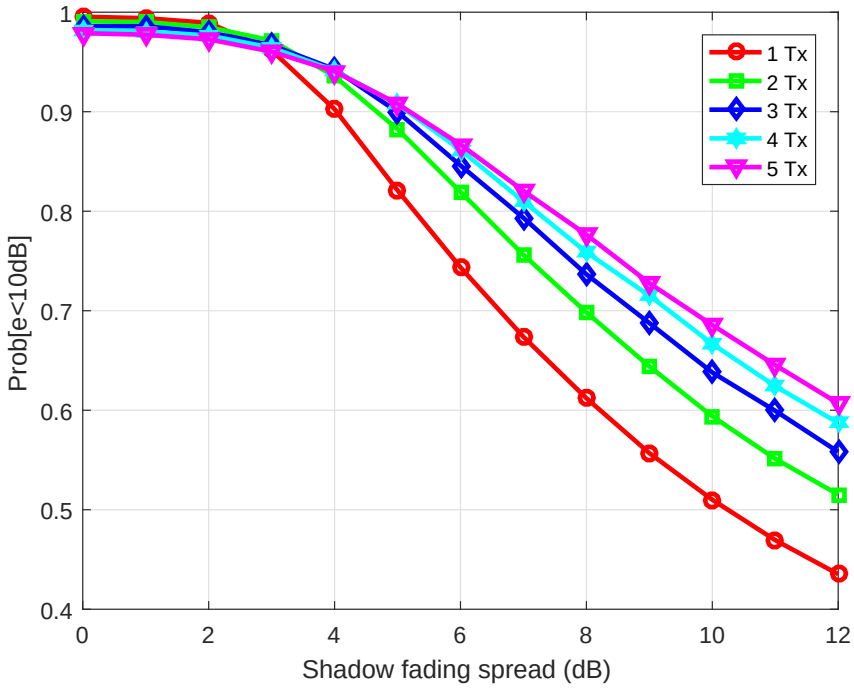

Figure 3.27: Prob. of RSS estimation error being less than 10 dB as a function of shadowing spread for nearest neighbor interpolation for multiple emitters (N_t = 1 - 5, N_s = 200, $N_{selected}$ = 100, α = 2.5, P_t = 1 W, L = 1 km, grid size = 10 m by 10 m)

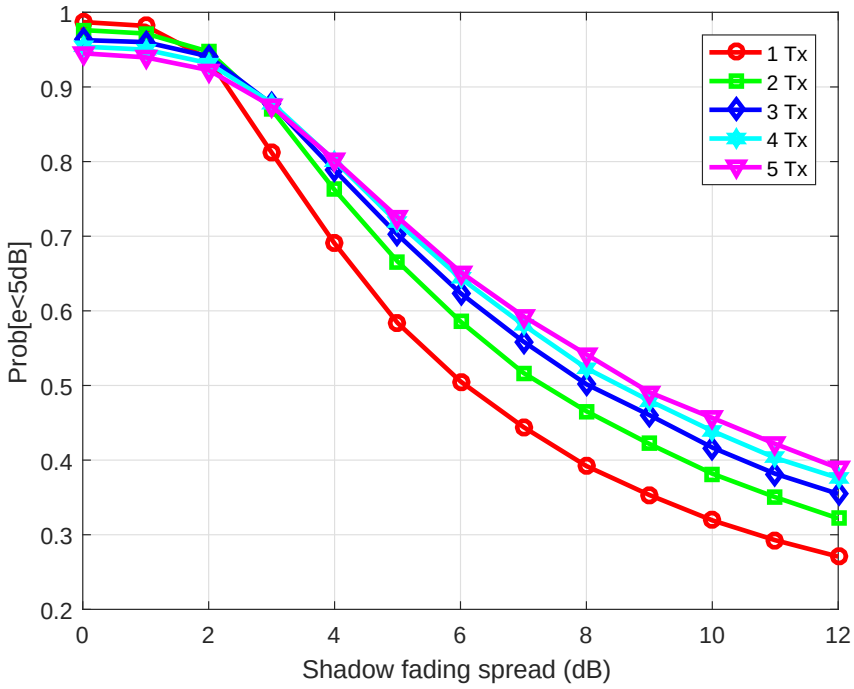

Figure 3.28: Prob. of RSS estimation error being less than 5 dB as a function of shadowing spread for natural neighbor interpolation for multiple emitters (N_t = 1 - 5, N_s = 200, $N_{selected}$ = 100, α = 2.5, P_t = 1 W, L = 1 km, grid size = 10 m by 10 m)

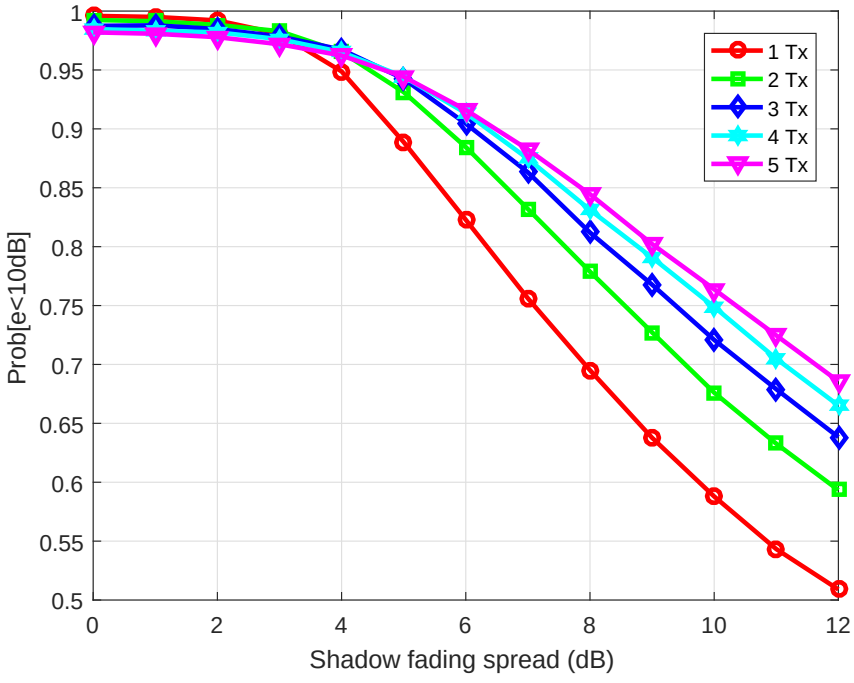

Figure 3.29: Prob. of RSS estimation error being less than 10 dB as a function of shadowing spread for natural neighbor interpolation for multiple emitters (N_t = 1 - 5, N_s = 200, $N_{selected}$ = 100, α = 2.5, P_t = 1 W, L = 1 km, grid size = 10 m by 10 m)

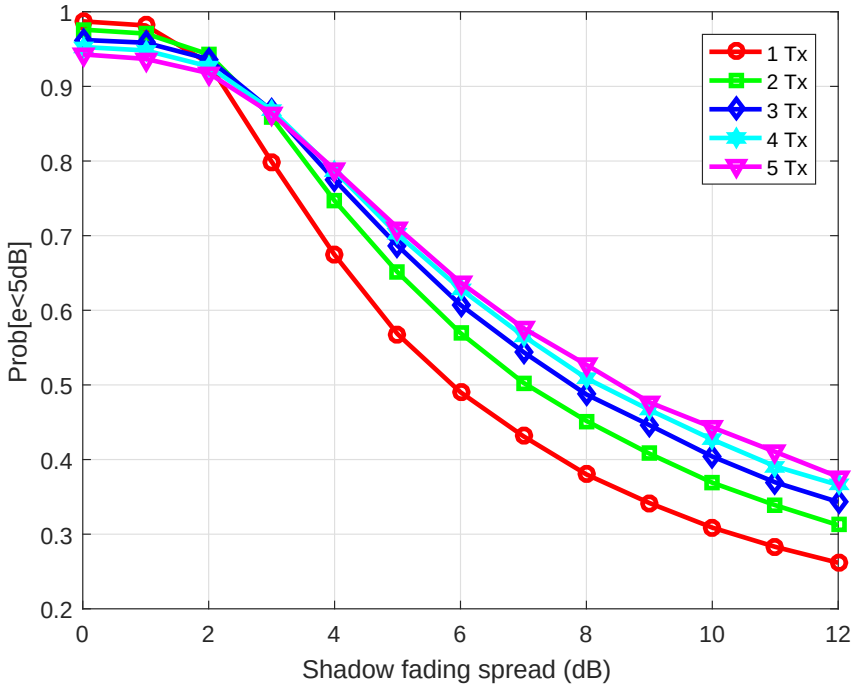

Figure 3.30: Prob. of RSS estimation error being less than 5 dB as a function of shadowing spread for linear interpolation for multiple emitters (N_t = 1 - 5, $N_s = 200$, $N_{selected} = 100$, $\alpha = 2.5$, $P_t = 1$ W, $L = 1$ km, grid size = 10 m by 10 m)

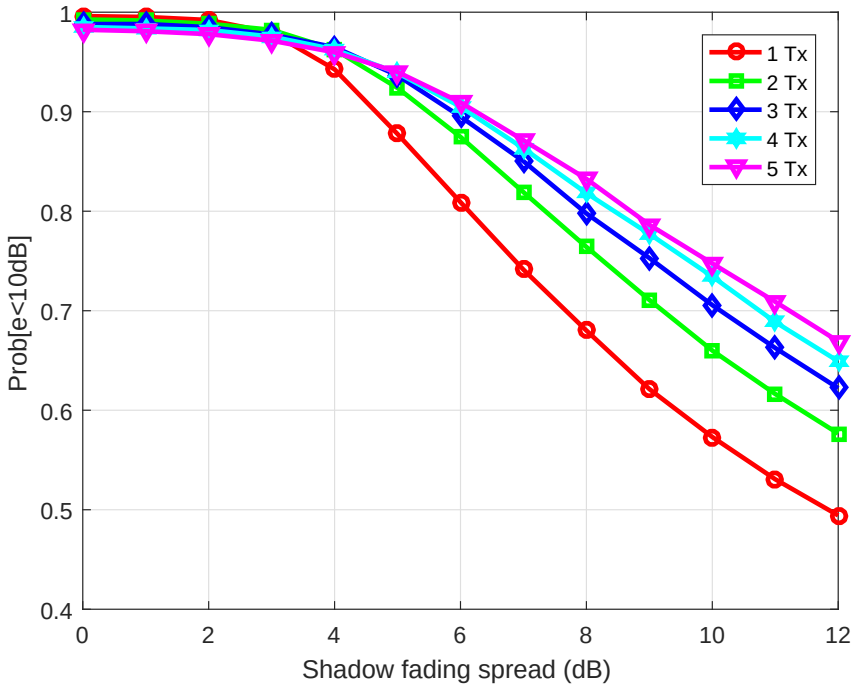

Figure 3.31: Prob. of RSS estimation error being less than 10 dB as a function of shadowing spread for natural neighbor interpolation for multiple emitters (N_t = 1 - 5, $N_s = 200$, $N_{selected} = 100$, $\alpha = 2.5$, $P_t = 1$ W, $L = 1$ km, grid size = 10 m by 10 m)

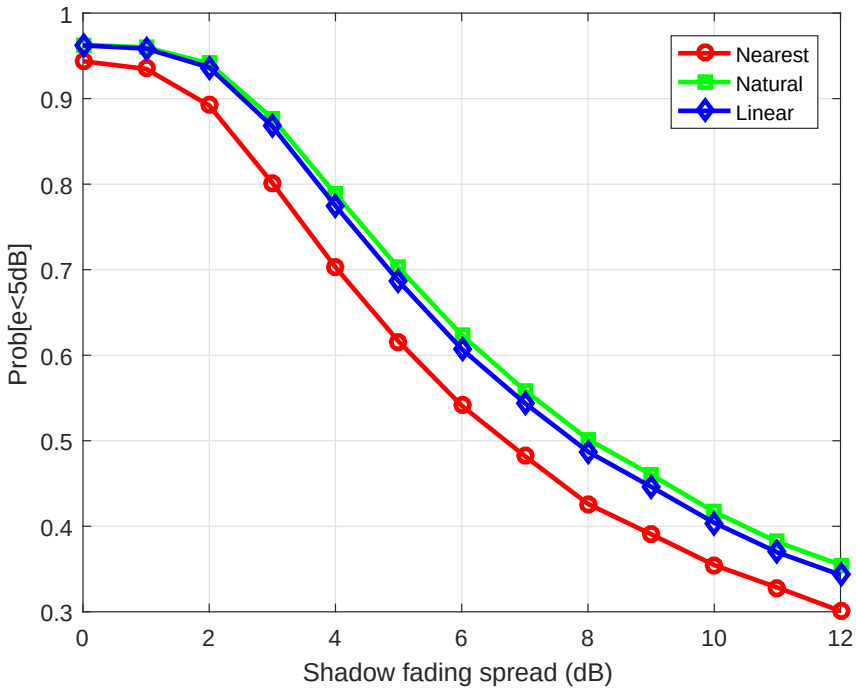

Figure 3.32: Comparison of RSS estimation error probability for 5 dB for nearest n., natural n. and linear interpolation methods at different shadowing spread values ($N_t = 3$, $N_s = 200$, $N_{selected} = 100$, $\alpha = 2.5$, $P_t = 1$ W, $L = 1$ km, grid size= 10 m by 10 m)

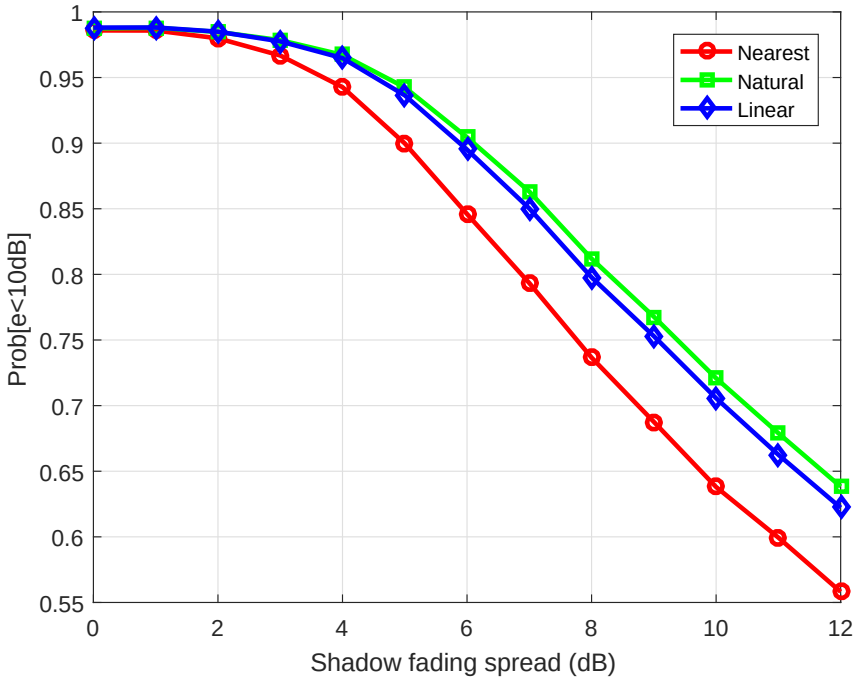

Figure 3.33: Comparison of RSS estimation error probability for 10 dB for nearest n., natural n. and linear interpolation methods at different shadowing spread values ($N_t = 3$, $N_s = 200$, $N_{selected} = 100$, $\alpha = 2.5$, $P_t = 1$ W, $L = 1$ km, grid size= 10 m by 10 m)

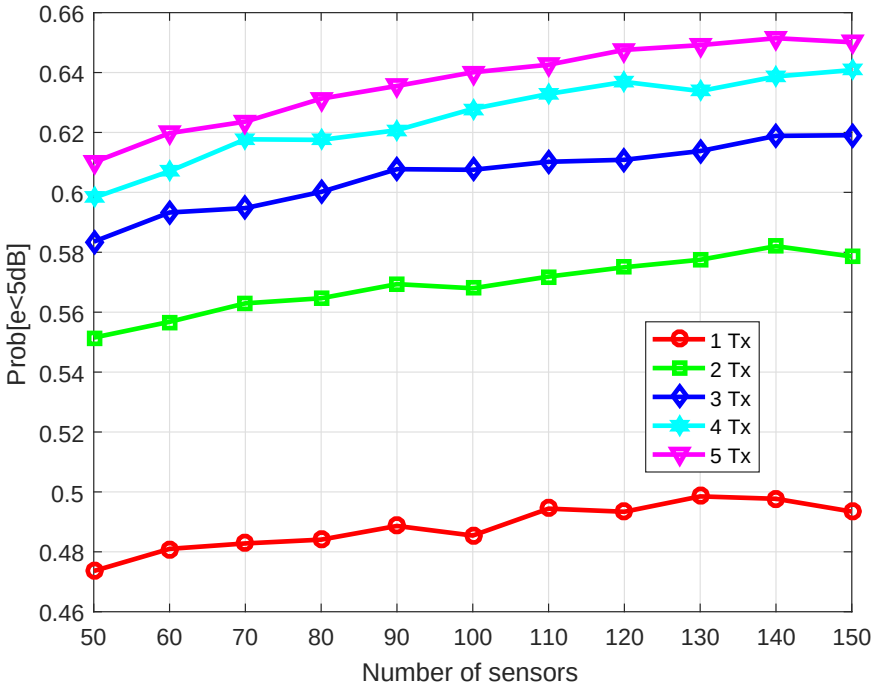

Figure 3.34: Prob. of RSS estimation error being less than 5 dB as a function of number of sensors for linear interpolation for multiple emitters ($N_t = 1 - 5$, $N_s = 200$, $N_{selected} = 50 - 150$, $\alpha = 2.5$, $\sigma = 6$ dB, $P_t = 1$ W, $L = 1$ km, grid size= 10 m by 10 m)

of linear interpolation method is also plotted for 6 dB shadowing spread and 100 sensors in Fig. 3.36 to provide further insights.

A comparison of received power estimation error for 5 dB and 10 dB as a function of number of sensors for three transmitters under 6 dB shadowing spread is plotted for the three interpolation methods in Fig. 3.37 and Fig. 3.38 respectively. As seen from the figure, the estimation error decreases with the increased number of sensors. The nearest neighbour interpolation technique has the worst performance among the three interpolation methods and natural neighbor and linear interpolation methods provide comparable performance levels. Between natural neighbor and linear interpolation, linear interpolation has lower computational complexity than natural neighbor interpolation.

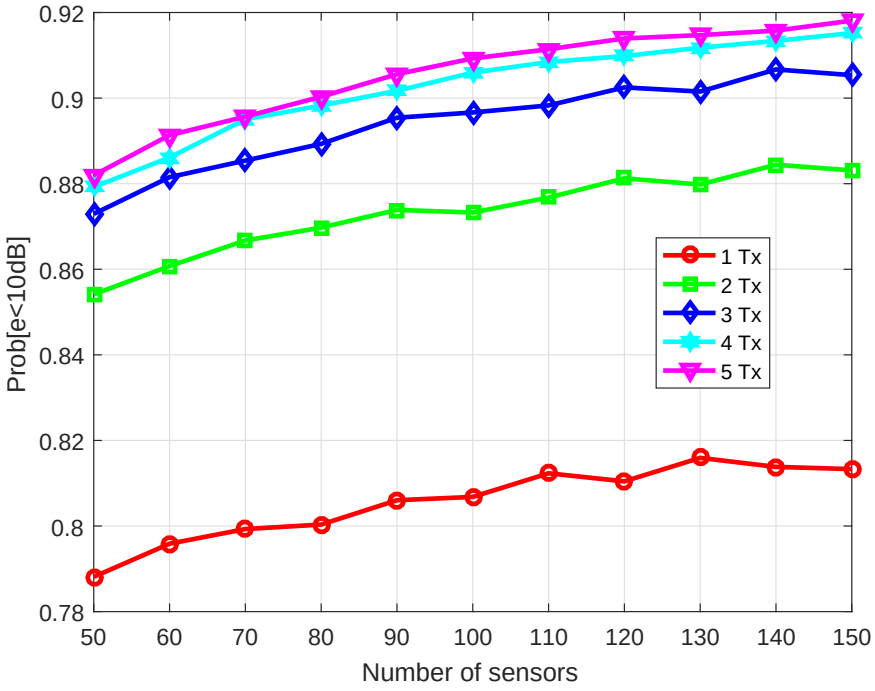

Figure 3.35: Prob. of RSS estimation error being less than 10 dB as a function of number of sensors for linear interpolation for multiple emitters (N_t = 1 - 5, $N_s = 200$, $N_{selected} = 50 - 150$, $\alpha = 2.5$, $\sigma = 6$ dB, $P_t = 1$ W, $L = 1$ km, grid size= 10 m by 10 m)

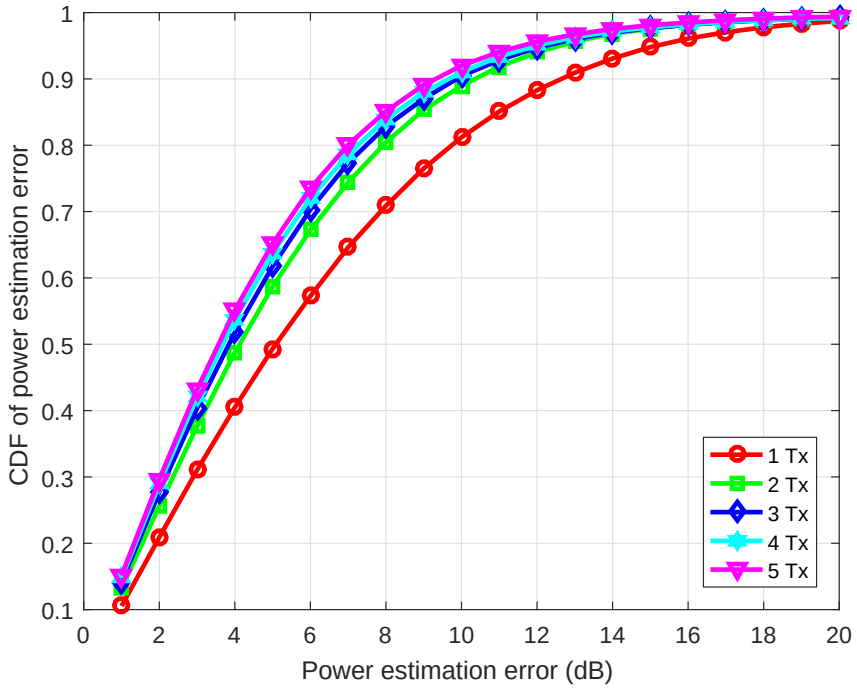

Figure 3.36: CDF of RSS estimation error for linear interpolation based on Delaunay triangulation ($N_s = 200$, $N_{selected} = 100$, $\alpha = 2.5$, $\sigma = 6$ dB, $P_t = 1$ W, $L = 1$ km, grid size = 10 m by 10 m)

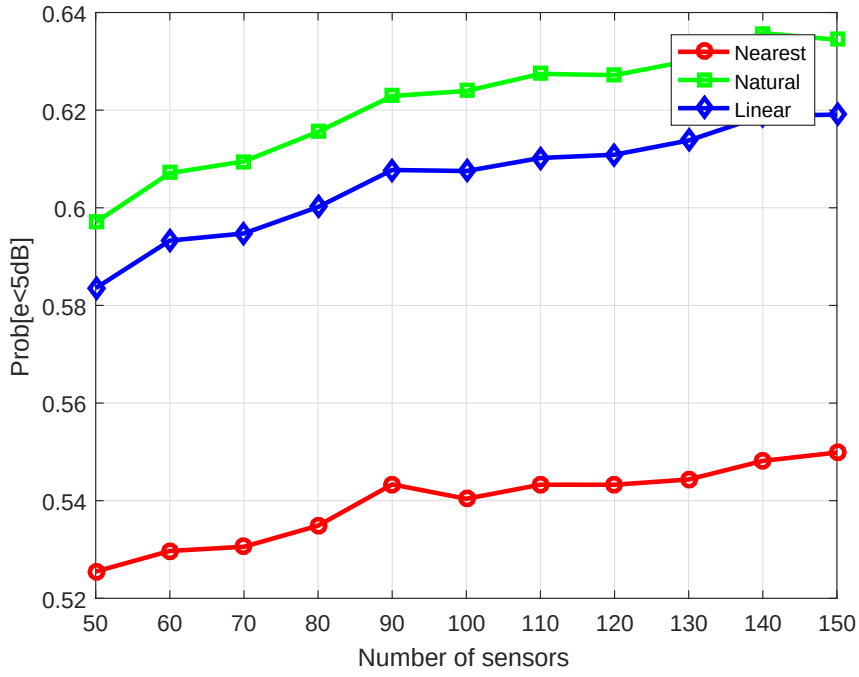

Figure 3.37: Comparison of RSS estimation error probability for 5 dB as a function of number of sensors for three transmitters ($N_t = 3$, $N_s = 200$, $N_{selected} = 50 - 150$, $\alpha = 2.5$, $\sigma = 6$ dB, $P_t = 1$ W, $L = 1$ km, grid size= 10 m by 10 m)

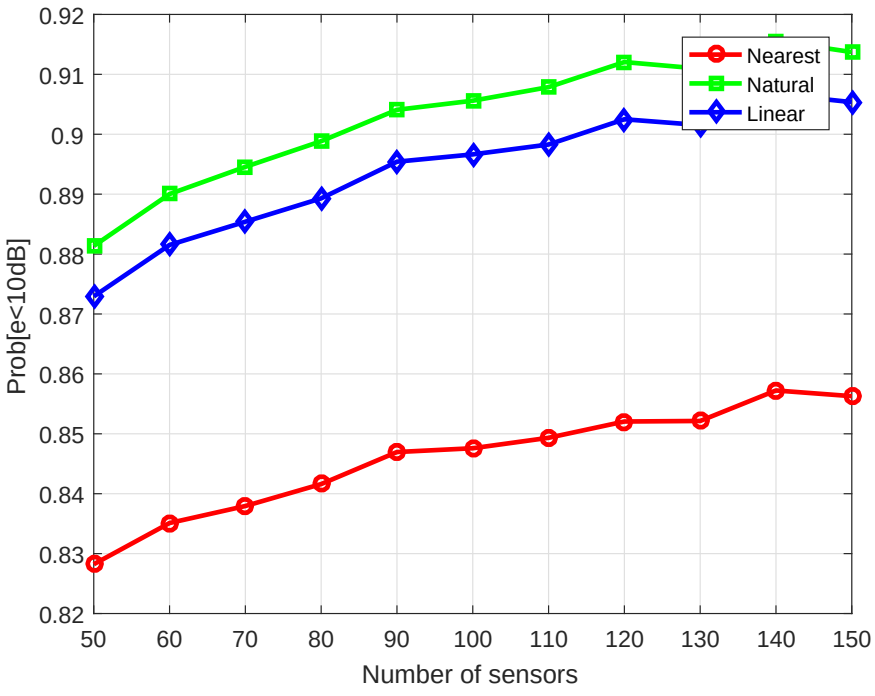

Figure 3.38: Comparison of RSS estimation error probability for 10 dB as a function of number of sensors for three transmitters ($N_t = 3$, $N_s = 200$, $N_{selected} = 50 - 150$, $\alpha = 2.5$, $\sigma = 6$ dB, $P_t = 1$ W, $L = 1$ km, grid size= 10 m by 10 m)

Chapter 4

Improving Emitter Localization Accuracy

As shown in the previous section (see Fig. 3.17 and 3.18), the location estimates obtained from interference maps are not very accurate. Specifically the interference map introduces estimation errors even when there is no uncertainty due to shadowing because of using limited sensor measurements to predict the RF strength values at grid locations throughout the entire region of interest (ROI). Interpolation is a suboptimal estimator because it does not use any knowledge that may be available regarding the propagation model and/or any parameter related with the environment such as path-loss exponent. This type of localization can only give us rough estimates of the emitter location. However this information can be further utilized to initialize more accurate localization algorithms. A detailed study on initialization of an emitter localization algorithms by the information extracted from a REM is presented in Chapter 5. As a result, a need to look for more accurate algorithms arises for emitter localization problem in the thesis.

As mentioned in the literature survey, there is an extensive work on efficient algorithms for accurate localization. Among RSS-based emitter localization techniques, MLE method is the most attractive approach as it is an unbiased linear estimator and gives estimates that are close to the Cramer Rao lower bound (CRLB) [65]. We will first study the MLE technique for improving the localization accuracy and analyze its performance in comparison with the bound. However, it is important to analyze CRLB and investigate the effects of model parameters on the bound to understand inter-relation between the parameters and the estimation accuracy. A theoretical background and some simulation results for CRLB is presented in the next section.

For simplicity, before we delve into more accurate localization algorithms for multiple emitter localization, we first study these algorithms and evaluate their performances for single emitter localization problem.

4.1 Single Emitter Localization

4.1.1 Cramer Rao Lower Bound for Emitter Localization Error

The accuracy of the RSS-based emitter location estimators can be best understood by analyzing the CRLB of the estimates which provide information on the optimal performance achievable for unbiased estimators.

The CRLB is a bound on the covariance matrix of Fisher information matrix of unbiased estimates of the model parameters such as emitter locations, transmission power and/or path-loss exponent. In particular, the diagonal elements of the inverse of Fisher information matrix determine the CRLB bound on the variance of the unbiased estimates of the corresponding parameter. The components of the **Fisher information matrix (FIM)**, $J_{i,j}$ are defined by;

$$J_{i,j} = -E\left\{\frac{\partial^2 ln(Ł)}{\partial z_i \partial z_j}\right\} \tag{4.1}$$

where $ln(Ł)$ is the log-likelihood function, E denotes the statistical expectation operator, z is the unknown parameter to be estimated [45]. Here i and j represent the row and column index of FIM.

By computing the CRLB, we determine the lowest possible estimation variance we can achieve, regardless of which algorithm or method is used in the estimation process. A variance equal to the CRLB is not necessarily achievable, but in practice it is usually possible to get very close to the bound with some estimators. In this section, we compute the CRLB for the emitter location parameter only and use the bound to analyze the performances of different location estimators under different simulation conditions.

There are many papers where the accuracy of RSS-based location estimators has been analyzed through the explicit computation of the Fisher information matrix for unbiased location estimators. In [80], a CRLB was derived for estimates of the 2D coordinates and omni-directional transmit power of the source using RSS measurements. Similarly in [55], the CRLB and a maximum likelihood (ML) estimator were derived under the same conditions for self-localization of a network of sensors, in which few of the sensors in the network were reference nodes at known locations. In [78], ML emitter location estimators are derived for both RSS and RSS difference (RRSD) information under the assumption of a log-normal path loss model and these two ML estimators are shown to be identical. To provide a reference standard, the Fisher information matrix and the CRLB for the root mean square (RMS) of emitter localization error which is defined as average miss distance in [78], have also been derived for unbiased RSSD-based emitter estimators. In [79], CRLB of the RMS of localization error for RSS-based geolocation is derived under the same assumptions. It is shown that the bound derived in this paper is affected by the number of sensors, the path-loss exponent, the shadowing spread and a particular parameter G, which depends only on the relative positions of the emitter and receivers and is called the **geometric dilution of precision (GDOP)** for the given emitter-sensor geometry.

Similarly in [42], a CRLB derivation for location under the log normal model is reviewed as well.

To provide a good practical understanding of the CRLB, we calculate the bound values for shadowing spread values ranging from 1 dB to 12 dB by using equations that are derived in [79] and [42] for a given emitter-sensor geometry. The CRLB expressions used in these two papers are in fact identical, except that the one in [42] is just the matrix representation of the form given in [79] which is given below.

The CRLB for the RMS of emitter localization error for RSS-based geo-localization under log-normal shadowing is given by [79];

$$CRLB(\kappa) = \frac{\ln 10}{10} \frac{\sigma}{\alpha\sqrt{N_s}} G \tag{4.2}$$

where

$$\kappa = \sqrt{E\Big((\widehat{T_x} - T_x)^2 + (\widehat{T_y} - T_y)^2\Big)} \tag{4.3}$$

Recall N_s is the number of sensors, T_x, T_y, $\widehat{T_x}$, and $\widehat{T_y}$ are the actual and estimated emitter locations in x and y directions, respectively, σ is the shadowing spread and α is the path-loss exponent. Here $E(.)$ represents the statistical expectation operator and the parameter G is given by;

$$G = \sqrt{\frac{\overline{\tau^2} + \overline{\rho^2} - (\overline{\tau})^2 - (\overline{\rho})^2}{\begin{vmatrix} 1 & \overline{\tau} & \overline{\rho} \\ \bar{\tau} & \overline{\tau^2} & \overline{(\tau\rho)} \\ \overline{\rho} & \overline{(\tau\rho)} & \overline{\rho^2} \end{vmatrix}}} \tag{4.4}$$

Here, $\overline{\tau}$ and $\overline{\rho}$ are the averages of τ_j and ρ_j, $\overline{\tau^2}$ and $\overline{\rho^2}$ are the averages of τ_j^2 and ρ_j^2, $\tau_j = \frac{\cos(\phi_j)}{d_j}$, $\rho_j = \frac{\sin(\phi_j)}{d_j}$, $\overline{\tau\rho}$ is the average of $\tau_j\rho_j$, and ϕ_j is the angle between the vector emanating from the jth sensor to the emitter and the positive direction of the x-axis of the reference coordinate system and d_j the distance between the emitter and jth sensor. A sample figure that shows the distance and angle for an emitter located at [500, 500] and a sensor located at [650, 850] coordinates is depicted in Fig. 4.1. Note that the shadowing spread is assumed to be constant for each emitter-sensor pair. As seen from (4.4), the CRLB depends not only on the shadowing spread, path-loss exponent, the number of sensors, but the emitter-sensor geometry as well which means each unique emitter-sensor placement results in a different CRLB. However, the value of the emitter power has no effect on the bound.

CRLB Calculations for Uniform Geometries

To gain more insights of the CRLB, we plot CRLB bound values for random and uniform sensor geometries with three different scenarios. In all three scenarios, an independent log-normal shadowing of given dB spread value and a log-distance path-loss model with a

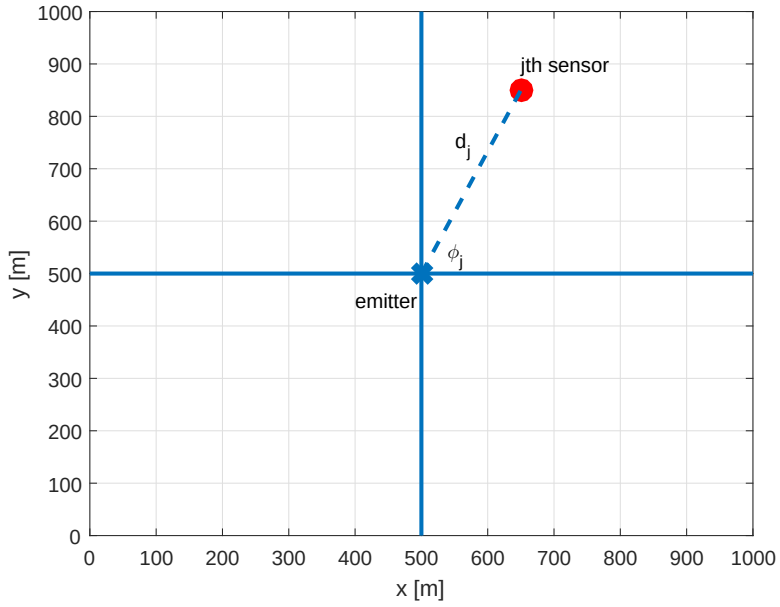

Figure 4.1: Distance and angle for parameter G in calculating CRLB

fixed path-loss exponent of 4 is assumed. In these scenarios, emitter and sensors are placed in a 1 km by 1 km square ROI.

Scenario 1: In this scenario, 100 sensors (denoted by black dots) are placed in a square lattice with uniform spacing between them and the emitter (denoted by red cross), is placed at the center of the ROI, as shown the Fig. 4.2. The CRLB for this case is calculated for dB spread values of 1 to 12 dB and plotted in Fig. 4.4 as the red line.

CRLB Calculations for Random Geometries

Scenario 2: In this scenario, the emitter and the sensors are placed randomly with uniform distribution in the ROI. One random realization of this placement is depicted in Fig. 4.3. The mean, minimum and maximum CRLB values calculated over 1000 different realizations are plotted in Fig. 4.4. As seen from the Fig. 4.4, uniform emitter sensor geometry generally results in smaller CRLB values when compared to the random placement geometries. However, there are some random placements that give smaller bound values than the uniform placement.

Scenario 3: In this case, 100 sensors are placed in a square lattice with uniform spacing between them as in Scenario 1 over 1 km by 1 km area. The CRLB is calculated for each location where the emitter is assumed to be placed at the center of 10 m by 10 m grid locations, creating a 100 pixel by 100 pixel image, as shown in Fig. 4.5. In this image, CRLB values are color coded as shown in the color bar. The bound values from smaller to large are represented by blue to red color respectively. As seen from this figure, CRLB

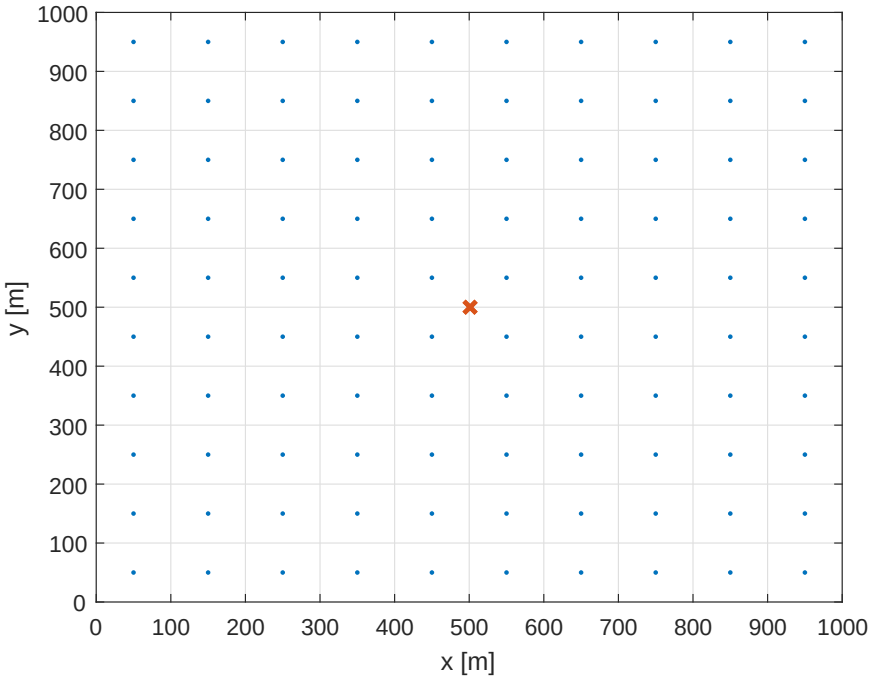

Figure 4.2: Uniform sensor geometry ($N_t = 1$, N_s=100, $L = 1$ km)

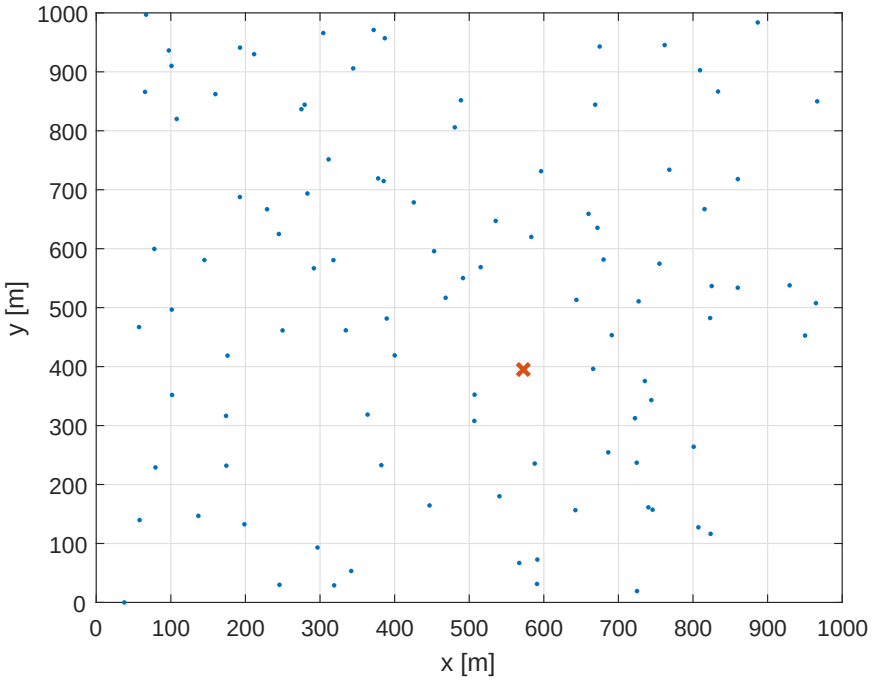

Figure 4.3: Random emitter sensor geometry ($N_t = 1$, N_s=100, $L = 1$ km)

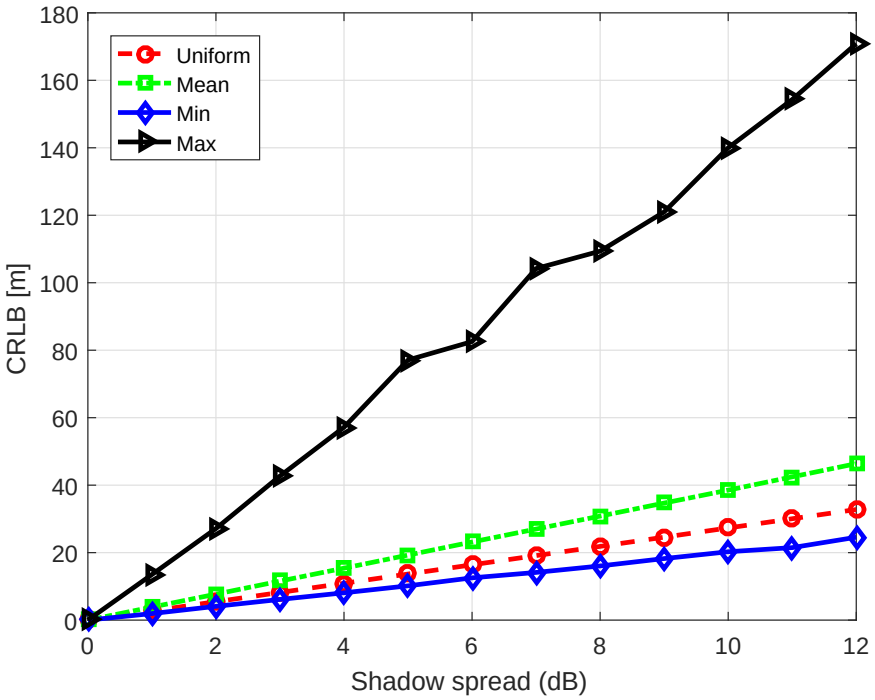

Figure 4.4: CRLB for the RMS of location error for uniform (see Fig. 4.2) and random emitter-sensor geometry (see Fig. 4.3) ($N_t = 1$, N_s= 100, $L = 1$ km, $\alpha = 4$)

values are smaller when the emitter is placed inside the region covered by the sensors, yielding more accurate location estimations. When an emitter is placed at the center of a grid where a sensor is placed, the value of the bound increases, yielding in poor location estimations.

As can be seen from Fig. 4.4 and Fig. 4.5, smaller CRLB values are achieved when sensors are placed around an emitter. In other words, bound values increase as the sensors are placed further away from the emitter. In accordance with this result, another result obtained in [20] showed that the optimal sensor placement is achieved when the sensors are distributed with uniform spacing around the emitter in a circle.

4.1.2 Single Emitter Localization Using MLE (Grid Search) Method

The emitter location and received power parameters in (3.11) are considered to be random variables. Assuming that the RSS values are independently distributed, each having a log-normal shadowing, the likelihood of observing all N_s sensor outputs given the signal model in (3.11) and (3.12) is written as

$$Ł = p(\mathbf{r}|M, \boldsymbol{\theta}) = \prod_{j=1}^{N_s} \frac{1}{\sigma\sqrt{2\pi}\epsilon r_j} e^{-\frac{\left(10\log_{10} r_j - 10log_{10} s_j\right)^2}{2\sigma^2}} \tag{4.5}$$

where M denotes the specific choice of signal model and noise statistics, $\boldsymbol{\theta} = (T_x, T_y)$ is the unknown emitter's location parameter and $\mathbf{r} = [r_1\ r_2\ ...\ r_N]$ are the sensors' power

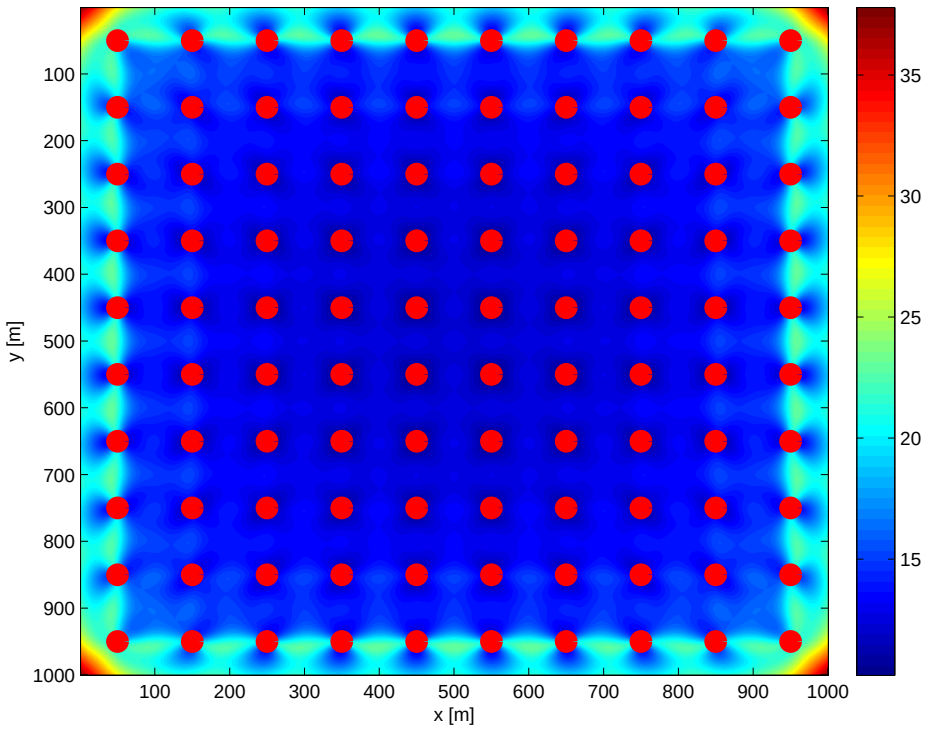

Figure 4.5: CRLB for uniform sensor placement for all emitter locations ($N_t = 1$, N_s= 100, $L = 1$ km, $\alpha = 4$, $\sigma = 4$ dB)

measurements. The shadowing spread σ can be considered as a nuisance parameter and can be integrated out analytically to obtain the following marginalized likelihood function, Ł$_{mar}$ (Refer to Appendix B.1).

$$Ł_{mar} = p(\mathbf{r}|M, \boldsymbol{\theta}) = K \left[\sum_{j=1}^{N_s} \log_{10}^2 \frac{r_j d_j^\alpha}{\rho P_t} \right]^{-\frac{N_s}{2}} \tag{4.6}$$

where $K = \frac{1}{2} \left(\frac{1}{\sqrt{2\pi\epsilon}} \right)^{N_s} \left(\prod_{j=1}^{N_s} r_j \right)^{-1} 50^{-\frac{N_s}{2}} \Gamma(\frac{N_s}{2})$ is a constant parameter (scaling factor), which is independent of emitter power and location. Here $\Gamma(.)$ represents the gamma function. The advantage of using the marginalized likelihood is that it eliminates the need for knowing or estimating the shadowing spread.

Obtaining the exact solution of the ML estimate requires taking the derivative of (4.6) with respect to the unknown parameter which cannot be carried out analytically. A numerical solution to this problem can be obtained by searching the value of the parameter that gives the maximum value of the likelihood function over a grid element, which is called grid-search method.

In a grid-search method, the solution space is divided into a number of grids and a cost function is calculated for each grid center. The cost function that gives the estimate of the location parameter, $\hat{\theta} = (\hat{T}_x, \hat{T}_y)$ can be obtained by minimizing the sum of squared

differences between each sensor's power estimate and average of all sensor estimates for each grid center [82]. Note that the emitter power is not known and the value of the cost function depends on the power estimates of each sensor in the network. The center of the grid that minimizes the cost function is selected as the solution:

$$\hat{\theta} = \min_{\widehat{T_x},\widehat{T_y}} \sum_{j=1}^{N_s} \left(\log\left(r_j d_{T,j}^{\alpha}\right) - \frac{1}{N_s} \sum_{i=1}^{N_s} \log\left(r_i d_{T,i}^{\alpha}\right) \right)^2 \tag{4.7}$$

where $d_{T,j}$ is the distance between jth sensor and the test grid location T. The derivation of the cost function in (4.7) is given in [82]. As can be seen from (4.7), the values of the transmit power and the shadowing spread are not required for cost function calculations. Thus, the MLE method is advantageous for the single emitter case scenarios where the emitter power and dB spread parameters are not known.

A sample grid is illustrated in Fig. 4.6 to show how the technique is used in estimating the location of a single emitter using five sensors. In this example, 1 km by 1 km simulation region is divided into smaller squares of length 100 m. The total number of grid elements Q, that is required to search is 100. The sensors are shown with circles whereas the actual emitter location is marked with a diamond shape. The emitter power is assumed to be unknown, however the received power measurements at sensor locations are generated due to 1 W transmit power for our simulations. The values of the cost function calculated in each grid location are also shown in the figure. As seen from the figure, the minimum value of the cost function which is 3 for this example, is obtained around the actual emitter location. The estimated emitter location is shown with a square at the center of the grid for which the cost is minimum.

In order to compare the performance of grid search based ML estimator to the CRLB, two different emitter-sensor geometries have been considered. In both cases, we assume independent log-normal shadowing of given dB spread and log-distance path-loss model with a fixed path-loss exponent of 4. The emitter power is not known and the grid-size is set to 10 m by 10 m.

In the first case, the emitter is located at the center of the area of 1200 m by 1200 m and 6 sensors are evenly positioned on the circle centered at the emitter with a radius of 500 m as shown in Fig. 4.7 for comparison to [78]. The RMS of estimation error is plotted for dB spread values of 1 to 12 dB for 1000 simulations in Fig. 4.8. As can be seen from the figure, the performance of the full grid search based on the ML approach is close to the Cramer-Rao lower bound for shadowing spread values of 6 dB and under.

In the second case, a network of 100 sensors distributed placed in a square lattice with uniform spacing between them in a 1 km by 1 km area and a primary emitter located at the center of the area as in Fig. 4.2. The RMS of estimation error is plotted for dB spread values of 1 to 12 dB for 100 simulations in Fig. 4.9.

As seen from Fig. 4.9, the performance of the ML estimator approaches to CRLB when the shadowing spread values are between 3 dB and 9 dB. However the performance degrades with higher dB spread values since higher shadowing effect degrades the estimation

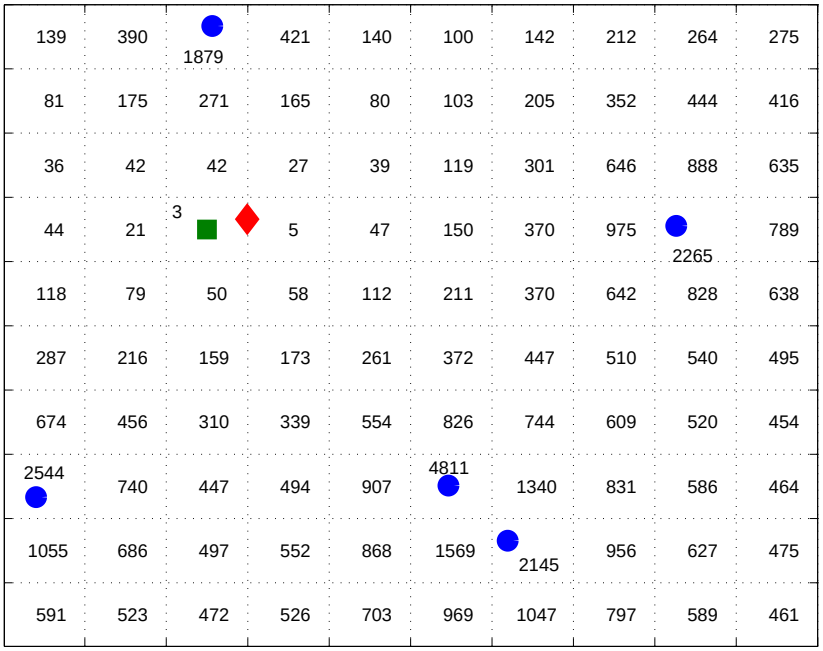

Figure 4.6: Uniform grid structure for full search ($N_t = 1$, N_s=5, $L = 1$ km, grid size = 100 m by 100 m, $P_t = 1$ W)

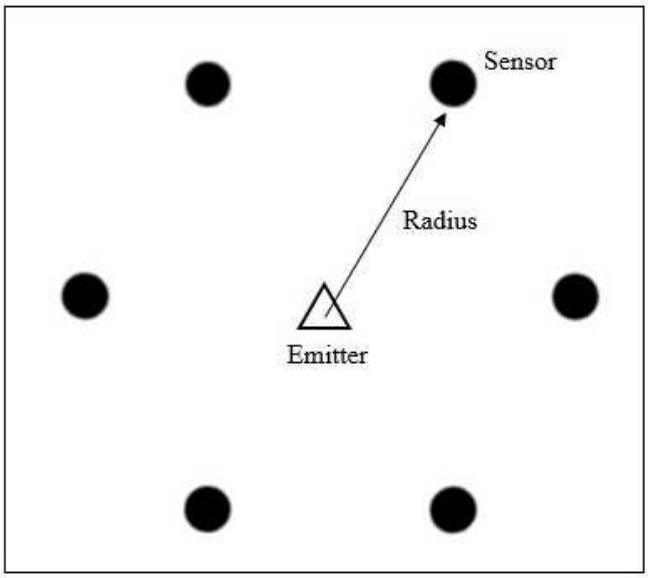

Figure 4.7: Sensors positioned on the circle centered at the emitter

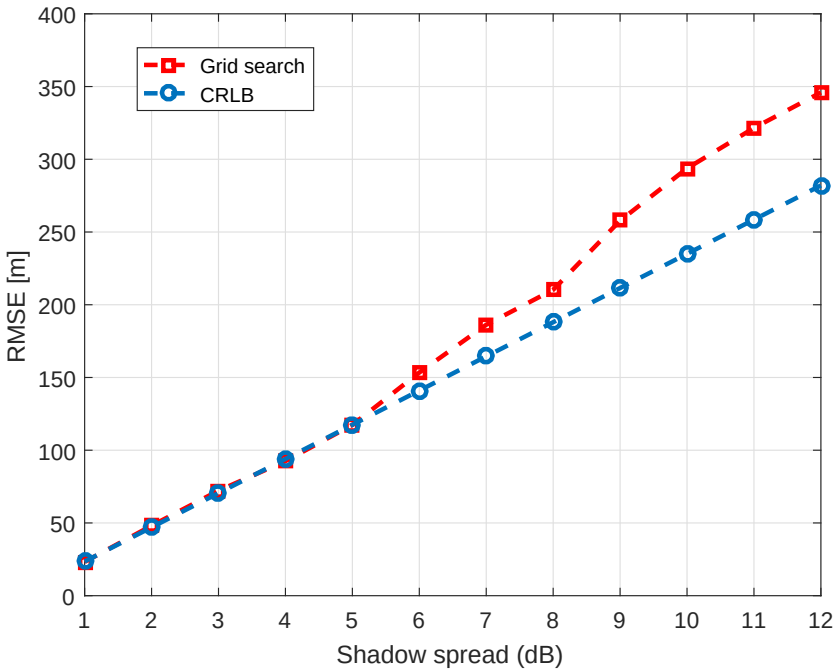

Figure 4.8: Performance of full grid search compared to CRLB for six sensors that are evenly positioned on the circle centered at the emitter with a radius of 500 m ($N_t = 1$, $N_s = 6$, $L = 1200$ m, $\alpha = 4$, grid size = 10 m by 10 m, $P_t = 1$ W)

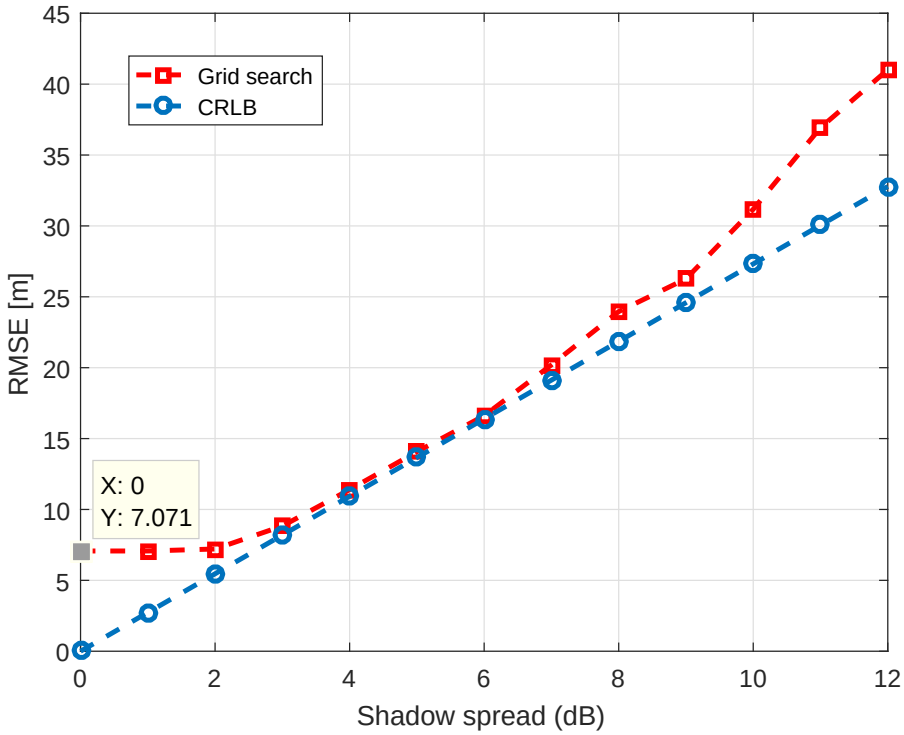

Figure 4.9: CRLB and the RMSE of the grid search for uniform sensor placement ($N_t = 1$, $N_s = 100$, grid size = 10 m by 10 m, $L = 1$ km, $\alpha = 4$, $P_t = 1$ W)

performance. Moreover, the quantization noise due to selecting large grid sizes becomes more pronounced than the shadowing effect below 4 dB, therefore deviations from the CRLB is observed at smaller shadowing spread values. When there is no shadowing, the RMS of emitter localization error with the grid search method is calculated as 7.071 for a grid size of 10 m and it is depicted in the figure as (X:0, Y:7.071). This is due to the position of emitter being in the corner of the grid where it resides as in Fig. 4.2 and its estimated location is found to be in the center of that grid. Therefore the distance between the corner and the center of a grid which is $\frac{gridsize}{2}\sqrt{2}$, determines the quantization error for that particular emitter-sensor geometry.

4.1.3 Computational Complexity of Grid Search Method

The RMSE of the MLE method based on full grid search closely achieves the Cramer-Rao lower bound at small shadowing variances as it is shown in the previous section. However, full grid search is a complex search method that requires the algorithm to scan all possible grid points in the localization space and also requires the size of the grid elements to be chosen small to reduce the quantization error induced by the grid size and obtain more accurate location estimates. There is a trade-off between the estimation accuracy and the computational complexity; smaller grid sizes provide more accurate estimates at a cost of increased computational complexity. The algorithm becomes even more complex for multiple primary emitter localization problems as it increases the calculation of the likelihood function for all grid points related with the number of primary emitters considered in the network. The number of computations is given by;

$$\text{Number of computations} = \binom{Q}{N_t} \tag{4.8}$$

where Q is the number of grid locations and N_t is the number of emitters. For example for two emitter scenario, the number of calculations is $Q(Q-1)/2$ where in one emitter case it is Q that is the total number of grid elements. The number of computations versus the number of emitters is plotted in Fig. 4.10. As can be seen from the figure, the complexity increases exponentially with respect to the number of unknown parameters to be estimated.

In the case of estimating multiple parameters such as emitter location, emitter power, path-loss exponent, joint parameter estimation is not possible with the grid search method. Instead, each parameter is estimated one at a time. This situation yields in accumulating estimation errors for the last estimated parameters. For example, for a single emitter case scenario, where the problem is to estimate both the transmit power and its location, the error that arises from location estimation will affect the transmit power estimate. Therefore for multiple parameter estimation problems, this method is not preferred.

Additionally, any prior knowledge about the location of the transmitter or any statistical characterization of its transmit power is not considered with the ML estimator, which is called as blind estimation.

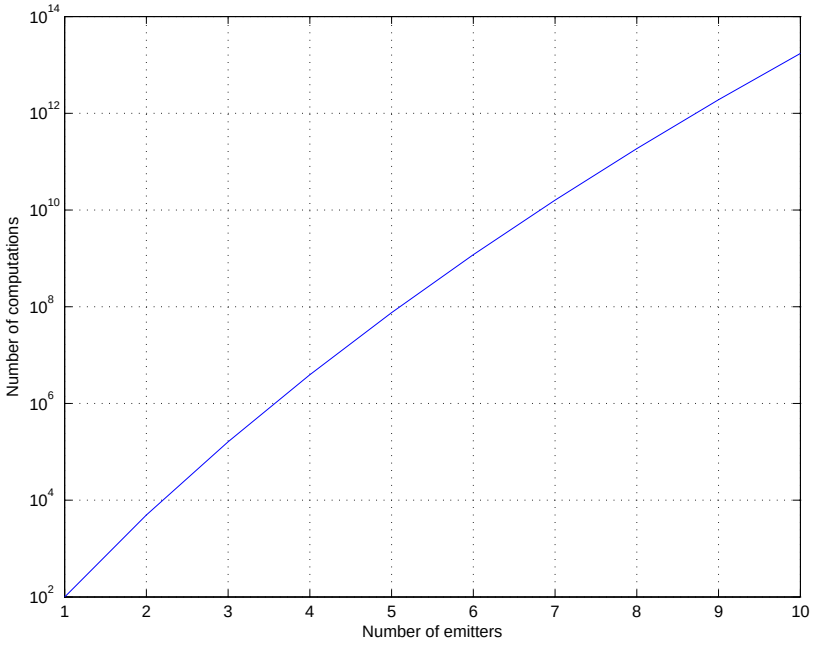

Figure 4.10: Computational complexity of the MLE method for $Q = 100$

4.1.4 Single Emitter Localization Using MCMC Method

The problems with the grid search method that are discussed in the previous section, arises the need to look for another numerical solution that can also account for the shadowing uncertainty introduced by the wireless channel. In this section, we will look into numerical approaches based on generating samples from the joint posterior of the unknown parameters with MCMC methods, as an alternative for highly computationally complex full grid search method. The reason to propose a MCMC method for maximizing the likelihood function given in (4.6) is that the MCMC methods provide computationally efficient sampling strategies especially when the number of parameters to be estimated is large, which is the case for multiple emitter scenarios. Besides, the MCMC estimator has a Bayesian approach in which a prior knowledge can be used for better estimates. The rough emitter location estimates we have obtained from generated REM in the previous chapter is taken as a prior knowledge and it is proposed to initialize the MCMC algorithm for reducing the number of iterations required for convergence as described in Section 5.2. Moreover, the quantization error we have encountered in the grid search technique is not a concern with any of the MCMC methods.

Basically, for maximizing the likelihood function given in (4.6), samples are generated from this likelihood function using an MCMC thechnique. The simulated samples generated by this process are then used for making inferences about the emitter's location.

Metropolis Hastings (MH) Algorithm

MCMC methods are a class of iterative algorithms for sampling from probability distributions based on constructing a Markov chain that has the desired distribution as its equilibrium distribution [60]. The state of the chain after a large number of steps is then used as a sample of the desired distribution. The quality of the sample improves as a function of the number of iterations. Samples of the Markov chain are generated by using Metropolis Hasting (MH) algorithm [17], an MCMC method that is based on **Accept-Reject** technique. As a motivation for the MH algorithm, we first present the theory that lies behind the Accept -Reject idea.

Simulation methods that are for pseudo-random number sampling are based on the production of uniform random variables, originally independent random variables that are distributed according to a distribution p, that is not necessarily explicitly known. The uniform distribution $U(0,1)$ provides the basic probabilistic representation of randomness and the generation of uniform random variables is the key point in the behavior of simulation methods for other probability distributions since those distributions can be represented as a deterministic transformation of uniform random variables. For example, inverse transform sampling, also known as inverse transform method is one of the basic methods for pseudo-random number sampling, i.e. for generating sample numbers at random (random variables) from any probability distribution given its invertible cumulative distribution function (cdf) [60]. Similarly, when a distribution p is linked in a relatively simple way to another distribution that is easy to simulate, this relationship can often be exploited to construct an algorithm to simulate variables from p. There are many transformation algorithms for generating non uniform random variables using relationships between the distributions. For example Box-Muller algorithm is used for normal variable generation connected to the uniform distribution. Similarly, Poisson distribution can be simulated by generating exponential random variables. However there are many distributions from which it is difficult, or even impossible to directly simulate by an inverse transform. Moreover, in some cases, we are not even able to represent the distribution in a usable form such as transformation. In such settings, it is impossible to exploit direct probabilistic probabilities to derive a simulation method. We thus turn to another class of methods that only requires us to know the functional form of the density p of interest up to a multiplicative constant; no deep analytical study of p is necessary. The key to this method is to use a simpler (simulation wise) density q from which the simulation is actually done. For a given density q, called the instrumental density, there are thus many densities p, called the target densities, which can be simulated this way. The corresponding algorithm, called Accept-Reject, is based on a simple connection with the uniform distribution and can be explained as follows.

Consider an envelope distribution as an instrumental distribution around the underlying target distribution $p(x)$. In the simplest case it can be a uniform distribution around it. Then choose (x, y) such that:

$x \sim U(A, B)$

$y \sim U(0, max(f(x)))$ If y is under the $p(x)$ curve accept x, otherwise reject it. An example can be found in Fig. 4.11 [13].

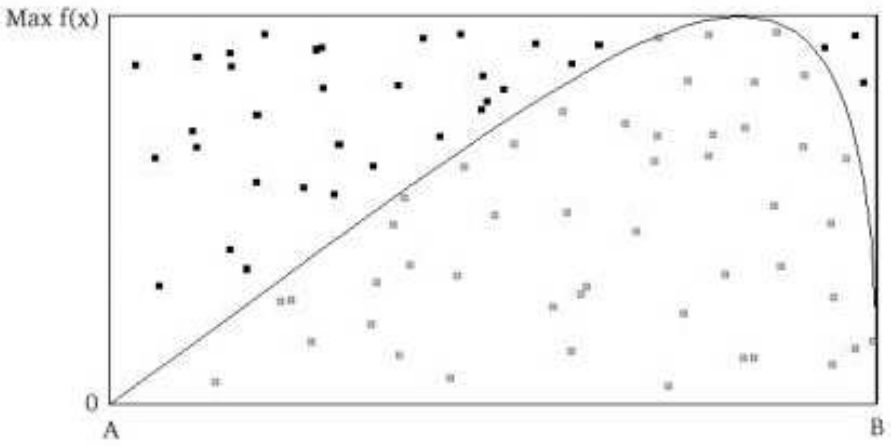

Figure 4.11: An example for Accept-Reject technique, uniform envelope

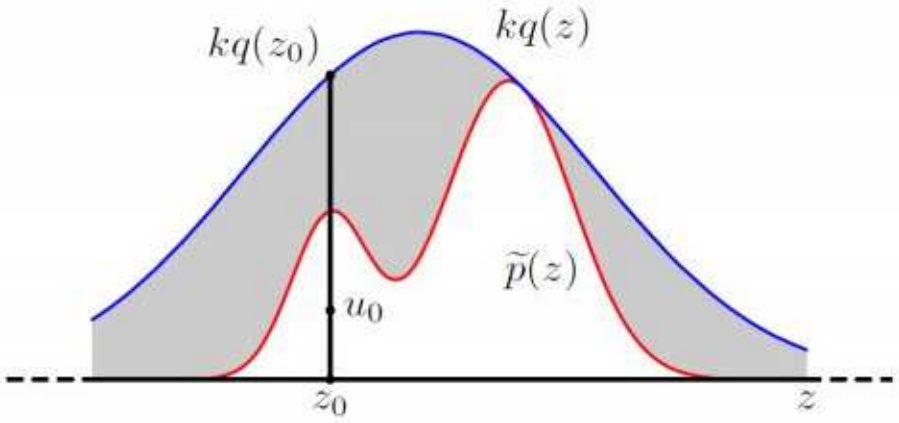

Figure 4.12: An example for Accept-Reject technique, scaled Gaussian envelope

We can generalize the envelope distribution. For example, we may have a Gaussian distribution instead of a uniform. If the Gaussian (or any other envelope distribution), $q(x)$, can not envelope the underlying distribution, $p(x)$, we can simply scale it with a scale k, to have $kq(x)$ that envelops $p(x)$; $p(x) < kq(x)\ \forall x$. Furthermore, to be more in the area of interest, we can sample x from the Gaussian distribution. In other words, we choose (x, y) such that:

$x \sim q(x)$

$y \sim U(0, kq(x))$

If y is under the $p(x)$ curve accept x, otherwise reject it. An example for a scaled Gaussian envelope can be found in Fig. 4.12 [13].

The Metropolis Hasting (MH) algorithm [17] is based on the Accept-Reject technique for obtaining a sequence of random samples from a probability distribution for which direct sampling is difficult. This sequence can be used to generate a histogram and compute an integral, such as an expected value of the distribution. The general idea of the algorithm is to use a Markov chain that generates states depending on the likelihood ratio of the states. In MH algorithm, sample generation is based on a proposal density that resembles the likelihood as much as possible. Even though any proposal density eventually generates samples from the target density, inappropriate proposal selections may result in increased convergence time.

In MH algorithm, the Markov chain starts from a random initial state $\boldsymbol{\theta_i}$ where $\boldsymbol{\theta}$ represents the unknown location parameter to be estimated. It generates a new state $\boldsymbol{\theta_{new}}$ that depends only on the previous state which is the current state $\boldsymbol{\theta_c}$. By using a proposal density $R(\boldsymbol{\theta_p}; \boldsymbol{\theta_c})$, which depends on the current state $\boldsymbol{\theta_c}$, a new proposed sample $\boldsymbol{\theta_p}$ is generated. This proposal is accepted as the next value by checking the **acceptance ratio**, a defined as follows:

$a = \min(1, b)$ where $b = b_1 b_2$,

$b_1 = P(\boldsymbol{\theta_p})/P(\boldsymbol{\theta_c})$ is the posterior ratio between the proposed sample $\boldsymbol{\theta_p}$ and the previous sample $\boldsymbol{\theta_c}$. If there is no prior information available for the unknown parameter, then the posterior ratio is equal to the **likelihood ratio** $Ł_p/Ł_c$, where $Ł_p$ and $Ł_c$ represent the likelihood of proposed and current locations respectively. As we recall Bayes rule, the posterior probability of a parameter is the likelihood probability of that parameter multiplied by its prior pdf. Due to the lack of prior knowledge of the parameter, the prior ratio is taken as 1 [70].

$b_2 = R(\boldsymbol{\theta_c}; \boldsymbol{\theta_p})/R(\boldsymbol{\theta_p}; \boldsymbol{\theta_c})$ is the ratio of the proposal density in two directions from $\boldsymbol{\theta_c}$ to $\boldsymbol{\theta_p}$ and vice versa. This ratio is equal to 1 if the proposal density is symmetric. Then the new state $\boldsymbol{\theta_{new}}$ is chosen according to the value of a.

$$\boldsymbol{\theta_{new}} = \begin{cases} \boldsymbol{\theta_p} & \text{if } b \geq 1 \\ \boldsymbol{\theta_p} & \text{if } a > u, u \sim U(0,1) \\ \boldsymbol{\theta_c} & \text{if } a \leq u \end{cases}$$

The Markov chain is run for many iterations until the chain reaches to a convergence. The samples for which the initial state is forgotten are discarded and known as **burn-in samples**. The remaining set of accepted values of $\boldsymbol{\theta}$ represents a sample from the distribution $P(\boldsymbol{\theta})$. This algorithm works better when the proposal density matches the shape of the target distribution $P(\boldsymbol{\theta})$ that is; $R(\boldsymbol{\theta_p}; \boldsymbol{\theta_c}) \sim P(\boldsymbol{\theta})$.

Large sample theory states that the posterior distribution of the parameter approaches a multivariate normal distribution therefore as proposal distribution, a normal distribution is selected often in practice:

$R(\boldsymbol{\theta_p}; \boldsymbol{\theta_c}) \sim N(\boldsymbol{\theta_c}, \sigma^2)$

Here $R(\boldsymbol{\theta_p}; \boldsymbol{\theta_c})$ is the probability density function for $\boldsymbol{\theta_p}$ given the previous value $\boldsymbol{\theta_c}$. This proposal density would generate samples centered on the current state $\boldsymbol{\theta_c}$ with variance σ^2. The variance parameter has to be tuned during the burn-in period. This is usually done by calculating the acceptance rate which is the ratio of the accepted samples to the total number of the last N generated samples. If the variance is too large, almost all steps under the MH algorithm will be rejected and the acceptance rate will be very low because the proposals are likely to land in regions of much lower probability density, then the chain will converge very slowly. On the other hand, if it is too small, almost all steps will be accepted and the acceptance rate will be high but successive samples will move around the space slowly and the chain will again converge only slowly to $P(\boldsymbol{\theta})$. Thus the MH algorithm requires reasonable tuning of the variance. There is no general rule for automatic tuning and off-line tuning may require extensive experimentation.

The MH algorithm as applied to single emitter location estimation problem is presented as follows with a simulated example. The algorithm takes the received power values at each sensor and generates samples from the posterior distribution. In this example, an independent log-normal shadowing of 12 dB and a path-loss exponent of 3.5 is assumed. The primary emitter and 50 sensors are randomly placed in a 10 km by 10 km square ROI for convinence. The emitter power is fixed at 1 W and the close-in distance, d_0 is at 1 m. The algorithm can be summarized as follows:

1. Simulating the received power levels at the sensors for given emitter-sensor geometry
    - Place the emitter and the sensors randomly within the defined area
    - Calculate the distances between the transmitter and the sensors, d_j, $j = 1, .., N_s$.
    - Calculate mean received power level at jth sensor, s_j,$s_j = \frac{\rho P_t}{d_j^{\alpha}}$, $j = 1, .., N_s$.
    - Generate random variables from normal distribution with a variance of dB spread to simulate log-normal shadowing.
    - Include shadowing $r_j = s_j 10^{\frac{X}{10}}$ where $X \sim N(0, \sigma^2)$, $j = 1, .., N_s$.
2. Calculating the likelihood of initial value

- Let the initial estimate of the emitter location, θ_i be $(\hat{T}_x, \hat{T}_y)$ which is randomly chosen. $(\theta_i = \theta_c)$
- Calculate the distances between the sensors and the initial emitter location $\hat{d}_j$, $j = 1, .., N_s$.
- Calculate the likelihood of initial location as the likelihood of current location, Ł$_c$ using $\hat{d}_j$ in (4.6).

3. Calculating the likelihood of proposed value
   - Propose a new estimated emitter location, θ_p based on the current location, θ_c and proposal density. Δ (the **step size** of MH algorithm) is the variance of the proposal density function and taken as 200 m after a tedious fine tuning stage based on extensive trial and error process. The pdf of the location parameter is chosen as Gaussian for the proposed location value to be symmetric around the current location values. Note that, even though any proposal density eventually generates samples from the target density, inappropriate proposal selections may result in an increased convergence time. Make sure that the proposed value is within the simulation area.

     Ł$_p$ = Ł$_c$ + $Z\Delta$ where $Z \sim N(0, 1)$
   - Calculate the likelihood of proposed location Ł$_p$ using $\hat{d}_j$ in (4.6).
4. Determining whether to accept or reject the proposed value:
   - Calculate the likelihood ratio $Ł_R = \frac{Ł_p}{Ł_c}$
   - Calculate the acceptance ratio $a = \min(1, Ł_R)$
   - Generate a uniform random number and compare it to a. If a is bigger than the uniform random number, accept the proposed location otherwise keep the current location
5. Estimating the emitter location
   - Generate location samples for a given number of iterations by repeating the above process
   - Discard burn-in samples. The remaining set of samples represents the samples from target posterior distribution.
   - Estimate the emitter location by averaging samples from the target distribution

An example simulation output is shown in Fig. 4.13. In this figure, the actual emitter location is represented with a red circle at (2200 m, 7200 m) and the estimated location is represented with a green cross at (2600 m, 6500 m). The chain starts from the initial location (9750 m, 1250 m). The burn-in samples are in red and the remaining ones are in blue. Estimation is performed by calculating the expected value of the blue samples.

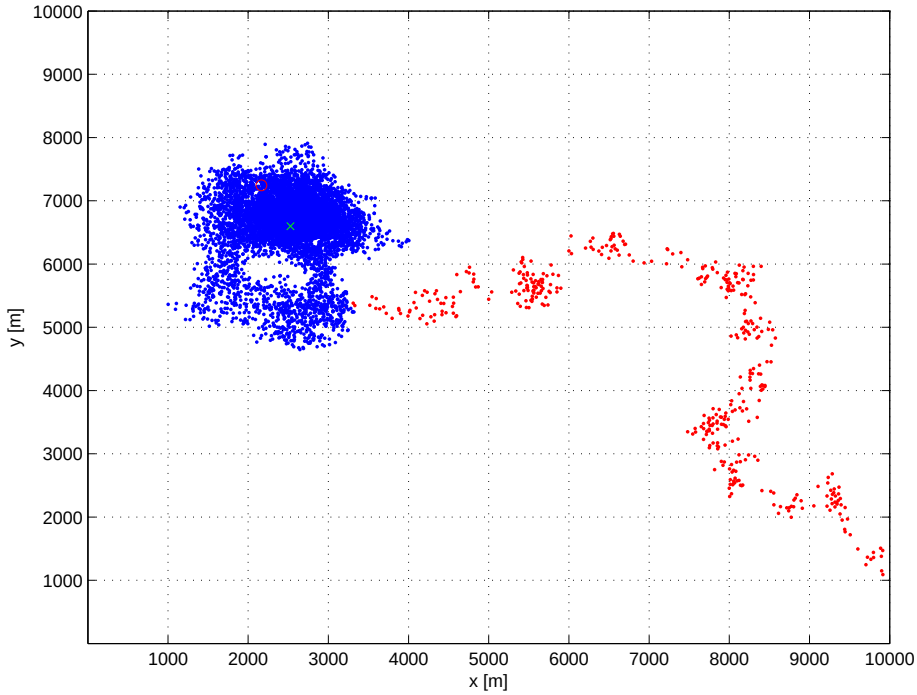

Figure 4.13: A simulation example: Single emitter localization using MCMC ($N_t = 1$, $N_s = 50$, $P_t = 1$ W, $L = 10$ km, $\alpha = 3.5$, $\sigma = 12$ dB, Markov chain starting point at (9750,1250) and end point at the vicinity of (2600,6500))

Performance Analysis of MH Algorithm

The performance of the MH based localization algorithm is compared to the CRLB under the following simulation conditions:

The primary emitter is located at the centre of the 1km by 1km square ROI and 16 sensors are placed at the centres of 250 m by 250 m grid locations. We assume independent log-normal shadowing of given dB spread and log-distance path-loss model with a fixed path-loss exponent of 4. The step-size of the MH algorithm, Δ is set to 200 m after a tedious fine tuning stage based on extensive trial and error process with a consideration of the value of proposed location being in the simulation area. In each simulation, the MH-algorithm is run for 10000 iterations and the first 1000 samples are discarded as burn-in samples. The performance results are presented in terms of the RMS of the estimation error given in (4.3). The calculated estimation error values and the resulting CRLB are plotted in Fig. 4.14 for shadowing spread values ranging from 1 to 12 dB. As shown in the figure, for shadowing values of 6 dB and under, the MH based location estimator gives similar performance to the CRLB, but above 6 dB the estimators performance degrades with the increasing dB values. Also shown in this figure is the performance of two interpolation based localization algorithms, nearest neighbor and linear interpolation methods, given in Section 3.2.2. These analyses have been made to compare the performance of MH algorithm with a simpler method of localization that can be obtained from an interpolated interference map [71], [72] which is generated by a given number of sensor measurements

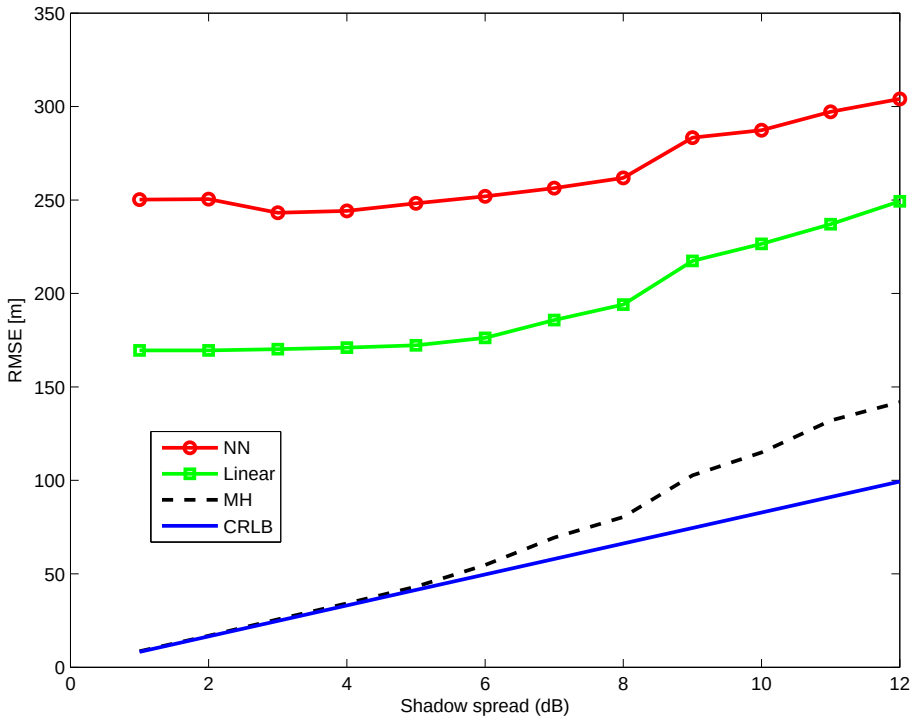

Figure 4.14: RMSE performances of MH and interpolation based techniques ($N_t = 1$, $N_s = 16$ uniformly placed sensors, $P_t = 1$ W, $L = 1$ km, $\alpha = 4$, $\Delta = 200$ m, number of iterations = 10000, number of burn-in samples = 1000)

and their locations. In these cases the performances at each shadowing spread value were obtained by averaging over 1000 different realizations of the shadowing noise. As seen from these curves, linear interpolation performs slightly better than the NN interpolation based localization, but both techniques perform poorly compared to the MH based localization algorithm.

However, the performance of the MH based localization technique is affected by several design parameters such as the selection of the proposal density and its parameters and the numbers of iterations and burn-in samples. Even though the algorithm is guaranteed to converge asymptotically, improper selection of the parameters may slow down the convergence leading to increased computational complexity. Particularly, if the Markov chain is initialized with a value far from the actual emitter location and the step size is small, then the chain will require large number of iterations to converge. In order to investigate the effect of parameter selection to the estimation error, we have simulated network scenarios where a primary emitter and 20 sensors are placed randomly chosen locations within the ROI. In these simulations, we evaluate the performance of the MH algorithm in terms of number of burn-in samples and iterations as well as the value of the step-size. Fig. 4.15 shows the performance as a function of number of MH iterations for different step-sizes. As seen from this figure, the performance is affected by the selection of step-size when the number of iterations is small. The best performance is achieved at $\Delta = 200$ m. As the number of iterations increases, the performance difference becomes negligible.

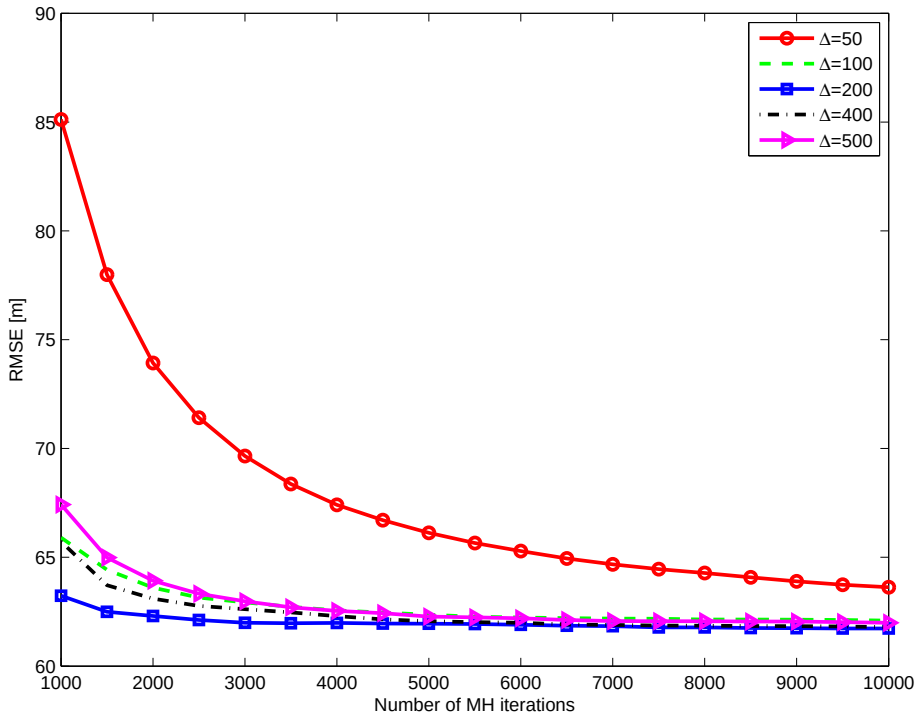

Figure 4.15: RMSE performance versus number of MH iterations for different step-sizes ($N_t = 1$, $N_s = 20$, $P_t = 1$ W, $\alpha = 4$, $\sigma = 6$ dB)

Fig. 4.16 shows the performance of the MH algorithm in terms of the number of burn-in samples for different step sizes. As seen from this figure, the number of burn-in samples does not affect the performance significantly except when the step-size is set to $\Delta = 50$ m. In this case, at least 2000 burn-in iterations are required for the algorithm to converge.

In order for improving the convergence and reducing the complexity of the MH estimator, a smart initialization technique is presented in Chapter 5. Our simulation results in Section 5.2 show that smart initialization of the MH algorithm eliminates tedious parameter tuning process and achieves significantly better localization performance compared to the randomly initialized MH algorithm at a fraction of iterations.

4.2 Multiple Emitter Localization

In this section, the MLE estimator discussed in the previous section for single emitter case is extended to multiple emitter localization problem. We begin the section by describing the challenges of multiple emitter localization. The MLE estimator used for multiple emitter localization require an analytical expression for sum of log-normal distributions. Therefore an investigation of sum of log-normal approximations is presented first. Among various approximations, Fenton-Wilkinson's approach has been chosen due to its simplicity and applicability to non-independent and identically distributed (non-iid) log-normal random variables that represent different mean received power values for each emitter sensor pair

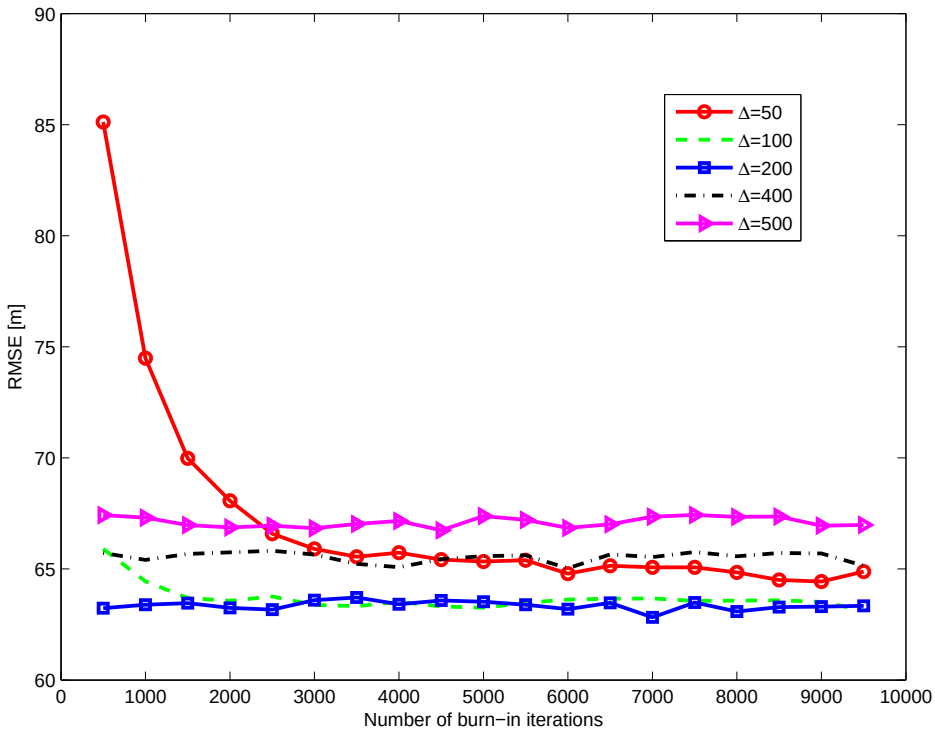

Figure 4.16: RMSE performance vs number of burn-in iterations for different step-sizes ($N_t = 1$, $N_s = 20$, $P_t = 1$ W, $\alpha = 4$)

in the network. We present performance analysis and simulation results of the estimation accuracy of this approach and propose a novel approximation that addresses weaknesses of the Fenton-Wilkinson's approach to achieve higher accuracy at high dB spread values. In our proposed approach, the pdf of sum of log-normals is estimated from a set of simulated data. The simulation results of the MLE based localization algorithm with the proposed approach is also presented.

4.2.1 Challenges of Multiple Emitter Localization

The localization problem in a non-cooperative wireless network is more challenging than the standard problem of localization since there is no cooperation or feedback with the transmitters. When only one transmitter is present, the transmitter location can be determined from three received power measurements via trilateration, or from a large number of sensors via the least-squares estimate. However when there are multiple transmitters contributing unknown portions of the observed power at each receiver, the non-cooperative localization problem does not allow a straightforward solution. In [58], an experimental study of transmitter localization performance is presented and it is stated that localizing multiple transmitters that are simultaneously active is too difficult when only signal strength is observed.

When there are multiple sources transmitting in the same band, energy detection tech-

niques are insufficient to localize the transmitters when they are simultaneously transmitting. This is because each transmitter contributes different unknown portions of power at the sensor nodes. Simple methods based on received power measurements are inconclusive. Isolating each transmitter based on the transmitters signature is essential to localize the transmitters in this scenario. There is a trade-off between the cost and complexity of the sensors. When we require complex signal processing algorithms in the cognitive radio sensors, the cost of the devices increases. Thus, there is a need for signal processing and detection algorithms which can be implemented at low cost. The time taken for localization directly impacts the time to find the white spaces in the spectrum. In highly dynamic networks, where white spaces do not last long, time to localize needs to be short so that secondary users can make better use of white spaces. Hence algorithms that take less time to localize are preferable in cognitive radio networks.

4.2.2 Investigation into Sum of Log-normals

The first step in all likelihood based parameter estimation techniques is to obtain the likelihood expression, which requires the knowledge of the pdf of the parameter to be estimated. In emitter localization problem, the received signal at the sensors will have a sum of log normal distribution in log-normal shadowing case when there are multiple emitters, as shown below.

Consider a scenario where there are N_s sensors measuring the received power r_{ij}, $j = 1, .., N_s$, and $i = 1, ..., N_t$ where N_t is the number of emitters transmitting simultaneously at the same frequency. When all emitters transmit at the same time, the received power at the sensor j will be r_j, which is the sum of the received powers due to all emitters:

$$r_j = \sum_{i=1}^{N_t} r_{ij} \tag{4.9}$$

where $r_{ij} = s_{ij} 10^{\frac{W}{10}}$ and $W \sim N(0, \sigma^2)$, s_{ij} is the mean received power at jth sensor due to ith emitter. W is a normally distributed random variable with zero mean and σ^2 variance, which is the shadowing variance or dB spread. Note that σ^2 is assumed to be known and same for each transmitter-receiver pair. Recalling that pdf of a log-normal variable z with scale parameters of μ_z and σ_z as plotted in Fig. 4.17 is,

$$f(z|\mu_z, \sigma_z) = \frac{1}{z\sigma_z\sqrt{2\pi}} e^{-\frac{(\ln(z)-\mu_z)^2}{2\sigma_z^2}} \tag{4.10}$$

then r_j will have a pdf that is a sum of log-normal distributions. However, there is no closed form expression for the pdf of the sum of log-normals.

The investigation of the pdf of sum of log-normals is an active research area and there is an extensive literature on this topic. A large portion of the effort in this area is focused on finding approximate analytic expressions for the pdf of the sum of log-normals. There exists several proposals for the analytic expression of the pdf of the sum of log-normals, with their weaknesses and strengths. For example, some of the proposals work only when the number

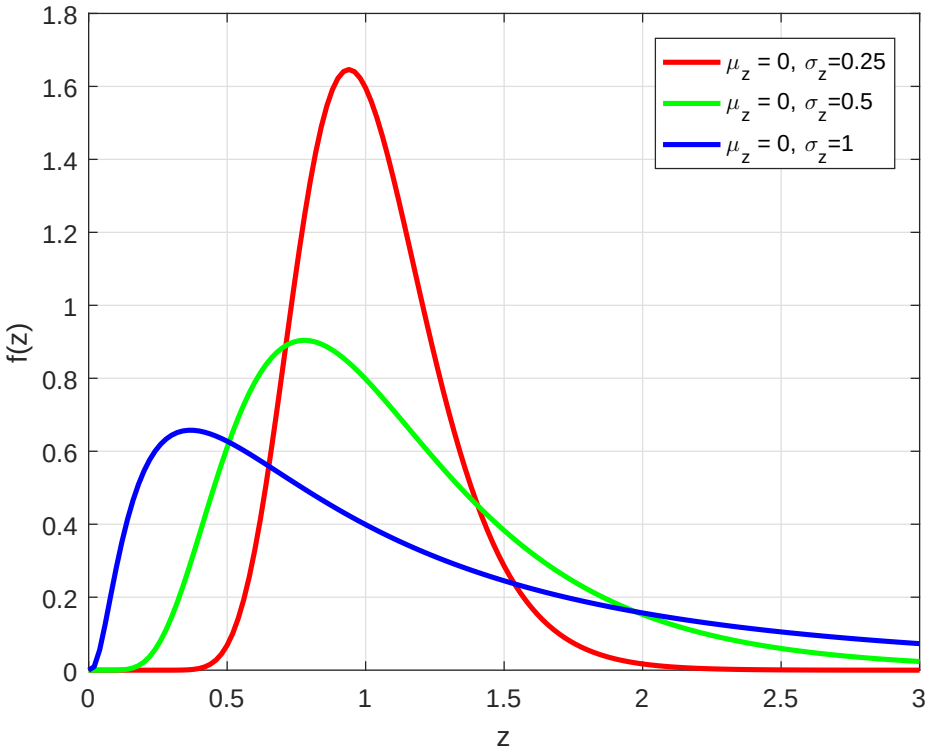

Figure 4.17: Examples of log-normal density functions with different scale parameters of μ_z and σ_z

of added log normal components is low whereas others work only for small shadowing spread values. Some of these approximations assume that the mean and/or variance of the added components are the same, i.e. the summands are assumed to be independent and identically distributed (iid) random variables. Besides, there is also complexity and implementation issues. Because search techniques require computing the likelihood function for a large number of iterations, it is also important to have a computationally efficient analytical pdf form.

Most of the proposed methods in the literature approximate the log-normal sum distributions with another log-normal random variable [9], [47], [64]. Fenton-Wilkinson [64], Schwartz-Yeh [64], Farley [64], and Beaulieu-Xie [9] methods are based on this approximation.

Fenton-Wilkinson method matches the first and second central moments of random variables in order to compute the mean and the standard deviation of the log-normal sum distribution. The method breaks down in computing the first and the second moments when standard deviation of the summands are more than 4 dB [64], [15]. Therefore, Fenton-Wilkinson method cannot compute these moments accurately when the shadowing spread values ranges from 4 to 12 dB. In contrast, Schwartz Yeah method performs very well in a wide range of standard deviations including the 4 to 12 dB range. The method can be applied to non-iid random variables and uses moments of the random variables in the log-domain [63]. However, this approach is much more complex than the straight for-

ward Fenton-Wilkinson method. Schleher method, a modified version of Fenton-Wilkinson method, is based on matching successively the first and the second, the second and the third, and the third and the fourth cumulants of the reference distribution against the cumulants of the sum distribution. Beaulieu-Xie method [9] maps the cdf of the log-normal sum in a log domain for probability by using a transformation that linearizes the log-normal distribution. With this mapping, a log-normal cdf is sketched as a straight line. Using a minimax approximation in the transformed domain, an optimal log-normal approximation to log-normal sum is achieved. The transformed domain magnifies the large and the small values of the probability; hence this method is only accurate on the approximation of the head and the tail of the cdf. The summands are assumed to be non-iid random variables and it is computationally too complex since it requires numerical integration for each summand having different mean and standard values.

Rajwani and Beaulieu [57] apply a curve fitting technique, on the cdf of the log-normal sum, which approximates the cdf very well. A log-normal cdf plots a straight line whereas the cdf of sum of log-normals plots a smooth curve and becomes increasingly convex as the number of log-normals increases. A parabolic function is considered to approximate the cdf curves and the coefficients of the parabola are determined for particular number of sums and dB spread values. The authors have used a nonlinear least squares method to optimize the values of the constants. The approximated pdf is shown to be accurate over a large dB spread range while Fenton-Wilkinson's approximation is only accurate for one tail of the pdf. This approximation assumes the mean values of summands are zero (iid random variables) but can be generalized to be different than zero. This method is more accurate than Fenton-Wilkinson's approach and the analytical approximation is not very complex. However, as the curve fitting parameters depend on the statistical characteristics of the non-iid random variables, and due to the diversity of these random variables, the computation is infeasible in practice.

In [1], a recursive approximation is proposed based on curve fitting to approximate the sum of two log-normally distributed random variables with identical standard deviations and different means. A recursive method based on surface fitting is developed for approximating the sum of more than two log-normal random variables. This method can approximate the first and the second moments of the resulting RV very well and has less complexity compared to Shwartz-Yeh method.

Assuming iid summands, Lian and Ding [84] apply a quadratic polynomial curve fitting technique on the pdf of the log-normal sum. The coefficients of the polynomial are determined based on the standard deviation and the number of summands. Mehta [47] deploy Gauss-Hermite expansion of the moment generation function to approximate the log-normal sum. Although the method has less complexity than Schwartz-Yeh method, it is still more complex compared to Fenton-Wilkinson, Beaulieu-Xie, Rajwani-Beaulieu, and Lian-Ding methods.

In the course of this thesis work, three major criteria are our concern for selecting the appropriate approximation for sum of log-normals pdf among various approximations studied in the literature. As we study multiple emitter localization problem by using the MLE method with the assumption of two transmitting emitters in the network, we need a

pdf approximation for only two summands of log-normals as the first criteria. Second, the approximation we are investigating for our problem needs to be applicable to non-iid log-normal random variables with different means and same standard deviation values since the total received power at the sensors due to two emitters will differ but the shadowing spread for every transmitter-receiver pair is assumed to be constant which is the most commonly used model in the literature. Third, the pdf approximation also needs to be easy to compute as the grid search algorithm requires likelihood calculations for every possible emitters' positions at grid centers.

Similar to our problem, in [48] the average power estimation problem of two transmitting sources which is based on the measurements of the power received by sensors that are placed in known locations in a given area is studied. The randomness in the received power collected by the sensors is introduced by the shadow fading component which is modelled as log-normally distributed random variable in the paper, therefore resulting in a sum of log normal distributed sensor measurements. The authors in [48] use Fenton and Wilkinson approximation for the sum of log-normals pdf. This simple approximation is based on the assumption that the sum of log-normal distributions can be modelled as another log-normal pdf with given mean, s_j and variance $\sigma_{sum_j^2}$ given as follows.

$$f(r_j|s_j,\sigma^2_{sum_j}) = \frac{1}{r_j\sigma_{sum}\sqrt{2\pi}} e^{-\frac{(\ln(r_j)-s_j)^2}{2\sigma^2_{sum_j}}} \tag{4.11}$$

where

$$s_j = \ln\Big(\sum_{i=1}^{N_t} s_{ij} + \epsilon^2\frac{\sigma^2}{2} - \frac{\sigma^2_{sum_j}}{2}\Big) \tag{4.12}$$

$$\sigma^2_{sum_j} = \ln\Big((e^{\epsilon^2\sigma^2}-1)\frac{\Sigma_{i=1}^{N_t} s_{ij}^2}{(\Sigma_{i=1}^{N_t} s_{ij})^2} + 1\Big) \tag{4.13}$$

and $\epsilon = \frac{\ln 10}{10}$. Here s_j represents the total mean received power at the jth sensor and r_j represents the received power affected by shadowing at the same sensor. s_{ij} represents the portion of s_j due to ith emitter. σ^2, which is assumed to be known, is the variance of log-normal shadowing and same for all sensor-emitter pairs. $\sigma_{sum_j^2}$ is the variance of the log-normal sum.

In Section 4.2.3, we have performed a preliminary analysis of this approximation technique to see its applicability to our problem. By using this approximation, one can write the likelihood expression Ł for multiple emitter localization problem under independent log-normal shadowing:

$$
\begin{aligned}
Ł &= \prod_{j=1}^{N_s} \frac{1}{r_j \sigma_{sum_j}\sqrt{2\pi}} e^{-\frac{(\ln(r_j)-s_j)^2}{2\sigma^2_{sum_j}}} \\
&= \frac{1}{r_1 \sigma_{sum_1}\sqrt{2\pi}} e^{-\frac{(\ln(r_1)-s_1)^2}{2\sigma^2_{sum_1}}} \frac{1}{r_2 \sigma_{sum_2}\sqrt{2\pi}} e^{-\frac{(\ln(r_2)-s_2)^2}{2\sigma^2_{sum_2}}} \ldots \frac{1}{r_{N_s} \sigma_{sum_{N_s}}\sqrt{2\pi}} e^{-\frac{(\ln(r_{N_s})-s_{N_s})^2}{2\sigma^2_{sum_{N_s}}}}
\end{aligned}
\tag{4.14}
$$

By taking the logarithm of (4.14) and following the steps given in Appendix B.2, the log-likelihood expression becomes:

$$
\ln(Ł) = -\sum_{j=1}^{N_s} \ln(r_j \sigma_{sum_j}) - \frac{1}{2} \sum_{j=1}^{N_s} \frac{(\ln(r_j) - s_j)^2}{\sigma^2_{sum_j}} \tag{4.15}
$$

Our preliminary experimentation with (4.15) shows that even though the analytical expression is suitable for our multiple emitter localization problem, its performance degrades at high shadowing spread values (refer to Section 4.2.3). Therefore, we propose a novel sum of log-normal pdf approximation that is also accurate at high shadowing spread values, specifically greater than 6dB in the next section.

4.2.3 A Sum of Log-normal Approximation from Simulated Data

In this section, we introduce a technique to find approximations to the sum of log-normal distributions. The proposed three stage approach is given as follows:

Stage 1: Simulate random numbers from the desired distribution Let Y_1 and Y_2 be two log-normally distributed random variables with means μ_1 and μ_2 and standard deviations σ. Here μ_1 and μ_2 represent the portion of mean received power values at a sensor due to each emitter, i.e. s_{1j}= μ_1 and s_{2j}=μ_2 in (4.9) and σ represents the dB spread of shadowing for an emitter-receiver pair. Then $Y = Y_1 + Y_2$ will have a sum of log-normal distribution with parameters μ_j, σ_{sumj} which are functions of μ_1, μ_2 and σ. Here μ_j represents the total mean received power s_j at the jth sensor.

$Y_1 \sim LN(\mu_1, \sigma)$

$Y_2 \sim LN(\mu_2, \sigma)$

$Y = Y_1 + Y_2, Y \sim SLN(\mu_j, \sigma_{sumj})$ where $\mu_j = f_1(\mu_1, \mu_2, \sigma)$ and $\sigma_{sumj} = f_2(\mu_1, \mu_2, \sigma)$

Therefore, in order to generate a random variable that has a sum of log-normal distribution, two log-normal random variables Y_1 and Y_2 are simulated and then added.

Stage 2: Generate a candidate model set using simulated numbers A set of a number of candidate pdfs are generated based on simulated data. This is an ad hoc approach where candidates can be determined intuitively by using the empirical distribution (e.g. histogram) of the simulated data generated in Stage 1. If, for example, the empirical pdf looks like a gamma distribution, then a gamma pdf is included in the template set. Other candidates can be added into the set based on their use in the literature. For example, a widely accepted approximate form of a sum of log-normal distribution is another log-normal distribution; therefore it can be used as a candidate solution in our approach.

Stage 3: Evaluate the merit of each candidate solution The merit of each candidate solution is calculated and the candidate that provides the largest merit is selected. In this work, we use the likelihood value as a measure of merit. The likelihood of observing the simulated data for each proposed template function is calculated and the one that provides the largest likelihood value is selected as the best fit among other proposals.

A simulation study has been performed with the following assumptions to test the proposed approach: Mean received power values μ_1 and μ_2 at a sensor due to two emitters is bounded in between -100 dBm and 0 dBm. Using a resolution of 1 dB, $101x101 = 10,201$ combinations of mean received power values (μ_1, μ_2) are generated and stored in a look-up table (LUT). Even though the received power values in LUT range from -100 dBm to 0 dBm, only power values between -16 dBm and -82 dBm are used for localization in the scenarios defined in Section 4.2.5.

We generate one million random numbers from two different log-normal distributions with (μ_1, σ) and (μ_2, σ) for each (μ_1, μ_2). These simulated data are then summed up to obtain random numbers with sum of log-normal distributions.

We fit gamma, log-normal, and Gaussian mixture distributions to simulation data. We estimate the parameters of gamma and log-normal distribution using maximum likelihood technique whereas the parameters of Gaussian mixtures are estimated by using expectation maximization (EM) technique.

Once the parameters μ_j and σ_{sumj} are estimated for each distribution, then the likelihood of observing the simulated data for each proposed model is calculated. The distribution fit that gives the highest likelihood value is selected.

In our simulations, the log-normal model provided the best fit as shown in Figures 4.18 and 4.19. Fig.4.18 shows the likelihood difference between log-normal and gamma distributions, and Fig.4.19 shows the likelihood difference between log-normal and Gaussian mixture (with 2 mixtures) distributions, for a shadowing spread of 6 dB. As seen from these two figures, the likelihood differences for every μ_1 and μ_2 values are always greater than zero which means that the likelihood of observing the simulated data under log-normal distribution is higher than that of gamma and Gaussian mixtures distributions.

There are well-known sum of log-normal approximations in the literature. For example, Fenton technique is a simple and computationally efficient approach that fits a log-normal distribution to sum of log- normals by matching first and second central moments of random variables [48]. Therefore it is interesting to investigate how our proposed approach

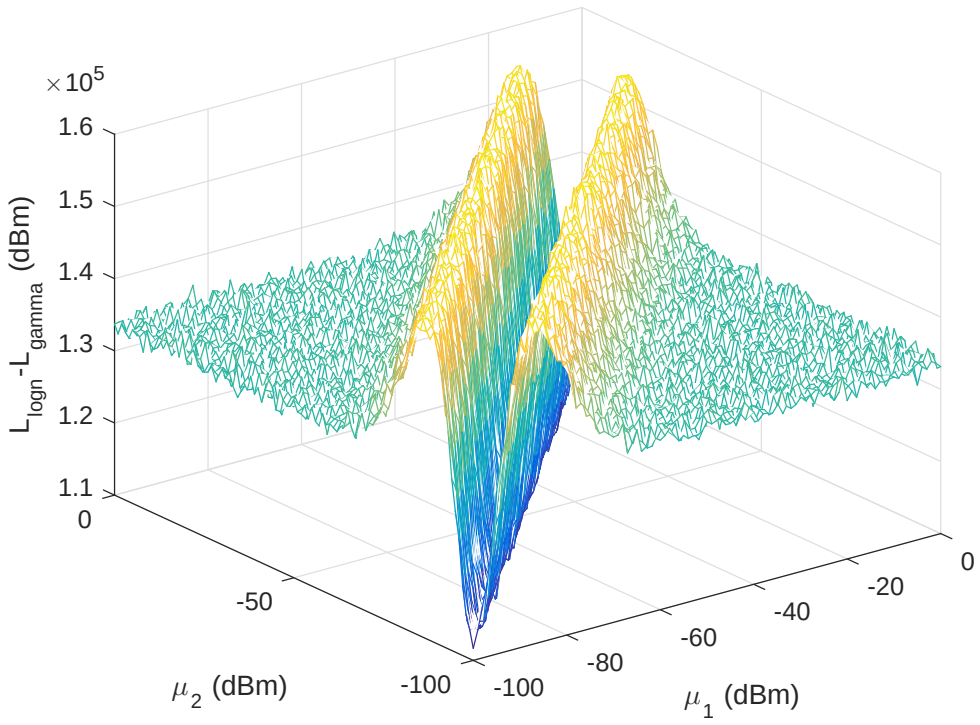

Figure 4.18: Likelihood difference between log-normal and gamma approaches ($\sigma = 6$ dB)

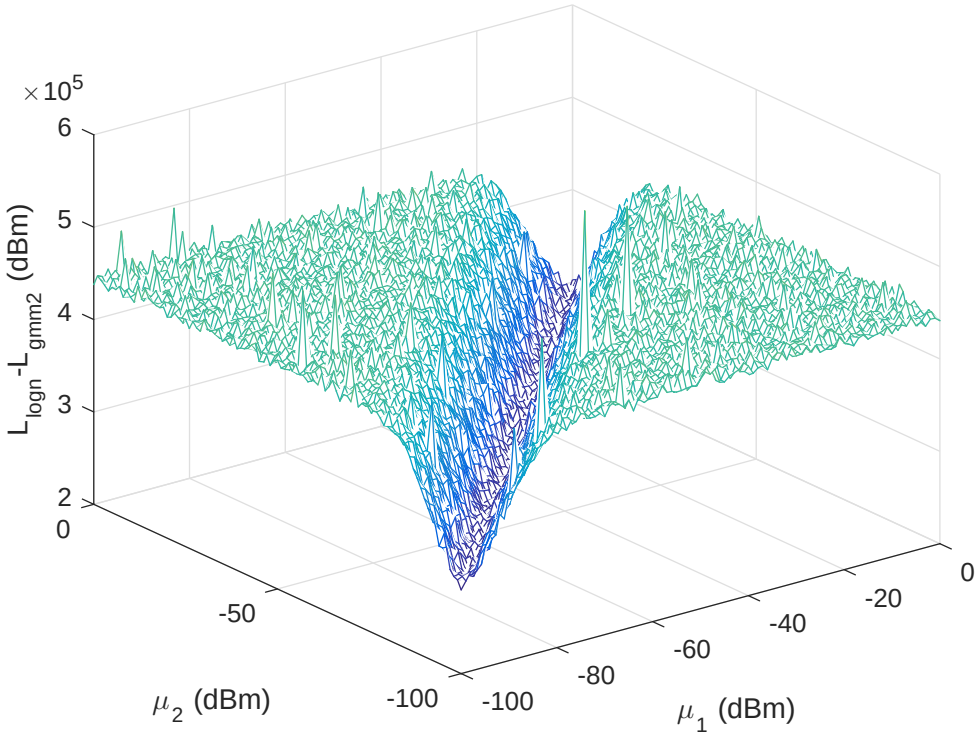

Figure 4.19: Likelihood difference between log-normal and Gaussian mixture (2 mixtures) approaches ($\sigma = 6$ dB)

compares with Fenton's technique. In order to compare the two approaches, we compare their localization errors using the grid search technique which is described in the next section.

4.2.4 Multiple Emitter Localization Using Grid Search

In this section we study the localization of two emitters, transmitting at the same frequency with known and equal transmit power in the ROI by using the full grid search method. The grid search algorithm required to localize two emitters is similar to the algorithm described in Section 4.1.2 for single emitter case scenario and it is summarized below.

The search space is divided into a number of grids and the grid locations are set as grid centers. To do the full search, the first emitter is placed at the first grid and the second emitter is placed at the rest of the grid locations successively. Then the first emitter is placed to the next grid and the second emitter is placed at the remaining grid locations. This is repeated for all unique emitter pair location configurations. Repeated emitter location configurations are unnecessary, therefore they can be omitted to reduce complexity. The likelihood of observing the received power measurements at all sensors is calculated for each unique configuration using the equation (4.15). The emitter pair configuration which gives the maximum calculated likelihood value determines the estimated locations. Thus, the centers of the grid pair for that particular configuration are selected to be the estimated locations of the two emitters. Since the transmit power values of the emitters are equal, a matching of the estimated locations to emitters is not required. It should also be noted that, unlike the assumption we make here, the emitter power is not known for single emitter localization problem studied in Section 4.1.2 and values of the cost function that depends on the power estimations are calculated instead of likelihood values at grid locations.

4.2.5 Comparison of the Proposed Approach with Fenton's Approximation

In order to compare the localization performance of the sum of log-normal approach proposed in Section 4.2.3 with Fenton's approach, the grid search algorithm is applied to 4 different case scenarios (small/large area and dense/sparse GSM network) with the given network assumptions and constraints.

For all of our scenarios, we consider a micro cellular network with a cluster size of 3 and a cell size of 100 m. The reuse distance which is the required distance between base stations in each cell transmitting at the same frequency is then calculated as, $cellsize\sqrt{3clustersize} =$ 300 m. This determines a constraint on the emitter geometry. Therefore, the transmitters using the same frequency are assumed to be separated by at least 300 m, reflecting the physical reality that primary transmitters using the same frequency band would interfere if they were too close together. The second constraint is, all sensors are assumed to be at least twice the reference distance (assumed to be 1 m for our simulations) from all emitters.

This is a constraint required to guarantee that the log-distance propagation model yields realistic results [28] and taken as 10 m or 100 m depending on the given network scenario. The minimum distance between sensors is also taken as 10 m or 100 m depending on the selected network scenario. We set the frequency of transmit power to 900 MHz which is a typical value of frequency of a GSM operator and the propagation exponent to 2.5. Received power values measured at sensors vary between -82 dBm and -16 dBm. Hence the minimum received power is above the receiver sensitivity which is typically -112 dBm and less than maximum input power rating, that is typically 10 dBm. Considering each emitter pair location configuration and each sensors location, parameter (μ_j, σ_{sumj}) is calculated using the LUT prepared in Section 4.2.3. For Fenton's approach, parameters are calculated directly by using the two equations, 4.12 and 4.13. Likelihood values for both approaches are then calculated by using the derived equation in 4.15. The overall localization error is calculated by averaging the two estimation errors e_1 and e_2, which are the estimation errors for the first and the second emitter respectively. 500 simulations are run for dB spread values of 1 to 10 dB. The resulting figures are given in from Fig. 4.20 to Fig. 4.23 for four scenarios.

Scenario 1: Small area, dense network In this scenario, 100 sensors and two emitters are randomly deployed in a 1 km by 1 km square area. All sensors are placed at least 10 m apart from the emitters and from each other. The emitter power is 1 W. The grid size is chosen as 50 m. In this configuration, the received power values at sensors vary between -70 dBm and -17 dBm. The localization error for this configuration is plotted in Fig. 4.20.

Scenario 2: Small area, sparse network In this scenario, 20 sensors and two emitters are randomly deployed in a 1 km by 1 km square area. All sensors are placed at least 10m apart from the emitters and each other. The emitter power is 1 W. The grid size is chosen as 50 m. In this configuration, the received power values at sensors vary between -70 dBm and -17 dBm. The localization error for this configuration is plotted in Fig. 4.21.

Scenario 3: Large area, dense network In this scenario, 100 sensors and two emitters are randomly deployed in a larger square area of 3 km by 3 km. All sensors are placed at least 10 m apart from the emitters and each other. The emitter power is 10 W. The grid size is chosen as 150 m. In this configuration, the received power values at sensors vary between -82 dBm and -16 dBm. The localization error for this configuration is plotted in Fig. 4.22.

Scenario 4: Large area, sparse network In this scenario, 20 sensors and two emitters are randomly deployed in a larger square area of 3 km by 3 km. All sensors are placed at least 100 m apart from the emitters and each other. The emitter power is 10 W. The grid size is chosen as 150 m. In this configuration, the received power values at sensors vary between -82 dBm and -42 dBm. The localization error for this configuration is plotted in Fig. 4.23.

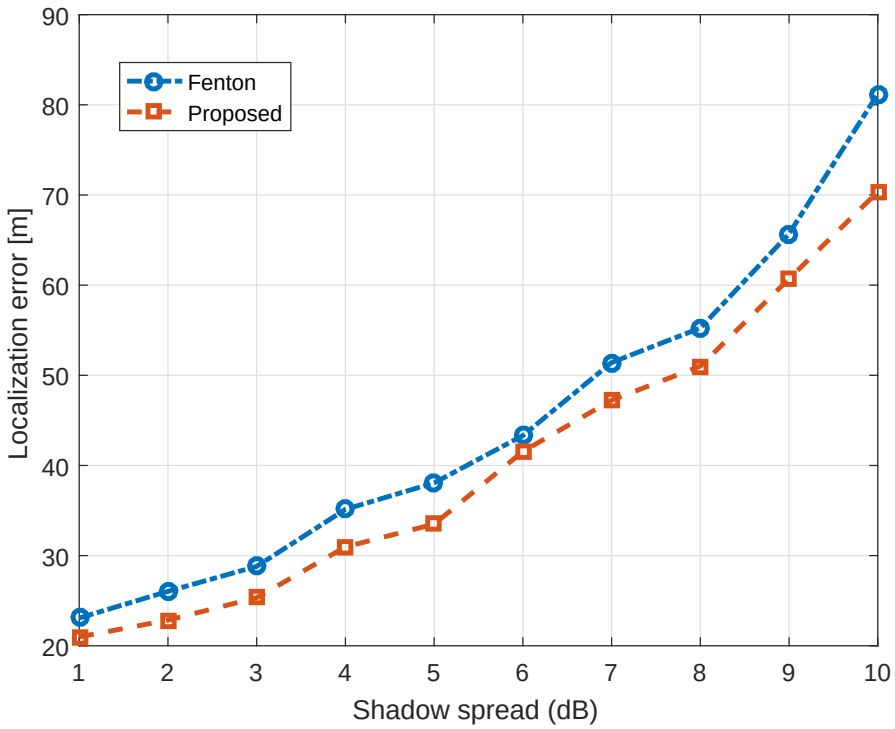

Figure 4.20: Localization error for scenario 1 ($N_t = 2$, $N_s = 100$, $\alpha = 2.5$, $L = 1$ km, $P_t = 1$ W, frequency = 900 MHz, grid size = 50 m)

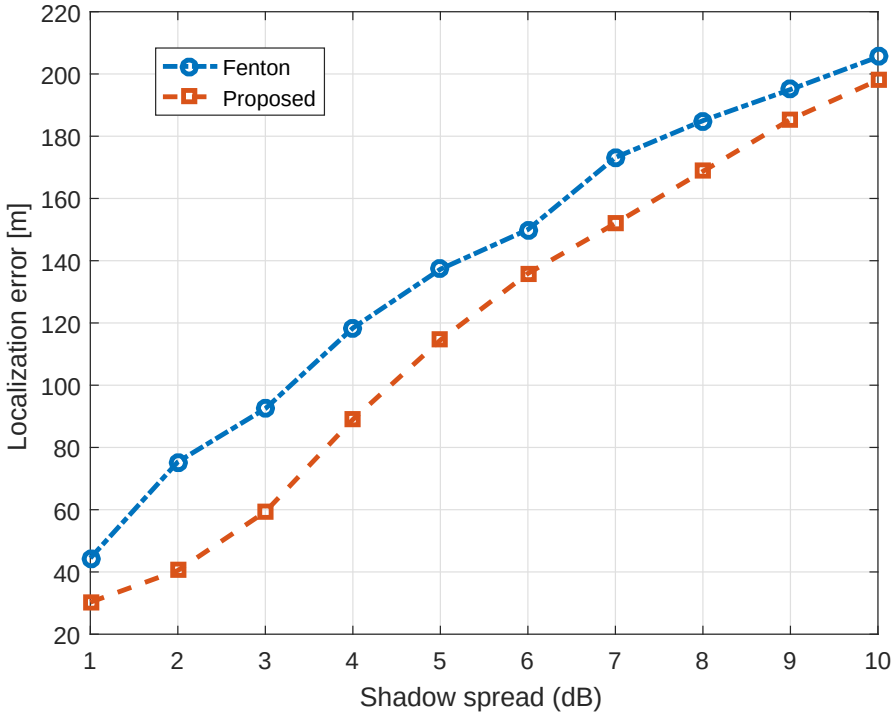

Figure 4.21: Localization error for scenario 2 ($N_t = 2$, $N_s = 20$, $\alpha = 2.5$, $L = 1$ km, $P_t = 1$ W, frequency = 900 MHz, grid size = 50 m)

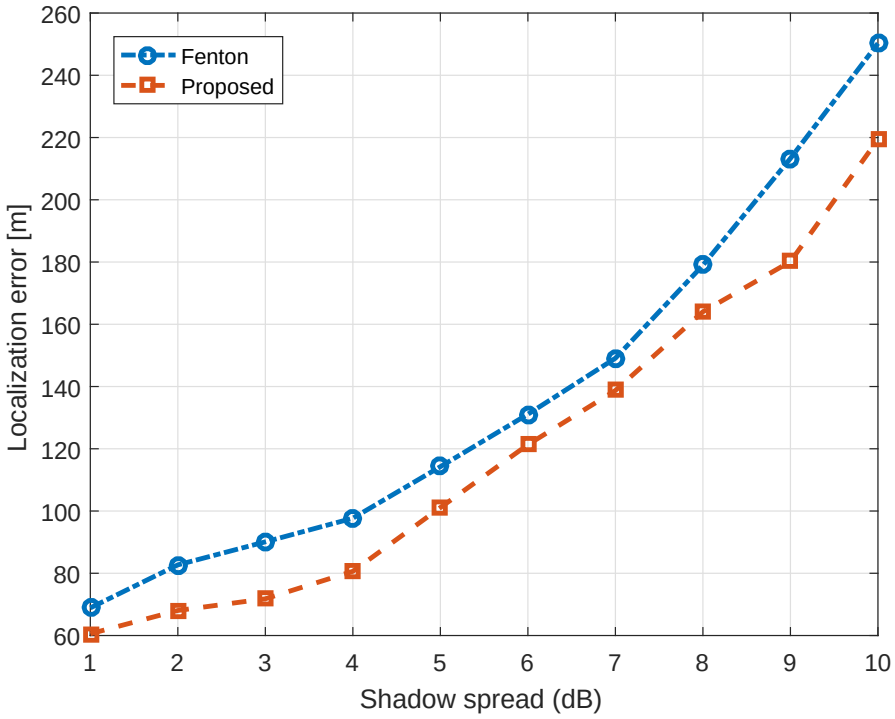

Figure 4.22: Localization error for scenario 3 ($N_t = 2$, $N_s = 100$, $\alpha = 2.5$, $L = 3$ km, $P_t = 10$ W, frequency = 900 MHz, grid size = 150 m)

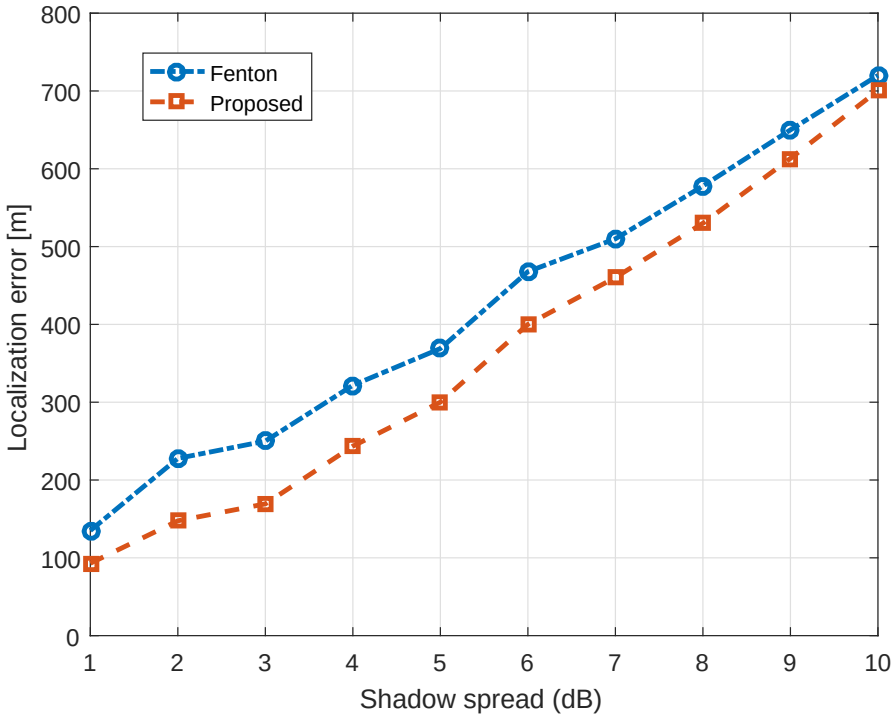

Figure 4.23: Localization error for scenario 4 ($N_t = 2$, $N_s = 20$, $\alpha = 2.5$, $L = 3$ km, $P_t = 10$ W, frequency = 900 MHz, grid size = 150 m)

As can be seen from Figures 4.20 to 4.23, the proposed pdf approximation approach outperforms Fenton's approach for all shadowing spread values.

Chapter 5

Complexity Reduction

In this chapter, we study the complexity reduction of the localization algorithms studied in Section 4.1.2 and 4.1.4. We present different iterative grid search techniques and smart initialization of MCMC techniques with their performance analysis.

5.1 Iterative Grid Search

In Section 4.1.3, we pointed that a major disadvantage of the MLE method we have studied in the thesis is its computational complexity. As we recall, it is based on a full grid search method and requires the algorithm to scan all possible grid points in the localization space. To obtain more accurate location estimates with this method, the size of the grid elements needs to be small and smaller grid size yields in increased number of computations, particularly when the algorithm does not use any scheme to reduce the complexity. The algorithm becomes even more complex for multiple primary emitter localization problems as it increases the calculation of the likelihood function for all grid points related with the number of primary emitters considered in the network. To address this problem, we propose an iterative grid search algorithm for locating the primary emitters with unknown power in this section. This technique is based on dividing the search space into a smaller number of candidate sub regions, selecting the best candidate that minimizes a cost function and repeating the process iteratively over the selections. We evaluate the performance of the proposed algorithm in independent shadowing scenarios and compare it with the performance of full search while comparing their complexity. We also look at the performance of our algorithm when the initial search space is specified based on two different data-aided approaches relying on sensor measurements. In contrast to the exhaustive full grid-search algorithm, the iterative grid-search avoids the complexity problem without significant performance loss.

5.1.1 Regular Iterative Grid Search

The proposed **iterative grid-search** algorithm is based on refining search space based on the minimization of the cost function given in (4.7). The performance of this method is studied and compared with the performance of the full search method under different grid-spacing values and/or with different number of iterations and the limits of the solution is also determined.

The iterative grid search algorithm can be initialized in different configurations based on the initial selection of the search partitions. For example, for a 2x2 partitioning, the ROI is divided into four quadrants and initial candidate locations are set at the centres of each quadrant. After calculating the cost function at each candidate location, search space is reduced to one fourth of the previous search area and it is re-centred at the location that provides the minimum of the calculated cost values. The iterations are run in this way for a given number of levels to achieve a desired grid resolution. An example of 2x2 partitioning ($Q = 4$) is illustrated in Fig. 5.1 for a 3 level iteration ($I = 3$) where level is the number of iterations. In this example, the same sensor and emitter placement of Fig. 4.6 is used. In the first iteration the cost values of 42, 646, 447 and 831 are obtained. Then in the second iteration the cost values of 185, 177, 35 and 19 are obtained. Finally at the third iteration values of 1, 31, 40 and 91 are obtained. As seen from the figure, the minimum cost values of 42, 19 and 1 are achieved at successive iterations. At the end of the third iteration, the emitter location is estimated to be the centre of the grid that results in minimum cost value of 1. In the figure the actual emitter location is shown with red diamond whereas the estimated location is shown with green square. Similarly higher number of partitions can be obtained by dividing the ROI into smaller areas. Increased partitioning reduces the grid resolution, however it results in increased number of computations as well.

As the iterative grid search algorithm requires computation of the likelihood function for each grid location at each iteration, the total number of required computations is given by QxI where Q is the number of grid elements (tiles) at each iteration and I is the number of iterations or levels. The computational complexity of this method is related with the iteration number and grid-spacing. The grid size at any iteration can be formulized as,

$$Gridsize = \frac{L}{Q^{\frac{I}{2}}} \tag{5.1}$$

where L is the length of square search area.

The algorithm for a square search area can be summarized as follows:

1. Initialize the iterations
2. Divide the given area into Q equal tiles depending on the defined grid spacing that is $\sqrt{Q}$ by $\sqrt{Q}$.
3. Calculate the metric at the center of each grid.

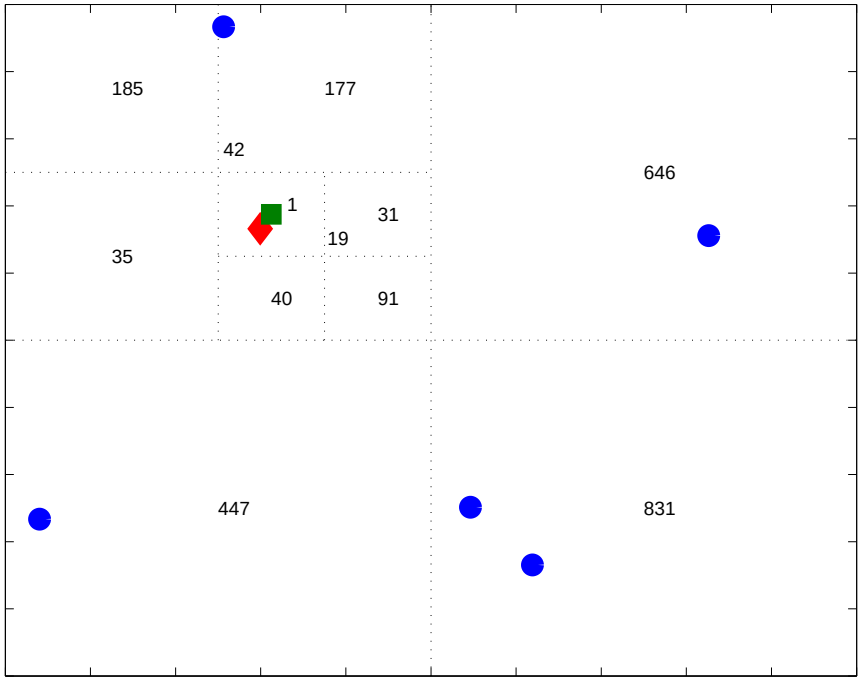

Figure 5.1: An example of 3 level 2x2 partitioning for iterative grid search ($N_t = 1$, $N_s = 5$, $L = 1$ km, $P_t = 1$ W)

4. Find the grid that has the minimum metric value and increase the iteration number. The center of this grid will be center of the search space at the next step.

5. Follow the algorithm from step 2 dividing the grid that was found in step 4 into Q smaller grids until the iteration number reaches to a defined value I.

6. The center of the grid that gives the minimum metric at the last iteration is estimated to be the emitter location.

Note that if the search area is a rectangle instead of a square assumed as above, then first divide the area into two squares and run the algorithm for one of the squares that has the minimum metric value at its center.

In order to evaluate the performance of the full search method with different grid sizes, we simulate random networks with 50 nodes and ran 1000 simulations at each dB spread value ranging from 0 to 12 dB for grid lengths of 10, 20, 25, 40, 50 and 100 m. The emitter power is assumed to be unknown and the path-loss exponent is assumed to be 3.5. The performance results are presented in terms of mean of the location estimation error, ME which is defined by

$$ME = \frac{1}{H} \sum_{i=1}^{H} \sqrt{(T_x - \hat{T}_x)^2 + (T_y - \hat{T}_y)^2} \tag{5.2}$$

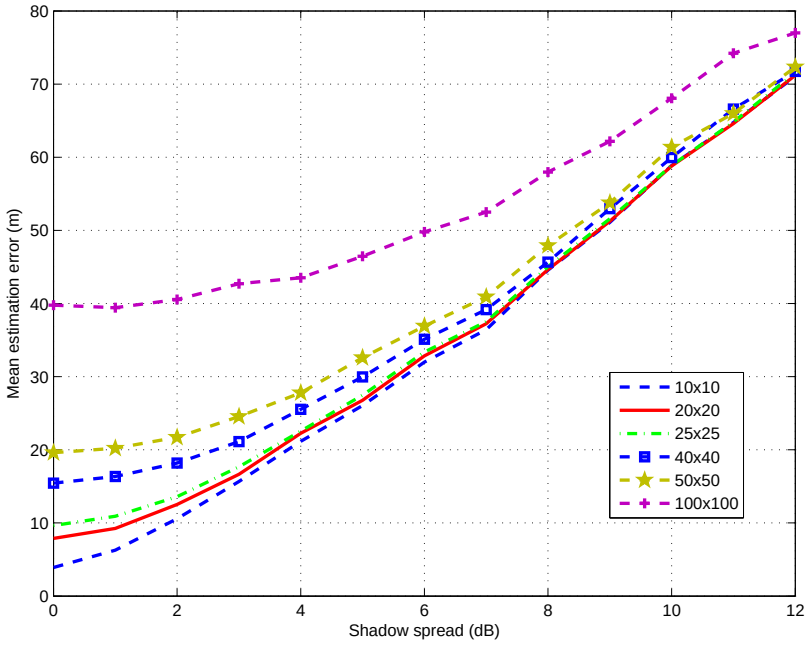

Figure 5.2: Full grid search performances with different grid sizes ($N_t = 1$, $N_s = 50$, $L = 1$ km, $\alpha = 3.5$, $P_t = 1$ W)

where (T_x, T_y) is the actual emitter location, $(\hat{T}_x, \hat{T}_y)$ is the estimated emitter location in ith simulation and H is the number of Monte Carlo simulations. The mean localization error is shown in Fig. 5.2. As seen from the figure, the grid search method performs better with the decreased grid size. However, the number of cost function calculations increases significantly with the reduced grid size. For grid sizes of 10, 20, 25, 40 and 50 m, the full search requires 10000, 2500, 1600, 625 and 400 cost function calculations, respectively. Note that, in Fig. 5.2 the mean localization error values are less than the maximum quantization error values induced by the grid size, that is $\frac{gridsize}{2}\sqrt{2}$ for each selected grid size at zero dB shadow spread, as expected. The error values at zero dB spread are 3.90, 7.88, 9.64, 15.44, 19.61 and 39.76 m for grid sizes of 10, 20, 25, 40, 50 and 100 m respectively. The analytical calculation of two dimensional quantization error in grid search method for zero shadowing spread, can also be found in Appendix C.

For performance evaluations of the iterative grid search algorithm, we run 1000 Monte Carlo simulations for 4 and 9 levels of 2x2 and 4x4 partitions. We evaluate the performance of the algorithm at different shadow spread values ranging from 0 to 12 dB. The results are shown in Fig. 5.3. Also shown in the figure is the performance of full grid search with a grid size of 10 m. As seen from this figure, the performance of the iterative grid search improves with an increase in the number of partitions and levels when the dB spread is less than 6 dB. However, when the dB spread is higher than about 6 dB, increasing the number of levels and/or the number of partitions does not improve the performance. For lower dB spread values the performance of 9 level 4x4 iterative grid search is very close to that of full search. The full search requires 10000 calculations whereas 9 level 4x4 iterative search requires only 144 calculations. The final grid size values at the last iteration for 4

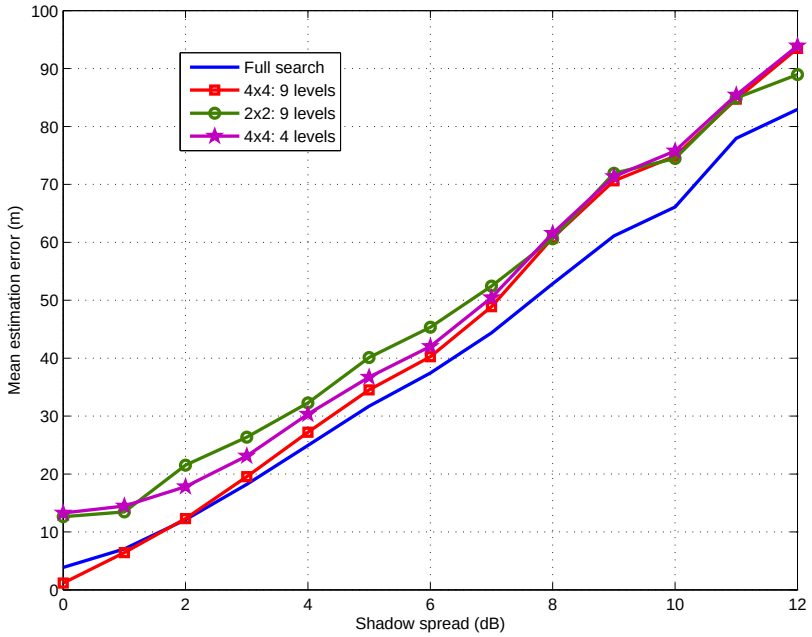

Figure 5.3: Performance comparison of full and iterative grid search vs shadowing spread ($N_t = 1$, $N_s = 50$, $L = 1$ km, $\alpha = 3.5$, $P_t = 1$ W, grid size for full search = 10 m, final grid size for 4x4 9 levels = 0.0000038 m, final grid size for 2x2 9 levels = 0.002 m, final grid size for 4x4 4 levels = 0.004 m)

and 9 levels of 2x2 and 4x4 partitions are also calculated using (5.1) and are given in the same figure.

We also evaluate the performance of the algorithm with different number of sensors ranging from 20 to 80 at a shadow spread of 6 dB and the results are shown in Fig. 5.4. As seen from the figure, the gap between the full and the iterative grid searches decreases as the number of sensors increases.

5.1.2 Search Space Initialization

Our regular iterative algorithm sets a search space centered at the origin of the ROI and it does not rely on any sensor measurements or sensor measurement related metric in setting the initial search space. In this section, we look at the performance of the iterative algorithm when the initial search space is set based on two different approaches. The first approach sets the search space around the sensor that reports the highest RSS (**the maximum approach**). The rational is that the sensor reporting the maximum RSS is more likely to be closer to the emitter than the rest of sensors. Even though this is true when the shadow spread is low, the condition may not be satisfied when the closest sensor is blocked by obstacles (hidden node problem). This approach is used in [34] to locate sound sources. In the second approach, the cost metric in (4.7) is calculated at a very close neighbourhood of each sensor location. This metric generates local maxima at the sensor neighbourhood and the sensor location that results in the minimum of these maxima is set

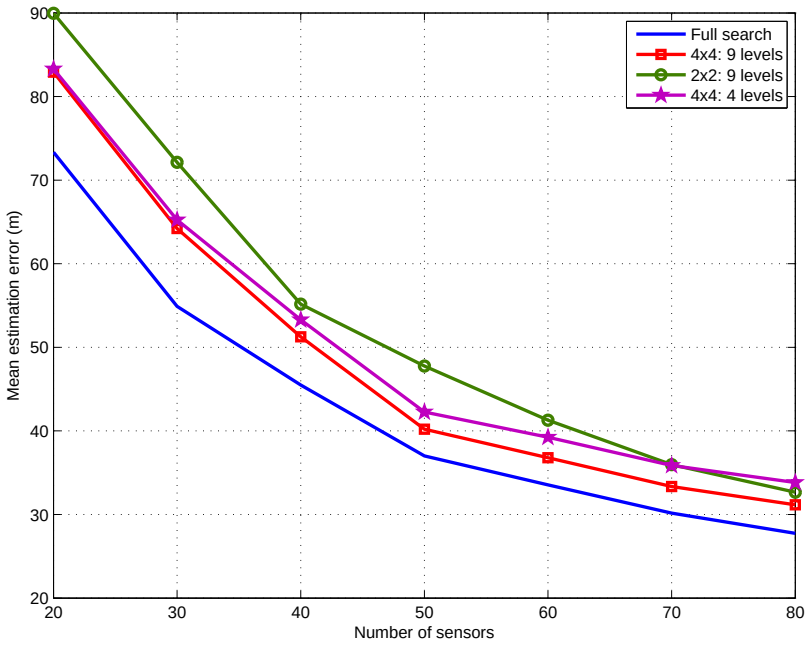

Figure 5.4: Performance comparison of full and iterative grid search vs number of sensors ($N_t = 1$, $\sigma = 6$ dB, $\alpha = 3.5$, $L = 1$ km, $P_t = 1$ W, grid size for full search = 10 m, final grid size for 4x4 9 levels = 0.0000038 m, final grid size for 2x2 9 levels = 0.002 m, final grid size for 4x4 4 levels = 0.004 m)

as the centre of the search space (**the minimax approach**). It is reported in [56] that this approach outperforms the naive approach that searches around the receiver reporting the largest RSS in emitter localization in shadow fading. Both the maximum and the the minimax approaches delimit a small geographical area that is the neighborhood of a prior location for initial search space. The prior location for the maximum approach is the sensor's location reading the maximum RSS whereas for the minimax approach, it is the sensor's location that gives the minimum of maximum cost function values as defined above. In contrast, the regular iterative grid search sets the whole ROI for the initial search space without having a prior knowledge of emitter's location.

We compared the performances of search space initialization schemes at different shadow spread values ranging from 0 to 12 dB for 9 level 2x2 partitions. At each dB spread value, we have performed 1000 Monte Carlo simulations and mean estimation errors are plotted in Fig. 5.5. In this figure, the maximum approach sets the search space around the sensor that reports the maximum RSS whereas the minimax approach sets the search space around the sensor that results in the minimum of maximum cost values. Both techniques use a search space of $L/2$ by $L/2$ whereas our proposed regular iterative approach performs the search inside L by L square centred at the origin. Here L is the length of the square search area. As seen from this figure, the minimax approach performs better than the maximum approach; however the regular approach outperforms both the minimax and the maximum approaches at higher dB spread values. Note that the minimax approach requires N_s additional cost function calculations compared to the maximum and the regular

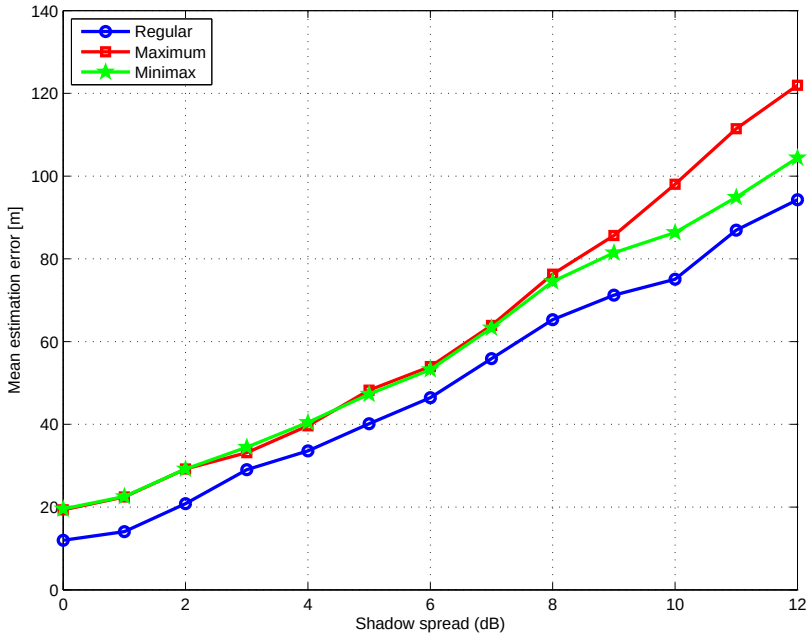

Figure 5.5: Performance comparison of regular, maximum and minimax approaches vs shadow spread for 9 level 2x2 partitions ($N_t = 1$, $N_s = 50$, $\alpha = 3.5$, $L = 1$ km, $P_t = 1$ W)

approaches.

In order to evaluate the effect of initial search space size on the performance of maximum and minimax approaches, we have performed simulations using different search space sizes of L, $L/4$, and $L/8$ in addition to $L/2$. However, this evaluation is not applicable for the regular iterative search approach since the emitter's location might be missed with any of the $L/2$, $L/4$, and $L/8$ initial space size selections due to the lack of a prior knowledge of emitter's location unlike the other two approaches. The performances of the maximum and the minimax techniques with different search space sizes are shown in Figs. 5.6 and 5.7, respectively. As seen from these figures, setting the initial search space too large or too small deteriorates the performances significantly. Comparing these figures to Fig. 5.5 reveals that the regular approach outperforms the two techniques irrespective of the initial search space size.

5.2 Smart Initialization of MCMC Methods

The iterative grid search method proposed to reduce the computational complexity of the full grid search method without significant performance loss, has coarser resolution at earlier stages. Therefore it is possible that the global minimum of the cost function given in (4.7) is sometimes missed, especially when the uncertainty is high due to larger shadowing spreads. The MCMC method we have proposed in Section 4.1.4 to address the problems of full grid search method can also address this problem, i.e. global minimum won't be missed, as the MCMC algorithm is guaranteed to converge as long as sufficient

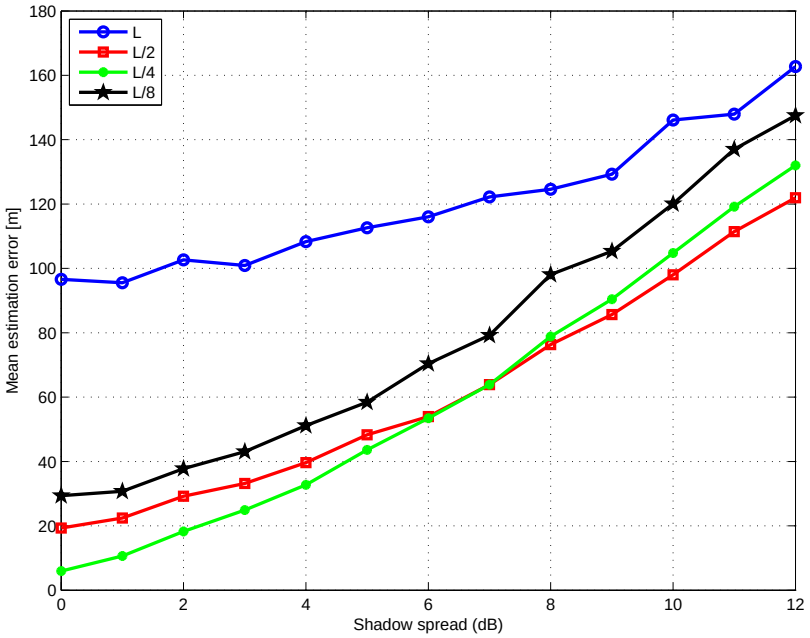

Figure 5.6: Performance of maximum approach vs shadow spread for different search space sizes for 9 level 2x2 partitions ($N_t = 1$, $N_s = 50$, $L = 1$ km, $\alpha = 3.5$, $P_t = 1$ W)

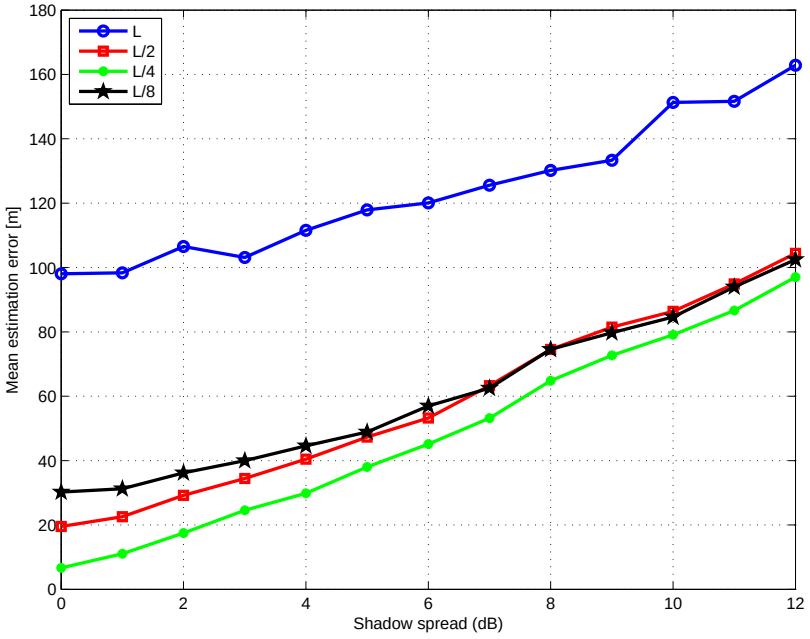

Figure 5.7: Performance of minimax approach vs shadow spread for different search space sizes for 9 level 2x2 partitions ($N_t = 1$, $N_s = 50$, $L = 1$ km, $\alpha = 3.5$, $P_t = 1$ W)

number of iterations is run. However, the convergence may be slow and the algorithm may require higher number of iterations leading to increased computational complexity due to improper selection of design parameters such as number of burn-in samples and step size.

In Section 4.1.4, we have shown that location estimation accuracy of the MH algorithm is affected by selection of these parameters and when they are not set judiciously, the algorithm needs to run a large number of iteration to converge. Here we study initializing the MH algorithm smartly so that the convergence of the algorithm improves. Our claim is that the required number of MH iteration can be reduced without significant performance loss if the algorithm is jump-started with an initial value obtained from the interference map (refer to Chapter 3) that the CR network has already created.

In order to support our claim, we ran simulations to compare performances of random and **smart initialized MH algorithms**. Randomly initialized MH algorithm starts at a location chosen arbitrarily within the region whereas the smart algorithm starts at the location where the interference map achieves its maximum. Interference maps are created using both NN and linear interpolation techniques. The grid size is set to 10 to interpolate the RF field strength values at grid centers by the interpolant functions for convenience. We set the step-size of the proposal density to 50, as this value is resulted in suboptimal performance in simulations performed in Section 4.1.4. Note that the optimal value of the step-size is not generally available unless the algorithm is tuned-up in advance which requires extensive off-line simulations. The reason for selecting a suboptimal step-size in simulations is due to our desire to compare the performances of both techniques under the worst case scenario.

In each simulation, MH algorithm is run for 500 iterations and first 250 samples from these iterations are discarded as burn-in samples. The expected a posteriori estimate of the emitter location is then obtained by averaging last 250 samples. The RMS of the location estimation errors are given in Figures 5.8 and 5.9. Fig. 5.8 is obtained by simulating 10000 networks with 30 sensors for each dB spread value ranging from 1 to 12 dB at 1 dB intervals to analyse the performance under shadow fading. Similarly, Fig. 5.9 is obtained by simulating 10000 networks as the number of sensors is changed from 20 to 50. The spread of shadow fading is set to 6 dB in these simulations.

As seen from Figures 5.8 and 5.9, randomly initialized MH performs poorly because the algorithm cannot converge due to insufficient number of iterations. In this case, the performance is even worse than the linear interpolation based estimation. When initialized with rough position information provided by the interference map, the MH algorithm achieves significantly better performance even when the number of iterations is small. The performance of the algorithm is the same for both NN and linear interpolation initialization. Even though the performance of the NN interpolation itself is poorer than the linear interpolation scheme, the performance of the MH is similar for both NN and linear interpolation initialization which shows that the algorithm is insensitive to the accuracy of the initial estimate.

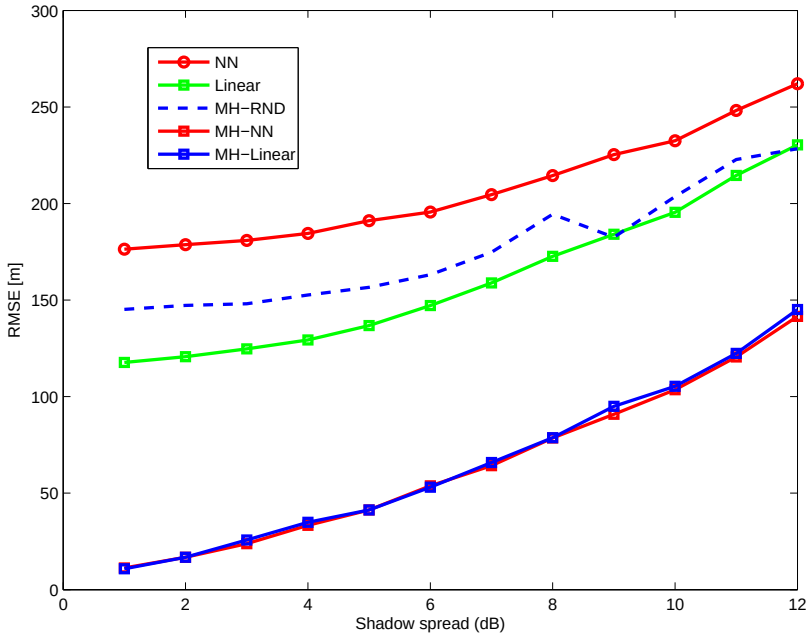

Figure 5.8: RMSE performance comparison of the smartly initialized MCMC techniques vs shadow spread ($N_t = 1$, $N_s = 30$, $P_t = 1$ W, $\alpha = 4$, $L = 1$ km, $\Delta = 50$, grid size for interpolation = 10 m, number of iterations = 500, number of burn-in samples = 250)

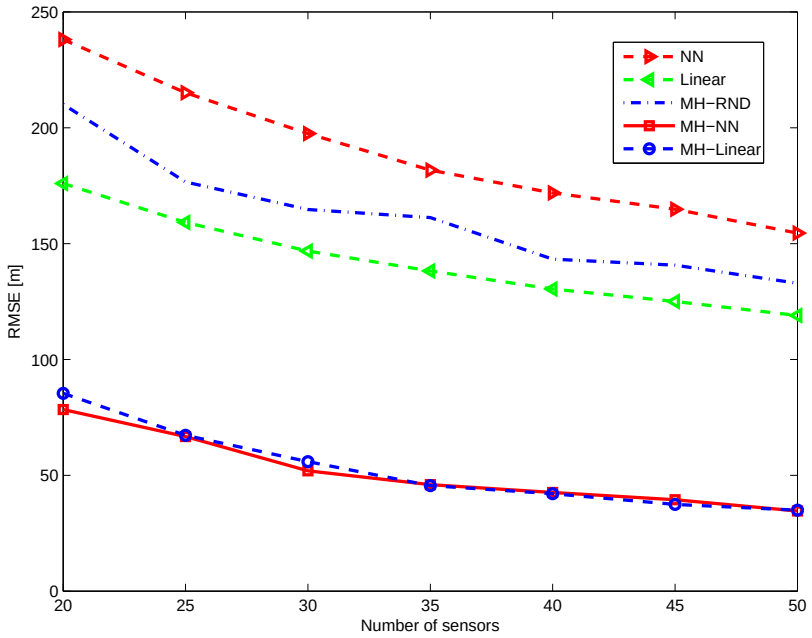

Figure 5.9: RMSE performance comparison of the smartly initialized MCMC techniques vs number of sensors ($N_t = 1$, $\sigma = 6$ dB, $P_t = 1$ W, $\alpha = 4$, $L = 1$ km, $\Delta = 50$, grid size for interpolation = 10 m, number of iterations = 500, number of burn-in samples = 250)

Chapter 6

Conclusions and Future Work

6.1 Conclusions

In this thesis, we have investigated RF cartography generation and multiple emitter localization problems in CR networks. We have investigated global and local interpolation methods, specifically Delaunay triangulation based interpolation techniques in generating interference maps as the use of existing triangulation provides a computationally attractive solution for the interference map generation problem. We have also investigated estimating the locations of primary emitters from the generated interference map and explore complexity-performance trade-offs of these interpolation techniques. We have shown that the accuracy of the estimation obtained from interference maps is low. So we have delved into more accurate algorithms such as MLE based grid search method and MCMC methods. The advantageous of these methods over another have been studied and their complexity issues have been addressed by using different iterative grid-search techniques and by smartly initializing the MCMC method. As the ML estimator we have used for multiple emitter localization is based on the approximation for sum of log-normal distributions, we also have investigated the sum of log-normal approximations that are studied in literature and proposed our own approximation that works well for the localization of two active primary emitters in a CR network.

In interference map generation problem, we have presented a comparative performance evaluation of the interpolation techniques used in interference cartography generation. The performances are evaluated in terms of RF field strength estimation efficiency and localization accuracy of multiple primary emitters. The kriging and the thin-plate spline methods evaluated in this thesis are global interpolation techniques and they require a central node to process the information from individual nodes. However, in the local interpolation methods each interpolation point requires the information only from the neighboring nodes; therefore a central fusion node is not required. This feature may provide desirable features such as robustness and better adaptation to local changes in CR networks. The local interpolations that are evaluated in this thesis are based on Delaunay triangulation. The Delaunay triangulation is used in several networking tasks and it is possible to utilize the actual triangulation for interference map generation as well. This provides a compu-

tational advantage to Delaunay based interpolation techniques over the global ones. The local interpolation methods studied in the thesis are nearest neighbor, natural neighbor, linear, cubic and quadratic interpolations. Among these methods, the nearest neighbor interpolation is the least complex method, however its performance is significantly worse than any one of the other local methods. Natural neighbor, linear, cubic and quadratic interpolation techniques have comparable performances, but linear interpolation is the least complex one in terms of computation. For all interpolation methods, the effect of the number of emitters to the RF power estimates depends on the shadowing spread. For shadowing spread under 3 dB, the power estimation error increases with the increased number of transmitters in all methods. However above 3 dB, the increase in number of transmitters decreases the power estimation error, therefore it helps reducing the shadowing effects for higher shadowing values.

We have calculated the CRLB of emitter location estimates that provides information on the best performance achievable for different emitter sensor geometries. We have shown that the CRLB, i.e. the estimation accuracy of an estimator is affected by the number of sensors used in the network, the shadowing spread, the path-loss exponent and the geometric configuration of the sensors and emitter which is called geometric dilution of precision. When the emitter is placed inside the region covered by the sensors, more accurate location estimations are obtained. In other words, the bound values increase as the sensors are placed further away from the emitter.

As the accuracy of the estimations obtained from interference maps is low, we have presented the MLE method based on full grid search method and have given its performance analysis in comparison with the Cramer Rao lower bound. In a grid-search method, the solution space is divided into a number of grids and a cost function is calculated for each grid center. The performance of the ML estimator approaches to CRLB when the shadowing spread values are between 3 dB and 9 dB. However the performance degrades with higher dB spread values since higher shadowing effect degrades the estimation performance. Besides its higher estimation accuracy, the full grid search is a complex search method that requires the algorithm to scan all possible grid points in the localization space and also requires the size of the grid elements to be chosen small to obtain more accurate location estimates. The algorithm becomes even more complex for multiple primary emitter localization problems as it increases the calculation of the likelihood function for all grid points related with the number of primary emitters considered in the network. Therefore we propose an efficient RSS-based localization algorithm, referred to as iterative grid-search method that closely approached the MLE method, particularly at small shadowing spread values with significantly reduced computational complexity. The iterative grid search considers a sequence of possible candidate grid points to compute on demand by recursively dividing the localization space into partitions, and then selecting only one partition where the target location should reside. Because the grid search has coarser resolution at earlier stages, it is possible that the global minimum of the cost function is missed, especially when the uncertainty is high due to larger shadowing spreads. We have also studied restricting the search space of the iterative search based on the maximum and minimax criteria and shown that this does not improve the performance of the iterative search algorithm at all.

In order to address the problems of grid search method, we have proposed to apply

an MCMC based technique that is Metropolis Hastings algorithm to single emitter localization problem. The main reason for this is, MCMC based techniques provide a lower computational complexity solutions to parameter estimation problems especially when the number of parameters to be estimated is large. The performance analysis of this method have showed that MH based location estimator gives similar performance to CRLB, i.e. it is highly an accurate estimator for shadowing values of 6 dB and under, but its performance degrades with higher dB spread values. A major disadvantage of these techniques is that they require large number of iterations to converge if its parameters are not tuned in advance. Parameters such as the selection of the proposal density, the number of iterations, the number of burn-in samples affect the convergence of the algorithm and they need tuning. Initializing the algorithm with the knowledge fed-back from the interference map generated by using low-complexity interpolation techniques overcomes this problem. Hence the smart initialization of MCMC technique we have proposed, eliminates tedious parameter tuning process and achieves significantly better localization performance than the randomly initialized MH method at a fraction of iterations.

The ML estimator we have used for multiple emitter localization require a sum of log-normal approximation for likelihood calculations at each emitter pair location configurations on a grid. We have investigated the sum of log-normal approximations that are studied in the literature. Among the approximations we reviewed, we have chosen Fenton-Wilkinson's approach due to its simplicity and applicability to non-iid log-normal rvs that represents different mean received power values for each emitter sensor pair in the network. However, the estimation accuracy of Fenton's approach is low at high dB spread values. Hence we propose a new approximation where the pdf of sum of log-normals is estimated from a set of simulated data. By using distribution fitting techniques, we have tried many different candidate distributions such as log-normal, gamma and Gaussian mixture pdfs to fit a curve that matches the histogram of the simulated data and calculated the likelihood values of each candidate distribution from their estimated parameters. Based on the comparison of the likelihood differences of distributions, we have decided that the best approach that fits the simulated data is the log-normal approximation. We have also compared the localization performance of our proposed approximation with Fenton‘s by using the grid search technique for different case scenarios. In these scenarios, localization of two emitters transmitting at the same frequency with equal transmit power in a dense or sparse GSM network within different sizes of areas is considered. Simulation results show that our proposed fitted log-normal approximation outperforms Fentons approximation for all shadowing spread values. The proposed pdf estimation approach is our novel contribution to the area of RSS-based multiple emitter localization.

6.2 Future Work

6.2.1 Applying MCMC Techniques to Multiple Emitter Localization

Localization of two active primary emitters using full grid search with our proposed fitted sum of log-normal approximation has been studied in Section 4.2.4. However, the MH-MCMC method hasnt been applied to our multiple emitter localization problem with the proposed approximation. As we have mentioned in Section 4.1.4, the reason to propose a MCMC method for maximizing the likelihood function given in (4.6) is that the MCMC methods provide computationally efficient sampling strategies when the number of parameters to be estimated is large, which is the case for multiple emitter scenarios. On the other hand, as we formulate our parameter estimation problem in a Bayesian framework, we sample from the joint posterior densities of the parameters so that inferences can be made. Any available prior information about the estimated parameters can be used to update the likelihood given in (B.8), using the Bayes formula. In this case, the joint posterior of the unknown parameter becomes

$$p(\theta|M, r) = p(r|M, \theta)p(\theta|M) \tag{6.1}$$

where M denotes the signal model and noise statistics, θ is the vector of unknown parameters and $r = [r_1, r_2, ., r_{N_s}]$ is the vector of the sensors power measurements. The samples generated from the joint posterior densities will form the marginal posteriors of the parameters and then be used to make inferences about the unknown parameters. This approach fits in with the MH algorithm we propose for our localization problem. To that end, an important area of future study is applying MCMC methods to multiple emitter localization problem.

Generating samples from non-standard multi-variate distributions is not a straight- forward task. Markov chain Monte Carlo algorithms have been shown to be very efficient for drawing samples from probability distributions [27]. The key idea is to build an ergodic Markov chain whose equilibrium distribution is the desired posterior distribution. At each iteration, a candidate value is drawn from a proposal distribution, which can be any distribution function that creates an irreducible and aperiodic chain over the entire parameter space, yet easy to draw samples. Even though any proposal distribution ultimately delivers samples from the target distribution, a distribution that closely approximates the desired posterior will improve the rate of convergence to the stationary distribution. Candidate samples drawn from the proposal distribution are randomly accepted according to an acceptance ratio that ensures reversibility. The state of the chain after a number of steps is then used as a sample from the desired distribution. Even though MCMC algorithm is guaranteed to converge, the convergence may be slow. It has been shown that the performance of MH algorithm is affected by several design parameters such as the selection of the proposal density and its parameters, number of iterations and burn-in samples [73].

6.2.2 Improving the Performance of MCMC Algorithms

Future studies related with MCMC algorithms are tuning the design parameters and improving their performance.

Initialization of MCMC algorithms: Any arbitrary point that is chosen to be the first state of the Markov chain is referred as the initial value. If the Markov chain is initialized with a value far from its actual value, the MH algorithm may require large number of iterations to converge. In [73], we have used the coarse estimate that is acquired from an interpolated interference map to initialize the MH algorithm for single emitter localization. We have observed that the smart initialization improved the convergence dramatically even without parameter tuning, therefore reduced the computational complexity in comparison with the randomly initialized MH algorithm. Similar methods for smart initialization for multiple emitter localization problem can be studied as well.

Selection of prior density functions: One's knowledge before observing the data is referred to as prior information. Prior distributions play an important role in Bayesian analysis. Different types of prior distributions can be used in the analysis based on the nature of the problem. For example, a non-informative prior, such as the uniform distribution, plays a minimal role on the posterior distribution and it is used when external information is not available or not reliable. Informative priors, on the other hand, have a stronger influence on the posterior distribution and they are typically obtained from past data. Therefore, investigating informative prior pdfs for the parameters of interest is another future study. We have used an uninformative prior for the location parameter for the single emitter localization problem in [73] since there is no prior information about the location of the emitter. However, cases where a prior pdf for location is available can be investigated and that can be used for improved performance for multiple emitter localization problem. For example, the knowledge that the primary emitters cannot be located very close to each other can be incorporated into a prior pdf model in multiple emitter localization problem.

Selection of proposal density functions: The MH algorithm obtains a sequence of random samples from a target probability distribution for which direct sampling is difficult. At each state a new value of the parameter is proposed according to the proposal density function. Even though any proposal density eventually generates samples from the target density, inappropriate proposal selections may result in an increased convergence time. Therefore, the algorithm works best if the proposal density matches the shape of the target distribution. If a Gaussian proposal density is used, the variance parameter has to be tuned during the burn-in period. This is usually done by calculating the acceptance rate, which is the fraction of proposed samples that is accepted in a window of the last N samples. In [73], we have used Gaussian distribution in our simulations to propose new location values because Gaussian pdf is symmetric around its mean value and symmetric proposal density function is preferred for the algorithm. The current parameter value at

each state is taken as the mean value of the distribution and the variance, i.e. the step size is tried with different values for the tuning process. The optimal value of the step size is not generally available unless the algorithm is tuned-up in advance which requires extensive off-line simulations.

Convergence tests: Even though MCMC algorithm is guaranteed to converge, the convergence may require large number of computations if its parameters are not tuned in advance. Unfortunately, there is no general rule for stopping MCMC iterations. In [73], the performance of MH algorithm for single emitter localization is studied as a function of number of MH iterations for different step-sizes. Simulation results show that the performance is affected by the selection of step-size when the number of iterations is small. As the number of iterations increases, the performance difference is shown to be negligible. For further studies, convergence tests for stopping MCMC algorithm for multiple emitter localization problem can be investigated.

Selection of number of burn-in samples: MCMC algorithms are started from arbitrary initial values and the algorithm is run for many iterations until this initial state is forgotten. The samples, which are discarded, are known as burn-in samples and selection of their number may affect the estimation accuracy. As for the number of convergence iterations, there is no general rule for determining the number of burn-in iterations. In [73], performance of the MH algorithm is evaluated in terms of number of burn-in samples and iterations as well as the value of the step-size. The results show that the number of burn-in samples effect the performance significantly when the step-size is set to a suboptimal performance in simulations. To that end, selection of the number of burn-in samples for multiple primary emitter localization problem can be investigated for further studies.

Sampling frequency of the parameters: When there are multiple parameters to estimate, each parameter is sampled in turn by the MCMC algorithm. Usually, each parameter is sampled at a different rate as they have different level of importance in the likelihood function. For example, in emitter location estimation problem when the emitter power is unknown, the location parameter needs to be sampled more often than the emitter power. Future investigations related with the parameter selection can also include the sampling frequency of the parameters.

6.2.3 Estimating the Number of Emitters (Reversible Jump MCMC)

In this thesis, we have studied multiple emitter localization problem with the assumption of knowing the number of active primary emitters. However there are cases when their number is unknown. The number of emitters sets the order of the model; therefore the number of parameters to be estimated (emitter locations) is unknown in that case. These problems are collectively known as model selection problems for which there is an extensive literature.

Regular MCMC methods, such as Metropolis-Hastings or Gibbs sampler [27], do not allow jumps between models; therefore they cannot be used in problems where the model order is unknown. The reversible jump MCMC (RJMCMC) sampler is an extension of the standard MCMC methods which allows for jumps between models and their parameter spaces of differing dimensions as the sampling proceeds [29]. In this approach, the move that requires the updating of parameters is implemented in the usual way as there is no change of dimensions and/or change of parameter spaces.

The RJMCMC technique has been successfully implemented in a variety of model selection and parameter estimation problems, for example: to determine the number of sinusoids and their parameters in [5], to obtain estimates of the number of scatters, their directions of arrival and their times of arrival in [37] and to segment SAR images in [67] and to estimate locations of multiple change points [29]. When applied to change point detection problems, the algorithm involves 4 move types in the sampling process: height and position moves and birth and death moves. Height and position moves update the amplitudes and change locations, whereas the birth and death moves change the number of change points, respectively. These last two moves allow reducing and increasing the model order during the sampling process.

In RJMCM algorithm, the acceptance of a new sample drawn from the proposal distribution depends on the acceptance ratio of moving from state θ to state θ^* , which is given by:

$$a = \min(1, \text{Likelihood ratio} \times \text{Prior ratio} \times \text{Proposal ratio} \times J) \tag{6.2}$$

where J is the Jacobian of the dimension matching transformation that allows the change in dimensionality. Note that (6.2) is the most general form of the acceptance ratio and its specific expression depends on the choice of the move type. For example, the Jacobian is only required when the order of the model is changed and for other move types $J = 1$. To our best knowledge, the RJMCMC technique has not been applied to multiple emitter localization problem. Implementation of the RJMCMC technique for estimating the location of unknown number of emitters requires developing move types suitable for this problem. At that point, the Jacobian expressions for the specific move type that requires dimension change can be derived and proper prior and proposal densities to accelerate the convergence of the algorithm can be proposed for further research.

6.2.4 RSS-based Localization with Different Case Scenarios

Unknown number of emitters In this scenario, a future study is the investigation of the multiple emitter localization problem when the number of emitters is unknown. In this case, emitters may have different or same transmit power levels.

Emitter power and/or path-loss exponent unknown The work performed in this thesis, in [51] and [4] has assumed that the transmitted power from the primary transmitters are known and equal. In practice, this assumption may not be true, the transmit

powers or even the path-loss exponent might not be known. In this section, a future study is investigating the case scenarios where the primary transmit powers are unknown and unequal or the path-loss exponent is unknown or both the transmit powers and the path-loss exponent are unknown. When emitter powers are unknown, location estimation ambiguity occurs as the path-loss range formula depends on transmit power, alpha and distance. When all of the parameters are unknown, the ambiguity increases. Here are the highlight studies that the RSS-based localization in the presence of unknown channel parameters are investigated. In [4], IS (interference subtraction) technique is proposed based on EM algorithm for jointly estimating transmitted powers and transmitter locations. In [76], a semi-definite programming approach by applying approximations and relaxations to ML estimator is derived to estimate the transmit power of a single emitter. A remarkable performance very close to the ML estimator is achieved with the derived algorithm with smaller number of computations that the ML estimator requires. Moreover, by linearizing the model, the partly least squares and weighted least squares algorithms are also derived to estimate the transmit power and their performances are also compared with each algorithm derived in the paper. In the existing studies, radio propagation path-loss model is assumed to be known a priori, which is a simplification in many application scenarios. But In [39], the joint estimation of the path-loss exponent parameter and unknown location coordinates of a single primary emitter in RSS-based localization systems is studied. Jointly estimating the path-loss exponent eliminates the need for extensive channel measurement and modeling and enables the algorithm to adaptively optimize its performance in dynamically changing environmental conditions. A nonlinear least-square estimator is presented in the paper and the performance of the algorithm is studied based on the CRLB analysis for a given emitter sensor geometry. Based on CRLB analysis in the referred paper, it is shown that unbiased RSS location estimators with unknown path-loss exponent are more sensitive to geometric parameters than unbiased RSS location estimators with known path-loss exponent, which indicates that jointly estimating the location and the path-loss exponent requires more careful planning of sensor deployment than the conventional location estimator. It is also shown that the variance of the estimation error increases with the unknown number of parameters. Similarly in [26], the localization of a single primary emitter problem based on RSS measurements is studied under the assumption of transmit-power or path-loss exponent is unknown. Because of non-convex behaviour of ML estimator, suitable approximations are used to formulate the localization problem as a general trust region sub-problem, which can be solved exactly under mild conditions. For future studies, algorithms can be developed to estimate all these unknown parameters jointly using the RJMCMC method when the number of emitters is also unknown. This will require simulating samples from the number of emitters, their locations, transmit powers and path-loss exponent parameters. In a scenario where all or most of these parameters are unknown, it may be very difficult to make accurate estimates of these parameters; however for some applications only a rough estimate of the emitter locations may be enough.

APPENDICES

Appendix A

Emitter Localization Methods for Different Case Scenarios

The following table gives the assumption of model parameters of different case scenarios and the relevant localization methods studied throughout the thesis.

	Number of emitters	**Power of emitters**	**Path-loss Exponent**	**dB spread**	**Methods and/or References**
1	Single	Unknown	Unknown	Unknown	**Localization using REM** [71] and [72]
2	Single	Unknown	Known	Unknown	**MLE method based on full and iterative grid search** [75] and [74]
3	Single	Known	Known	Unknown	**Localization using MCMC-MH method** [73]
4	Multiple(2 emitters)	Unknown	Unknown	Unknown	**Localization using REM** (Refer to Section 3.4.2)
5	Multiple(2 emitters)	Known and equal	Known	Known	**MLE method based on full grid search** (Refer to Section 4.2.4)

Appendix B

Derivation of Likelihood Expression for Likelihood Based Estimators

B.1 Single Emitter Localization Problem

Assumptions:

Number of emitters, N_t=1

Transmit power, P_t: unknown

Propagation exponent, α: known

Shadowing variance, σ^2: unknown

We consider N_s sensors to be located arbitrarily in known places in the region of interest measuring the power due to a randomly located emitter at a specific frequency and time instant with the above assumptions. The transmissions are omnidirectional and the signal propagation is governed by a log distance path-loss model. Received sensor measurements are assumed to have a log-normal shadowing.

For algorithms that require a likelihood function to estimate the location of the emitter $\boldsymbol{\theta} = (T_x, T_y)$, the derivation of the likelihood expression in MH algorithm is as follows:

The received power at the jth sensor with a distance d_j from the emitter is a log-normal random variable with mean s_j and variance σ^2 and is given by

$$r_j = s_j 10^{\frac{W}{10}} \tag{B.1}$$

where $W \sim \mathcal{N}(0, \sigma^2)$ is the gain/loss in dB due to shadowing and σ is the shadowing spread.

The mean received power at the jth sensor is given by

$$s_j = \frac{\beta P_t}{(d_j)^\alpha} \tag{B.2}$$

where P_t is the emitter power, β is a constant that reflects the carrier frequency and antenna properties given by $\beta = (\frac{\lambda}{4\pi})^2$, and λ is the wavelength.

The pdf of the received power is given by

$$p(r_j; s_j, \sigma) = \frac{1}{\sigma\sqrt{2\pi}\epsilon r_j} exp\left(-\frac{(10log_{10}r_j - 10log_{10}s_j)^2}{2\sigma^2}\right) \tag{B.3}$$

where $\epsilon = \frac{ln10}{10}$.

Assuming that each sensor experiences independent and identically distributed log-normal shadowing, the likelihood of observing all N_s sensor outputs for the given model M can be written as

Ł $= p(\mathbf{r}|M, \boldsymbol{\theta}) = \prod_{j=1}^{N_s} \frac{1}{\sigma\sqrt{2\pi}\epsilon r_j} e^{-\frac{\left(10log_{10}r_j - 10log_{10}s_j\right)^2}{2\sigma^2}}$

where $r = \begin{bmatrix} r_1 & r_2 & r_3 & \cdots & r_{N_s} \end{bmatrix}$ are the sensor's power measurements and $\boldsymbol{\theta} = (T_x, T_y)$ is the unknown emitter location parameter.

Ł $= (\frac{1}{\epsilon\sqrt{2\pi}})^{N_s} \frac{1}{\prod_{j=1}^{N_s} r_j} \sigma^{-N_s} e^{-\frac{1}{2\sigma^2}\sum_{j=1}^{N_s}(10log_{10}r_j - 10log_{10}s_j)^2}$

Let $K_1 = (\frac{1}{\epsilon\sqrt{2\pi}})^{N_s} \frac{1}{\prod_{j=1}^{N_s} r_j}$, $K_2 = \frac{1}{2\sigma^2}\sum_{j=1}^{N_s}(10log_{10}r_j - 10log_{10}s_j)^2$

The likelihood expression can be written as;

$$\text{Ł} = p(\mathbf{r}|M, \boldsymbol{\theta}) = K_1\sigma^{-N_s}e^{-K_2\sigma^{-2}} \tag{B.4}$$

If we know the value of shadowing spread σ, we can use (B.4) as the likelihood expression for estimating the location parameter with the MH algorithm. However, for the case where σ is unknown, non-informative prior information of dB spread can be used to update the likelihood given in (B.4) using the Bayes formula. Then the joint posterior pdf becomes,

$p(\boldsymbol{\theta}|M, \mathbf{r}) \propto p(\mathbf{r}|M, \boldsymbol{\theta})p(\boldsymbol{\theta}|M)p(\sigma|M)$ where $p(\sigma|M)$ is the prior pdf of σ which is $\frac{1}{\sigma}$.

The updated likelihood expression, $p(\mathbf{r}|M, \boldsymbol{\theta})p(\sigma|M)$ can be written as

$$\text{Ł}updated = p(\mathbf{r}|M, \boldsymbol{\theta})p(\sigma|M) = K_1\sigma^{-N_s}e^{-K_2\sigma^{-2}}\frac{1}{\sigma} \tag{B.5}$$

To obtain the marginalized likelihood expression Ł$_{mar}$, σ can be integrated out analytically in (B.5).

$$\text{Ł}_{mar} = \int_0^\infty K_1\sigma^{N_s-1}e^{-K_2\sigma^{-2}}d_\sigma \tag{B.6}$$

$Ł_{mar} = K_1 \int_0^\infty \sigma^{N_s-1} e^{-K_2\sigma^{-2}} d_\sigma$

Recall

$$\int_0^\infty x^{\alpha-1} e^{-Qx} d_x = \frac{\Gamma(\alpha)}{Q^\alpha} \tag{B.7}$$

where $\Gamma(.)$ represents the gamma function.

Let $\sigma^{-2} = x$, then $-2\sigma^{-3} d_\sigma = d_x$

$d_\sigma = \frac{1}{-2\sigma^{-3}} d_x = \frac{-1}{2}\sigma^3 d_x$

$x^{\alpha-1} = \sigma^{-N_s-1} = x^{\frac{N_s+1}{2}}$

Then, $\alpha - 1 = \frac{N_s+1}{2} \Rightarrow \alpha = \frac{N_s+3}{2}$

Plug $\sigma^{-N_s-1}, \sigma^-2, d_\sigma$ in (B.6).

$Ł_{mar} = K_1 \int_0^\infty \sigma^{N_s-1} e^{-K_2\sigma^{-2}} d_\sigma$

$= -K_1 \int_{-\infty}^0 x^{(\frac{N_s+1}{2})} e^{-K_2 x} \frac{1}{2}\sigma^3 d_x$

$= \frac{K_1}{2} \int_0^\infty x^{(\frac{N_s+1}{2})} e^{-K_2 x} x^{\frac{-3}{2}} d_x$

$= \frac{K_1}{2} \int_0^\infty x^{(\frac{N_s+1}{2} - \frac{3}{2})} e^{-K_2 x} d_x$

$= \frac{K_1}{2} \int_0^\infty x^{(\frac{N_s-2}{2})} e^{-K_2 x} d_x$

$= \frac{K_1}{2} \int_0^\infty x^{(\frac{N_s}{2}-1)} e^{-K_2 x} d_x$

Let $\alpha = \frac{N}{2}$ in (B.7), then the above equation becomes,

$= \frac{\frac{K_1}{2}\Gamma(\frac{N_s}{2})}{K_2^{\frac{N_s}{2}}}$

Plug K_2 in the above equation.

$$Ł_{mar} = \frac{\frac{K_1}{2}\Gamma(\frac{N_s}{2})}{\left(\frac{1}{2}\sum_{j=1}^{N_s}(10log_{10}r_j - s_j)^2\right)^{\frac{N_s}{2}}}$$

$$= \frac{\frac{K_1}{2}\Gamma(\frac{N_s}{2})2^{(\frac{N_s}{2})}}{\left(\sum_{j=1}^{N_s}(10log_{10}r_j - s_j)^2\right)^{\frac{N_s}{2}}}$$

$$= K_1 2^{(\frac{N_s}{2}-1)}\Gamma(\frac{N_s}{2})\left(\sum_{j=1}^{N_s}\left(10log_{10}r_j - 10log_{10}\frac{\rho P_t}{d_j^\alpha}\right)^2\right)^{\frac{-N_s}{2}}$$

$$= K_1 2^{(\frac{N_s}{2}-1)}\Gamma(\frac{N_s}{2})\left(\sum_{j=1}^{N_s}\left(10log_{10}\frac{r_j d_j^\alpha}{\rho P_t}\right)^2\right)^{\frac{-N_s}{2}}$$

$$= K_1 2^{(\frac{N_s}{2}-1)}\Gamma(\frac{N_s}{2})100^{\frac{-N_s}{2}}\left(\sum_{j=1}^{N_s}\left(10log_{10}\frac{r_j d_j^\alpha}{\rho P_t}\right)^2\right)^{\frac{-N_s}{2}},\ 100^{\frac{-N_s}{2}}2^{(\frac{N_s}{2}-1)} = \frac{50^{\frac{-N_s}{2}}}{2}$$

$$= \frac{1}{2}K_1\Gamma(\frac{N_s}{2})50^{\frac{-N_s}{2}}\left(\sum_{j=1}^{N_s}\left(10log_{10}\frac{r_j d_j^\alpha}{\rho P_t}\right)^2\right)^{\frac{-N_s}{2}}$$

$$Ł_{mar} = K\left(\sum_{j=1}^{N_s}\left(10log_{10}\frac{r_j d_j^\alpha}{\rho P_t}\right)^2\right)^{\frac{-N_s}{2}} \text{ where } K = \frac{1}{2}K_1\Gamma(\frac{N_s}{2})50^{\frac{-N_s}{2}}$$

B.2 Multiple Emitter Localization Problem

The likelihood expression for multiple emitter localization problem which is given in (4.15) in Section 4.2.2 is obtained from (4.14) by taking the following steps:

$$Ł = \prod_{j=1}^{N_s}\frac{1}{r_j\sigma_{sum_j}\sqrt{2\pi}}e^{-\frac{(\ln(r_j)-s_j)^2}{2\sigma^2_{sum_j}}}$$

$$= \frac{1}{r_1\sigma_{sum_1}\sqrt{2\pi}}e^{-\frac{(\ln(r_1)-s_1)^2}{2\sigma^2_{sum_1}}}\frac{1}{r_2\sigma_{sum_2}\sqrt{2\pi}}e^{-\frac{(\ln(r_2)-s_2)^2}{2\sigma^2_{sum_2}}}\ldots\frac{1}{r_{N_s}\sigma_{sum_{N_s}}\sqrt{2\pi}}e^{-\frac{(\ln(r_{N_s})-s_{N_s})^2}{2\sigma^2_{sum_{N_s}}}}$$

$$Ł = \left(\frac{1}{\sqrt{2\pi}}\right)^{N_s}\left(\frac{1}{r_1\sigma_{sum_1}}\frac{1}{r_2\sigma_{sum_2}}\ldots\frac{1}{r_{N_s}\sigma_{sum_{N_s}}}\right)e^{-\frac{(\ln(r_1)-s_1)^2}{2\sigma^2_{sum_1}}}e^{-\frac{(\ln(r_2)-s_2)^2}{2\sigma^2_{sum_2}}}\ldots e^{-\frac{(\ln(r_{N_s})-s_{N_s})^2}{2\sigma^2_{sum_{N_s}}}}$$

Note that the constant term $\left(\frac{1}{\sqrt{2\pi}}\right)^{N_s}$ can be omitted without affecting the likelihood calculations.

$$\ln(Ł) = ln\left(\left(\frac{1}{r_1\sigma_{sum_1}}\frac{1}{r_2\sigma_{sum_2}}...\frac{1}{r_{N_s}\sigma_{sum_{N_s}}}\right)e^{-\frac{(\ln(r_1)-s_1)^2}{2\sigma^2_{sum_1}}}e^{-\frac{(\ln(r_2)-s_2)^2}{2\sigma^2_{sum_2}}}...e^{-\frac{(\ln(r_{N_s})-s_{N_s})^2}{2\sigma^2_{sum_{N_s}}}}\right)$$

$$= ln\left(\frac{1}{r_1\sigma_{sum_1}}\right) + ln\left(\frac{1}{r_2\sigma_{sum_2}}\right) + ... + ln\left(\frac{1}{r_{N_s}\sigma_{sum_{N_s}}}\right) - \frac{1}{2}\sum_{j=1}^{N_s}\frac{(\ln(r_j)-s_j)^2}{\sigma^2_{sum_j}}$$

$$\ln(Ł) = -\sum_{j=1}^{N_s}\ln(r_j\sigma_{sum_j}) - \frac{1}{2}\sum_{j=1}^{N_s}\frac{(\ln(r_j)-s_j)^2}{\sigma^2_{sum_j}} \tag{B.8}$$

Appendix C

Quantization Error Calculation in Grid Search Method

This section shows how to calculate the quantization error in grid search technique when there is no shadowing.

Let two dimensional quantization error be $\mathbf{z}$, which is the square root of the sum of squared quantization errors in x and y directions. We assume that the error in x and y directions are independent and have a uniform distribution within the interval $[D/2, D/2]$, where D is the grid size.

$$z = \sqrt{x^2 + y^2}$$

$$X \sim \mathcal{U}[-D/2, D/2]$$

$$Y \sim \mathcal{U}[-D/2, D/2]$$

The mean square error of z can be calculated for two different regions as shown below.

- Region 1

  The shaded region inside the circle with a radius z shown in Fig. C.1 can be represented by z, for values of $0 < z < D/2$. The cumulative probability distribution (cdf) of z for this region, $F_1(z)$ is given by

  $$F_1(z) = P(Z \leq z) = P(\sqrt{x^2 + y^2} \leq z) = \int_{y=-z}^{z} \int_{-\sqrt{z^2-y^2}}^{\sqrt{z^2-y^2}} f_{XY}(x, y) d_x d_y$$

  The probability distribution (pdf) of z can be obtained by differentiation [53],

  $$f_1(z) = \int_{y=-z}^{z} \frac{z}{\sqrt{z^2-y^2}} \Big(f_{XY}(\sqrt{z^2 - y^2}, y) + f_{XY}(-\sqrt{z^2 - y^2}, y) \Big) d_y$$

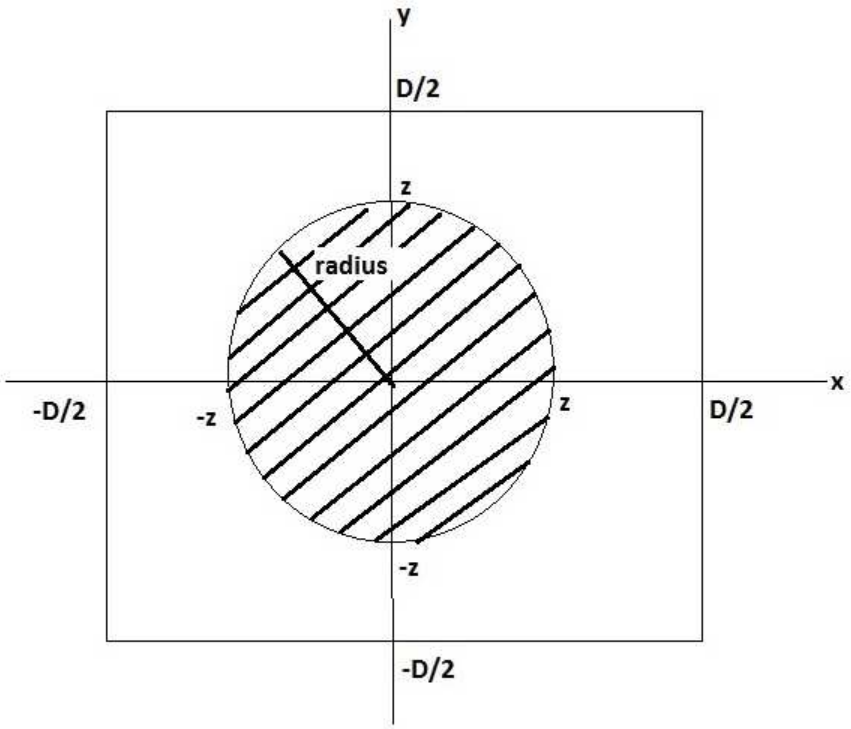

Figure C.1: Quantization error calculation in grid search for region 1

$f_{XY}(\sqrt{z^2-y^2}, y) = f_{XY}(x,y) = f_X(x)f_Y(y) = \frac{1}{D}\frac{1}{D} = \frac{1}{D^2}$

since X and Y are independent,

$f_1(z) = \int_{y=-z}^{z} \frac{z}{\sqrt{z^2-y^2}}\frac{2}{D^2}d_y = \frac{2z2}{D^2}\int_{y=0}^{z}\frac{1}{\sqrt{z^2-y^2}}d_y$

$\sin\theta = \frac{y}{z} \Rightarrow z = \frac{y}{\sin\theta} \Rightarrow z\cos\theta d_\theta = d_y$

$\frac{1}{\sqrt{z^2-y^2}} = \frac{1}{\sqrt{z^2-(\sin^2\theta)z^2}} = \frac{1}{\sqrt{z^2(1-\sin^2\theta)}} = \frac{1}{z\cos\theta}$

$f_1(z) = \frac{4z}{D^2}\int_0^{\pi/2}\frac{z\cos\theta}{z\cos\theta}d_\theta = \frac{4z}{D^2}\frac{\pi}{2} = \frac{2\pi z}{D^2}$

Therefore the pdf of z for Region 1 is,

$f_1(z) = \frac{2\pi z}{D^2}$

The mean square error for Region 1 can be given by,

$E_1(z^2) = \int_{z=0}^{D/2} f_1(z)z^2 d_z = \int_{z=0}^{D/2}\frac{2\pi z}{D^2}z^2 d_z = \frac{2\pi z^4}{4D^2}\Big|_0^{D/2} = \frac{2\pi(D/2)^4}{4D^2} = \frac{\pi L^2}{32}$

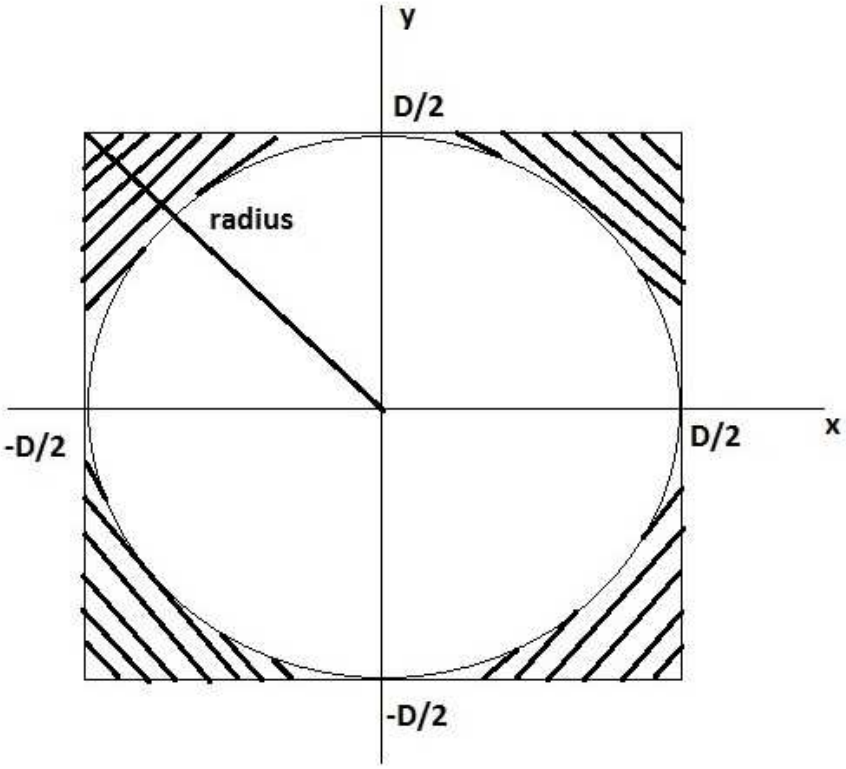

Figure C.2: Quantization error calculation in grid search for region 2

$E_1(z^2) = \frac{\pi D^2}{32}$

- Region 2

  The shaded region shown in Fig. C.2 is the part of the intersection of interior of two circles with radii of $D/\sqrt{2}$ and $D/2$, that remains in the grid. This region can also be represented by z, for values of $D/2 < z < D/\sqrt{2}$. The cdf of z for this region, $F_2(z)$ is given by

  $$F_2(z) = P(\sqrt{x^2+y^2} \leq z) = 1 - 4\int_{y=\sqrt{z^2-\frac{D^2}{4}}}^{D/2} \int_{x=\sqrt{z^2-y^2}}^{D/2} f_{XY}(x,y) d_x d_y$$

  By differentiation;

  $$f_2(z) = \frac{4z}{D^2}\left(\frac{\pi}{2} - 2\arctan\left(\frac{\sqrt{z^2-\frac{D^2}{4}}}{\frac{D}{2}}\right)\right)$$

  The mean square error for Region 2 can be given by,

  $E_2(z^2) = \int_{z=D/2}^{D/\sqrt{2}} f_2(z) z^2 d_z$

By using Wolfram integrator,

$$E_2(z^2) = \frac{\pi z^4}{2D^2} + \frac{(4z^2-D^2)^{\frac{3}{2}}}{24D} + \frac{1}{8}D\sqrt{4z^2-D^2} + \frac{1}{8}D^2 \arctan\left(\frac{D}{\sqrt{4z^2-D^2}}\right)$$

$$-\frac{(4z^2-D^2)(D^2+4z^2)\arctan\left(\frac{\sqrt{4z^2-D^2}}{D}\right)}{8D^2}\Bigg|_{D/2}^{D/\sqrt{2}}$$

$$\sqrt{4z^2-D^2}\Big|_{z=D/2} = 0$$

$$\sqrt{4z^2-D^2}\Big|_{z=D/\sqrt{2}} = D$$

$$4z^2+D^2\Big|_{z=D/2} = 2D^2$$

$$4z^2+D^2\Big|_{z=D/\sqrt{2}} = 3D^2$$

$$\implies E_2(z^2) = \left(\frac{\pi(\frac{D}{\sqrt{2}})^4}{2D^2} + \frac{(D^2)^{\frac{3}{2}}}{24D} + \frac{1}{8}DD + \frac{1}{8}D^2\arctan\left(\frac{D}{D}\right) - \frac{3D^2D^2}{8D^2}\arctan\left(\frac{D}{D}\right)\right)$$

$$-\left(\frac{\pi(\frac{D}{2})^4}{2D^2} + 0 + 0 + \frac{1}{8}D^2\arctan\left(\frac{D}{0}\right)\right)$$

$$E_2(z^2) = \frac{\pi D^4}{8D^2} + \frac{D^2}{24} + \frac{D^2}{8} + \frac{D^2\pi}{32} - \frac{3D^2\pi}{32} - \frac{\pi D^2}{32} - \frac{\pi D^2}{16}$$

By simplifying the expression,

$$E_2(z^2) = -\frac{\pi D^2}{32} + \frac{D^2}{6}$$

The total mean square error of z is the sum of mean square error for the two regions;

$$E(z^2) = E_1(z^2) + E_2(z^2) = \frac{\pi D^2}{32} - \frac{\pi D^2}{32} + \frac{D^2}{6}$$

$$E(z^2) = \frac{D^2}{6}$$

The root mean square of z is;

$$RMS(z) = \frac{D}{\sqrt{6}}$$

References

[1] R. Abaspour, M. Mehrjoo, S. Mohanna, and M. Rezaei. A recursive approximation approach of non-iid lognormal random variables summation in cellular systems. *International Journal of Communications and Information Technology*, 1(2):10–14, 2011.

[2] A. Alaya-Feki, S. B. Jemaa, B. Sayrac, P. Houze, and E. Moulines. Informed spectrum usage in cognitive radio networks: Interference cartography. In *IEEE 19th International Symposium on Personal, Indoor and Mobile Radio Communications (PIMRC)*, pages 1–5, 2008.

[3] A. I. Alhasant, B. S. Sharif, C. C. Tsimenidis, and J. A. Neasham. Low complexity least-square estimator for RSS-based localization in wireless sensor networks. In *IEEE International Conference on Communications and Information Technology (ICCIT)*, pages 331–335, 2012.

[4] J. E. Almodovar. *Multiple Transmitter Localization Using Received Signal Strength Measurements*. PhD thesis, George Mason University, 2012.

[5] C. Andrieu and A. Doucet. Joint bayesian model selection and estimation of noisy sinusoids via reversible jump MCMC. *IEEE Transactions on Signal Processing*, 47(10):2667–2676, 1999.

[6] J. Aspnes, T. Eren, D. K. Goldenberg, A. S. Morse, W. Whiteley, Y. R. Yang, B. D. Anderson, and P. N. Belhumeur. A theory of network localization. *IEEE Transactions on Mobile Computing*, 5(12):1663–1678, 2006.

[7] V. Atanasovski, J. Van de Beek, A. Dejonghe, D. Denkovski, L. Gavrilovska, S. Grimoud, P. Mähönen, M. Pavloski, V. Rakovic, and J. Riihijärvi. Constructing radio environment maps with heterogeneous spectrum sensors. In *IEEE Symposium on New Frontiers in Dynamic Spectrum Access Networks (DySPAN)*, pages 660–661, 2011.

[8] P. Bahl and V. N. Padmanabhan. Radar: An in-building rf-based user location and tracking system. In *IEEE INFOCOM, Nineteenth Annual Joint Conference of the IEEE Computer and Communications Societies, Proceedings*, volume 2, pages 775–784, 2000.

[9] N. C. Beaulieu and Q. Xie. An optimal lognormal approximation to lognormal sum distributions. *IEEE Transactions on Vehicular Technology*, 53(2):479–489, 2004.

[10] W. M. Bejuri, M. M. Mohamad, M. Sapri, and M. A. Rosly. Ubiquitous wlan/camera positioning using inverse intensity chromaticity space-based feature detection and matching: A preliminary result. *arXiv preprint arXiv:1204.2294*, 2012.

[11] D. Blatt and A. O. Hero III. Energy-based sensor network source localization via projection onto convex sets. *IEEE Transactions on Signal Processing*, 54(9):3614–3619, 2006.

[12] P. Bose and P. Morin. Online routing in triangulations. In *Algorithms and Computation*, pages 113–122. Springer, 1999.

[13] Brian C. Monte Carlo sampling methods, Lecture 7, Ohio State University, USA. http://web.cse.ohio-state.edu/~kulis/teaching/788_sp12/scribe_notes/, 2012.

[14] J.J. Caffery and G.L. Stuber. Overview of radiolocation in CDMA cellular systems. *IEEE Communications Magazine*, 36(4):38–45, Apr 1998.

[15] P. Cardieri and T. S. Rappaport. Statistical analysis of co-channel interference in wireless communications systems. *Wireless Communications and Mobile Computing*, 1(1):111–121, 2001.

[16] K. W. Cheung, H. So, W. Ma, and Y. Chan. A constrained least squares approach to mobile positioning: algorithms and optimality. *EURASIP Journal on Advances in Signal Processing*, 2006(1):1–23, 2006.

[17] S. Chib and E. Greenberg. Understanding the Metropolis-Hastings algorithm. *The American Statistician*, 49(4):327–335, 1995.

[18] A. J. Coulson, A. G. Williamson, and R. G. Vaughan. A statistical basis for lognormal shadowing effects in multipath fading channels. *IEEE Transactions on Communications*, 46(4):494–502, 1998.

[19] N. Cressie. Statistics for spatial data: Wiley series in probability and statistics. *Wiley-Interscience New York*, 15:16, 1993.

[20] S. Dasgupta, S. C. Ibeawuchi, and Z. Ding. Optimum sensor placement for localization under log-normal shadowing. In *IEEE International Symposium on Communications and Information Technologies (ISCIT)*, pages 204–208, 2010.

[21] A. Dogandzic, J. Riba, G. Seco, and A. L. Swindlehurst. Positioning and navigation with applications to communications. *IEEE Signal Processing Magazine*, 22(4):10–11, 2005.

[22] K. Doppler, M. Rinne, C. Wijting, C. B. Ribeiro, and K. Hugl. Device-to-device communication as an underlay to lte-advanced networks. *IEEE Communications Magazine*, 47(12):42–49, 2009.

[23] E. Elnahrawy, X. Li, and R. P. Martin. The limits of localization using signal strength: A comparative study. In *First Annual IEEE Communications Society Conference on Sensor and Ad Hoc Communications and Networks, IEEE SECON*, pages 406–414, 2004.

[24] I. Forkel, M. Schinnenburg, and M. Ang. Generation of two-dimensional correlated shadowing for mobile radio network simulation. *WPMC, Sep*, 21:43, 2004.

[25] M. P. Foster and A. N. Evans. An evaluation of interpolation techniques for reconstructing ionospheric tec maps. *IEEE Transactions on Geoscience and Remote Sensing*, 46(7):2153–2164, 2008.

[26] M. R. Gholami, R. M. Vaghefi, and E. G. Strom. RSS-based sensor localization in the presence of unknown channel parameters. *IEEE Transactions on Signal Processing*, 61(15):3752–3759, 2013.

[27] W. R. Gilks, S. Richardson, and D. J. Spiegelhalter. Introducing Markov chain Monte Carlo. In *Markov chain Monte Carlo in practice*, pages 1–19. Springer, 1996.

[28] A. Goldsmith. *Wireless communications*. Cambridge university press, 2005.

[29] P. J. Green. Reversible jump Markov chain Monte Carlo computation and Bayesian model determination. *Biometrika*, 82(4):711–732, 1995.

[30] S. Grimoud, B. Sayrac, S. B. Jemaa, and E. Moulines. An algorithm for fast REM construction. In *IEEE Sixth International ICST Conference on Cognitive Radio Oriented Wireless Networks and Communications (CROWNCOM)*, pages 251–255, 2011.

[31] J. Y. Hesterman, L. Caucci, M. A. Kupinski, H. H. Barrett, and L. R. Furenlid. Maximum-likelihood estimation with a contracting-grid search algorithm. *IEEE Transactions on Nuclear Science*, 57(3):1077–1084, 2010.

[32] B. Hofmann-Wellenhof, H. Lichtenegger, and J. Collins. Gps-global positioning system. theory and practice. *Austria, XXIII+ 389 p., ISBN 3-211-82839-7*, 1, 1997.

[33] L. Huang, G. Zhu, and X. Du. Cognitive femtocell networks: an opportunistic spectrum access for future indoor wireless coverage. *IEEE Wireless Communications*, 20(2):44–51, 2013.

[34] B. Johnston, X. Yin, A. Valenzuela, and P. Frantz. A fast algorithm and testbed evaluation for sound source localization using sensor networks. In *Proceedings of IEEE Vehicular Technology Conference*, 2005.

[35] S. K. Jones. *Evaluation of the performance of prototype TV-Band white space devices, phase II*. Technical Research Branch, Laboratory Division, Office of Engineering and Technology, Federal Communications Commission, 2008.

[36] S. Kim, H. Jeon, H. Lee, and J. S. Ma. Robust transmission power and position estimation in cognitive radio. In *Information Networking. Towards Ubiquitous Networking and Services*, pages 719–728. Springer, 2007.

[37] J-R Larocque and J. P. Reilly. Wide band channel characterisation in coloured noise using the reversible jump mcmc. In *IEEE International Conference on Acoustics, Speech, and Signal Processing, Proceedings,(ICASSP'01)*, volume 4, pages 2513–2516, 2001.

[38] A. Laya, K. Wang, A. A. Widaa, J. Alonso-Zarate, J. Markendahl, and L. Alonso. Device-to-device communications and small cells: enabling spectrum reuse for dense networks. *IEEE Wireless Communications*, 21(4):98–105, 2014.

[39] X. Li. Rss-based location estimation with unknown pathloss model. *IEEE Transactions on Wireless Communications*, 5(12):3626–3633, 2006.

[40] X. Li, G. Calinescu, P. Wan, and Y. Wang. Localized Delaunay triangulation with application in ad hoc wireless networks. *IEEE Transactions on Parallel and Distributed Systems*, 14(10):1035–1047, 2003.

[41] E. Maeland. On the comparison of interpolation methods. *IEEE Transactions on Medical Imaging*, 7(3):213–217, 1988.

[42] L. Mailaender. Geolocation bounds for received signal strength (RSS) in correlated shadow fading. In *IEEE Vehicular Technology Conference (VTC Fall)*, pages 1–6, 2011.

[43] G. Mao, B. Fidan, and B. D. Anderson. Wireless sensor network localization techniques. *Computer networks*, 51(10):2529–2553, 2007.

[44] B. L. Mark and A. O. Nasif. Estimation of maximum interference-free power level for opportunistic spectrum access. *IEEE Transactions on Wireless Communications*, 8(5):2505–2513, 2009.

[45] R. K. Martin and R. Thomas. Algorithms and bounds for estimating location, directionality, and environmental parameters of primary spectrum users. *IEEE Transactions on Wireless Communications*, 8(11):5692–5701, 2009.

[46] G. Mateos, J. Bazerque, and G. B. Giannakis. Spline-based spectrum cartography for cognitive radios. In *IEEE Conference Record of the Forty-Third Asilomar Conference on Signals, Systems and Computers*, pages 1025–1029, 2009.

[47] N. B. Mehta, J. Wu, A. F. Molisch, and J. Zhang. Approximating a sum of random variables with a lognormal. *IEEE Transactions on Wireless Communications*, 6(7):2690–2699, 2007.

[48] N. Miliou, A. Moustakas, and A. Polydoros. Interference source localization and transmit power estimation under log-normal shadowing. In *Proceedings of EUSIPCO*, 2011.

[49] A. O. Nasif and B. L. Mark. Measurement clustering criteria for localization of multiple transmitters. In *IEEE 43rd Annual Conference on Information Sciences and Systems*, pages 341–345, 2009.

[50] J. Nasreddine, N. Miliou, J. Riihijärvi, A. Polydoros, and P. Mähönen. Using geolocation information for dynamic spectrum access in cellular networks. In *Proceedings of the 6th ACM workshop on Performance monitoring and measurement of heterogeneous wireless and wired networks*, pages 75–82. ACM, 2011.

[51] J. K. Nelson, M. R Gupta, J. E. Almodovar, and W. H. Mortensen. A quasi em method for estimating multiple transmitter locations. *IEEE Signal Processing Letters*, 16(5):354–357, 2009.

[52] J. K. Nelson, M. U. Hazen, and M. R. Gupta. Global optimization for multiple transmitter localization. In *IEEE Military Communications Conference, MILCOM*, pages 1–7. IEEE, 2006.

[53] A. Papoulis and S. U. Pillai. *Probability, random variables, and stochastic processes*. Tata McGraw-Hill Education, 2002.

[54] N. Patwari, J. N Ash, S. Kyperountas, A. O. Hero, R. L. Moses, and N. S. Correal. Locating the nodes: cooperative localization in wireless sensor networks. *IEEE Signal Processing Magazine*, 22(4):54–69, 2005.

[55] N. Patwari, A. O. Hero, M. Perkins, N. S. Correal, and R. J. O'dea. Relative location estimation in wireless sensor networks. *IEEE Transactions on Signal Processing*, 51(8):2137–2148, 2003.

[56] J. S. Picard and A. J. Weiss. Theoretical facts on RSSI-based geolocation. In *IEEE 27th Convention of Electrical and Electronics Engineers in Israel*, pages 1–5, 2012.

[57] F. Rajwani and N. C. Beaulieu. Accurate simple closed-form approximations to distributions and densities of lognormal sum random variables. In *Vehicular Technology Conference, 2004. VTC2004-Fall. 2004 IEEE 60th*, volume 1, pages 111–114. IEEE, 2004.

[58] C. Raman, J. Kalyanam, I. Seskar, and N. Mandayam. Distributed spatio-temporal spectrum sensing: An experimental study. In *IEEE Forty-First Asilomar Conference on Signals, Systems and Computers*, pages 2063–2067, 2007.

[59] J. Riihijärvi, P. Mähönen, M. Wellens, and M. Gordziel. Characterization and modelling of spectrum for dynamic spectrum access with spatial statistics and random fields. In *IEEE 19th International Symposium on Personal, Indoor and Mobile Radio Communications, PIMRC*, pages 1–6, 2008.

[60] C. Robert and G. Casella. *Monte Carlo statistical methods*. Springer Science & Business Media, 2013.

[61] A. Sahoo and M. Souryal. Dynamic spectrum access: Current state of the art and future challenges. In *IEEE International Conference on Computing, Networking and Communications (ICNC)*, pages 226–230, 2014.

[62] A. H. Sayed, A. Tarighat, and N. Khajehnouri. Network-based wireless location: challenges faced in developing techniques for accurate wireless location information. *IEEE Signal Processing Magazine*, 22(4):24–40, 2005.

[63] D. C. Schleher. Generalized gram-charlier series with application to the sum of log-normal variates (corresp.). *IEEE Transactions on Information Theory*, 23(2):275–280, 1977.

[64] S. C. Schwartz and Y. Yeh. On the distribution function and moments of power sums with log-normal components. *Bell System Technical Journal*, 61(7):1441–1462, 1982.

[65] S. K. Sengijpta. Fundamentals of statistical signal processing: Estimation theory. *Technometrics*, 37(4):465–466, 1995.

[66] G. Sun, J. Chen, W. Guo, and K. J. R. Liu. Signal processing techniques in network-aided positioning: a survey of state-of-the-art positioning designs. *IEEE Signal Processing Magazine*, 22(4):12–23, 2005.

[67] S. Suparman, M. Doisy, and J. Tourneret. Changepoint detection using reversible jump mcmc methods. In *IEEE International Conference on Acoustics, Speech, and Signal Processing (ICASSP)*, volume 2, pages II–1569, 2002.

[68] MATLAB Signal Processing Toolbox. Natick. *Massachusetts, United States: The MathWorks Inc*, 2012.

[69] M. Umer, L. Kulik, and E. Tanin. Spatial interpolation in wireless sensor networks: localized algorithms for variogram modeling and kriging. *Geoinformatica*, 14(1):101–134, 2010.

[70] O. Ureten and T. J. Willink. Joint estimation of emitter power and location in cognitive radio networks. In *IEEE 12th International Workshop on Signal Processing Advances in Wireless Communications (SPAWC)*, pages 61–65, 2011.

[71] S. Ureten, A. Yongaçoğlu, and E. Petriu. A comparison of interference cartography generation techniques in cognitive radio networks. In *IEEE International Conference on Communications (ICC)*, pages 1879–1883, 2012.

[72] S. Ureten, A. Yongaçoğlu, and E. Petriu. Interference map generation based on Delaunay triangulation in cognitive radio networks. In *IEEE 13th International Workshop on Signal Processing Advances in Wireless Communications (SPAWC)*, pages 134–138, 2012.

[73] S. Ureten, A. Yongaçoğlu, and E. Petriu. Primary emitter localization using smartly initialized Metropolis-Hastings algorithm. In *IEEE Proceedings of the 21st European Signal Processing Conference (EUSIPCO)*, pages 1–5, 2013.

[74] S. Ureten, A. Yongaçoğlu, and E. Petriu. Iterative grid search for rss-based emitter localization. In *IEEE 22nd European Signal Processing Conference (EUSIPCO)*, pages 1507–1511, 2014.

[75] S. Ureten, A. Yongaçoğlu, and E. Petriu. A reduced complexity iterative grid search for rss-based emitter localization. In *IEEE 27th Biennial Symposium on Communications (QBSC)*, pages 149–152, 2014.

[76] R. M. Vaghefi, M. R. Gholami, and E. G. Strom. RSS-based sensor localization with unknown transmit power. In *IEEE International Conference on Acoustics, Speech and Signal Processing (ICASSP)*, pages 2480–2483, 2011.

[77] H. Wang and P. Chu. Voice source localization for automatic camera pointing system in videoconferencing. In *IEEE International Conference on Acoustics, Speech, and Signal Processing, ICASSP-97*, volume 1, pages 187–190, 1997.

[78] S. Wang, R. Inkol, and B. R. Jackson. Relationship between the maximum likelihood emitter location estimators based on received signal strength (RSS) and received signal strength difference (RSSD). In *IEEE 26th Biennial Symposium on Communications (QBSC)*, pages 64–69, 2012.

[79] S. Wang, B. R. Jackson, and R. J. Inkol. Impact of emitter-sensor geometry on accuracy of received signal strength based geolocation. In *IEEE Vehicular Technology Conference (VTC Fall)*, pages 1–5, 2011.

[80] A. J. Weiss. On the accuracy of a cellular location system based on RSS measurements. *IEEE Transactions on Vehicular Technology*, 52(6):1508–1518, 2003.

[81] M. A. Youssef, A. Agrawala, and A. U. Shankar. Wlan location determination via clustering and probability distributions. In *Proceedings of the First IEEE International Conference on Pervasive Computing and Communications, (PerCom)*, pages 143–150, 2003.

[82] M. Zafer, B. J. Ko, and IW-H Ho. Transmit power estimation using spatially diverse measurements under wireless fading. *IEEE/ACM Transactions on Networking*, 18(4):1171–1180, 2010.

[83] A. Zalonis, N. Dimitriou, A. Polydoros, J. Nasreddine, and P. Mahonen. Femtocell downlink power control based on radio environment maps. In *IEEE Wireless Communications and Networking Conference (WCNC)*, pages 1224–1228, 2012.

[84] L. Zhao and J. Ding. A strict approach to approximating lognormal sum distributions. In *IEEE Canadian Conference on Electrical and Computer Engineering (CCECE)*, pages 916–919. IEEE, 2006.

[85] Y. Zhao, J. Gaeddert, K. K. Bae, and J. H. Reed. Radio environment map enabled situation-aware cognitive radio learning algorithms. In *Proc. SDR Forum Technical Conference*, 2006.

[86] Y. Zhao, B. Le, and J. H. Reed. Network support–the radio environment map. *Cognitive radio technology*, pages 325–366, 2006.

[87] Y. Zhao, D. Raymond, Silva C., C.H. Reed, and Midkiff S.F. Performance evaluation of radio environment map-enabled cognitive spectrum-sharing networks. In *IEEE Military Communications Conference MILCOM*, pages 1–7, Oct 2007.

[88] X. Zhiqiang, L. Wei, and H. Qiang. An iterative multiple primary users localization algorithm based on clustering. In *IEEE 6th International ICST Conference on Communications and Networking in China (CHINACOM)*, pages 241–244, 2011.

[89] J. Zhu, S. Spain, T. Bhattacharya, and G. D. Durgin. Performance of an indoor/outdoor RSS signature cellular handset location method in Manhattan. In *IEEE Antennas and Propagation Society International Symposium*, pages 3069–3072, 2006.